NASA Technical Paper 3392

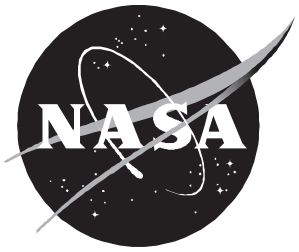

Experimental Studies of Transonic Flow Field Near a Longitudinally Slotted Wind Tunnel Wall

Joel L. Everhart and Percy J. Bobbitt

April 1994

NASA Technical Paper 3392

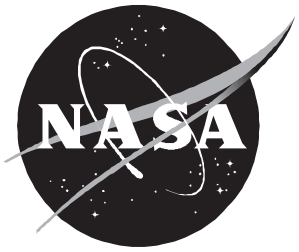

Experimental Studies of Transonic Flow Field Near a Longitudinally Slotted Wind Tunnel Wall

Joel L. Everhart and Percy J. Bobbitt
Langley Research Center • Hampton, Virginia

National Aeronautics and Space Administration
Langley Research Center • Hampton, Virginia 23681-0001

April 1994

The use of trademarks or names of manufacturers in this report is for accurate reporting and does not constitute an official endorsement, either expressed or implied, of such products or manufacturers by the National Aeronautics and Space Administration.

Acknowledgments

The first author gratefully appreciates the contributions of Richard W. Barnwell of the Langley Research Center and John L. Whitesides and Michael K. Myers of The George Washington University for serving on his examining committee and for their careful reviews of the material from which this report was taken.

Abstract

The results of detailed parametric experiments are presented for the near-wall flow field of a longitudinally slotted transonic wind tunnel. Existing data are reevaluated and new data obtained in the Langley 6- by 19-Inch Transonic Wind Tunnel are presented and analyzed. In the experiments, researchers systematically investigate many pertinent wall-geometry variables such as the wall openness and the number of slots along with the free-stream Mach number and model angle of attack. Flow-field surveys on the plane passing through the centerline of the slot were conducted and are presented. The effects of viscosity on the slot flow are considered in the analysis. The present experiments, combined with those of previous investigations, give a more complete physical characterization of the flow near and through the slotted wall of a transonic wind tunnel.

Introduction

Wind tunnels have long been used as tools for aerodynamic research, development, and testing so their use is relatively well understood. However, the uncertainties in the data acquired from these facilities may be excessive due to large interactions between the fluid and the geometric constraints of the tunnel circuit. The most important and variable portion of the circuit is the test-section segment that may have walls depending on the type of testing and the speed range. For low-speed testing, either closed-throat or open-jet test sections are typically used; transonic tunnels have either slotted- or porous-wall test sections. Supersonic and hypersonic tunnels typically have solid (closed-throat) test sections, which are almost a necessity for uniform flow.

Test sections with solid walls have zero normal flow at the wall, which constrains the flow about the model such that (for positive angles of attack) the upper surface velocities are higher than normal and the lower surface velocities are lower. Thus, a relatively larger value of lift is measured compared with the lift for the same model in free air.

For an open-jet test section, zero pressure drop exists across the interface between the jet and the "undisturbed" plenum. Open-jet tunnels force the local pressure at the interface to be equal to the plenum free-stream pressure that is greater than the pressure at an equivalent location in free air. Thus, for positive angles of attack, the measured value of lift is less than that in free air.

The closed-wall and open-jet test sections clearly provide flow conditions that differ from those about a body in free air. The resulting error in the model data acquired in these types of wind tunnels was analyzed for incompressible, two-dimensional flows as early as 1919 by Prandtl (see Glauert 1947). For approximately 30 years extending into the late 1940's, Prandtl's linear analysis methods were extended to include effects such as three-dimensional flow in wind tunnels with various cross-sectional geometries (e.g., see Theodorsen 1931) and compressible fluid flow (Allen and Vincenti 1944). Verification experiments were also conducted during that period. Several concise surveys of the resulting corrections are given by Garner et al. (1966), Pindzola and Lo (1969), Pope and Harper (1966), and Pankhurst and Holder (1965).

The first 30 years of wind tunnel wall-interference research yielded an important fact for modern wind tunnels; that is, theoretically and experimentally, solid-wall corrections are opposite in sign from those of open-jet test sections. Thus, if a wall is partially open, an adjustment to the geometric openness (porosity) should be possible to obtain a near-zero wall-interference correction and thereby allow a more realistic simulation of free-air conditions. Two major concepts have been advanced for constructing partially open walls—longitudinally slotting the wall in the free-stream direction and perforating the wall with discrete holes, typically with a uniform porosity.

Wright and Ward (1955) were the first researchers to determine theoretically the wall-induced interference of the slotted-wall tunnel by solving Laplace's equation for a circular cross-section wind tunnel with different numbers of slots. The tunnel disturbance was assumed to be caused by a doublet singularity the strength of which is matched to the blockage of the model. At the wall boundary, they alternately applied the solid-wall and open-jet conditions at the solid portions (slats) and the open portions (slots),

respectively. Their analysis showed the "possibility of obtaining zero blockage interference" in a slotted-wall test section. Based on these theoretical calculations, a slotted test section was constructed for the NACA Langley 8-Foot High-Speed Tunnel and placed in operation in early 1950 (Hansen 1987). Research conducted in that facility showed that by increasing the drive system power, slotted wind tunnels could operate at supersonic speeds and that at transonic speeds "the phenomenon of choking, characteristic of closed tunnels, did not occur in the slotted tunnel" (Wright and Ward 1955).

As with most advances in the state of the art, slotted walls introduced a new set of problems. Slotted walls have a mixed boundary composed of solid and open regions that generate a flow field for which the physics is poorly understood, particularly downstream of the model where flow returns to the test section from the plenum chamber. As a result, the viscous slotted-wall flow field is difficult to model mathematically, even with inviscid-flow assumptions. Several groups of researchers (Davis and Moore 1953; Chen and Mears 1957; Baldwin, Turner, and Knechtel 1954; Goethert 1961; Wood 1964; and Berndt and Sörensén 1976) have attempted to simplify the flow-field model and have derived what is now known as a homogeneous slotted-wall boundary condition. The term homogeneous results from the use of flow conditions in the far field of the slotted wall where the rapidly varying effect of the highly disturbed flow near and through the slot is averaged in the spanwise direction over many slots. Typically, the boundary condition prescribes the relationship between the pressure drop across the wall and the streamline curvature of the flow in the wind tunnel. Depending on the formulation, that relationship may depend on other quantities such as the flow angle in or near the slot. These slotted-wall boundary conditions contain coefficients that depend on the wall-geometry and tunnel-flow conditions, the values of which must be determined by appropriate theory or experiment. A discussion of these boundary conditions and of the resulting coefficients is given in a later section. Therefore, estimates of the wall-induced interference are difficult to determine with certainty, particularly at transonic speeds and with large model-span-to-tunnel-height ratios.

To resolve some of the problems associated with past slotted-wall studies and existing data, a combined theoretical and experimental study was initiated (Everhart 1988). Specific goals of the study were twofold: first, to increase understanding of the physics of the flow near the slotted wall by re-examining published slotted-wall data; second, to conduct an experiment in which wall-geometry parameters were varied systematically and in which appropriate flow measurements were made. With this increased understanding of the slotted-wall flow field, an improved mathematical model of the wall flow field was developed that can be used to improve interference predictions in existing slotted-wall tunnels. The model can also be used to design better walls for existing and new tunnels, walls that will reduce the interference in measured aerodynamic data.

The purpose of this paper is to present the experimental findings of this study. The paper begins with a brief summary of the historical development of the slotted-wall boundary condition, then proceeds with an examination of the terms and coefficients contained in the previous mathematical formulations. This historical development is presented to lay an appropriate foundation for subsequent sections in which the existing experimental database is reexamined for consistency and understanding. A new experiment that significantly expands on the database has been conducted in the Langley 6- by 19-Inch Transonic Tunnel. This experiment is described in detail, data are presented, and the major results are discussed. Finally, results from all experiments are summarized. The results indicate the need for additional slot-flow studies that focus on the slot–boundary-layer interaction and on the effects of changes in the slot cross-sectional geometry.

Part of the information presented in this report was included in a dissertation entitled "Theoretical and Experimental Studies of the Transonic Flow Field and Associated Boundary Conditions Near a Longitudinally-Slotted Wind-Tunnel Wall" submitted by Joel L. Everhart in partial fulfillment of the requirements for the Doctor of Science in Fluid Mechanics, George Washington University, Washington, DC, February 1988.

Symbols

A_{ls}, B_{ls}, C_{ls}	tunnel Mach number least-squares calibration coefficients (eq. (9))
a	slot spacing, in.
B	slotted-wall viscous coefficient
C_P	pressure coefficient, $\frac{p - p_\infty}{q_\infty}$
c	airfoil chord, in.
d	slot width, in.
h	tunnel semiheight, in.
K	slotted-wall streamline curvature coefficient

M	Mach number
P	pressure, psi
Q	plenum suction flow rate, ft^3/min
q	dynamic pressure, psi
R	unit Reynolds number, ft^{-1}
R_x	Reynolds number based on length x
T	temperature, °R
t	wall thickness, in.
U	longitudinal (axial) velocity component, ft/sec
u, v, w	perturbation velocity component in x, y, and z direction, respectively, ft/sec
V	transverse (crossflow) velocity component, ft/sec
W	lateral velocity component, ft/sec
x	longitudinal distance along tunnel, positive in downstream direction, in.
y	distance normal to top and bottom tunnel wall toward centerline, in.
$y\prime$	distance normal to slotted wall from centerline, in.
z	lateral distance normal to x-y plane, in.
α	angle of attack, deg
Δ	change in or drop across slotted wall
δ	boundary-layer thickness, in.
δ^*	boundary-layer displacement thickness, in.
ϵ	orifice discharge coefficient
θ	flow angle measured positive out of test section, deg
ρ	density, $slug/ft^3$
ϕ	potential, ft^2/sec
Subscripts:	
cal	calibrated
ff	far field
h	average
p	plenum
ref	reference
s	in slot
t	total
vc	at *vena contracta*
w	at wall
∞	in free stream
Abbreviations:	
AEDC	Arnold Engineering Development Center
DACU	data acquisition and control unit
DAS	data acquisition system
DFA	diffuser flow apparatus
ESP	electronically scanned pressure
HP	Hewlett Packard
IDT	Innovative Data Technologies
id	inside diameter
LE	leading edge (fig. 11)
NTF	National Transonic Facility
od	outside diameter
PCU	pressure calibrator unit
TE	trailing edge (fig. 11)

Slotted-Wall Geometry

A slotted-wall wind tunnel and its coordinate system are shown in figure 1(a). The longitudinal coordinate x is along the centerline of the tunnel, the coordinate y is normal to the centerline, and the coordinate z is normal to the x-y plane. The velocities U, V, and W correspond to the coordinates x, y, and z, respectively. A tunnel typically has a settling chamber upstream of the test section to allow the dampening of disturbances in the flow. Downstream of this chamber is a length of solid, converging walls through which the flow is accelerated to the desired test conditions. The test section has slotted walls extending both upstream and downstream of the model with the walls separated by distance $2h$. Upstream, the slots allow the flow to expand around the model into a plenum chamber that surrounds the test section. Downstream, the slots allow the flow to reenter the test section. The slotted-wall portion of different wind tunnel test sections may vary in the number of slots, openness ratios, and cross-sectional geometries. At the downstream end of the test section is a

reentry region that may have reentry flaps (depending on the construction of the tunnel) to allow the smooth transition of the flow into the diffuser section.

Figure 1(b) presents a cross-sectional view of a typical slotted wind tunnel wall, defines its geometric parameters, and gives a portion of the flow field as projected onto the crossflow plane. The slotted-wall configuration shown is composed of rectangular members called slats that are uniformly spaced distance a apart. The geometric slot width is denoted by d and the thickness or depth of the slot is denoted by t. Other geometric parameters such as variations in cross-sectional shape and slot-lip radius of curvature have not been illustrated for the sake of clarity. The local flow angles θ, as shown in figure 1(a), are measured with respect to the centerline of the tunnel and are positive for outflow. The approach velocity to the slotted wall v is the spanwise average of the velocity in the crossflow plane at some distance sufficiently far from the slot to avoid the large, rapidly varying flow into the slot. After entering the slot, the flow may separate from the wall and narrow to form a *vena contracta*. This narrowing forms the effective fluid slot width and is typically treated through the use of an orifice coefficient. Although not noted in the figure, the subscript s is used to denote the property "at the slot."

Slotted-Wall Boundary Condition

Historical Development

Davis and Moore (1953) and Chen and Mears (1957) each attempted to simplify the mathematical description of the wall and in the process derived what is now known as the classic or ideal form of the homogeneous slotted-wall boundary condition. In their theoretical analyses, they assumed that at the wall all perturbations from the free-stream velocity were small. This assumption allowed them to derive a relationship between the far-field average (homogeneous) pressure drop across the wall and the streamline curvature in the tunnel. Their formulation is given as

$$C_{P,w} - C_{P,s} = 2aK\frac{\partial \theta_w}{\partial x} \tag{1}$$

where the subscript w denotes the spanwise average of the flow property "at the wall." This average is in reality taken far from the slot in the tunnel where the rapidly varying changes due to the presence of the slot are negligible. The symbol $C_{P,s}$ represents the local far-field pressure coefficient on the plenum side of the slotted wall. The slotted-wall, geometry-dependent coefficient K must be determined either through theoretical analysis or appropriate experiment. The major difference between the theories of Chen and Mears and Davis and Moore is an attempt by the former pair to model the influence of slat thickness, whereas Davis and Moore considered slats of zero thickness. This difference appears in the theoretical value of the coefficient K.

Baldwin, Turner, and Knechtel (1954) proposed an empirical extension to equation (1) that accounts for viscous effects in the slots. Likewise, Goethert (1957) extended equation (1) by proposing a modification for slot configurations with porous cover plates. The resulting form of the boundary condition was the same in each case and is given by

$$C_{P,w} - C_{P,s} = 2aK\frac{\partial \theta_w}{\partial x} + B\theta_w \tag{2}$$

where the linear crossflow term $B\theta_w$ is the contribution of viscosity. Small velocity perturbations at the wall were again assumed. An estimate of the magnitude of the crossflow velocity for which equation (2) would apply was given by Baldwin, Turner, and Knechtel. Based on the present notation, that estimate is

$$\left(\frac{v}{U_\infty}\right)^2 \ll 2\sin\left(\pi\frac{d}{2a}\right)\frac{u}{U_\infty} \tag{3}$$

Thus, if a typical slotted-wall openness ratio $d/a = 0.05$, the square of the crossflow velocity perturbation must be much smaller than 0.01 times the longitudinal perturbation for the linear theory to apply. This places an unrealistic restriction on equations (1) and (2) for practical applications.

To remove the small crossflow restriction, Wood (1964) reasoned that crossflow in the slot would be larger than that typically allowed in the previous theoretical developments and that it would dominate the effect of the streamline curvature for slots of small width. His perturbation analysis yielded the nonlinear boundary condition,

$$C_{P,w} - C_{P,s} = \left(\frac{\pi + 2}{\pi}\,\frac{a}{d}\right)^2 \theta_w^2 \tag{4}$$

for both inflow and outflow through the slots. No published application of the boundary condition is known other than that of the original presentation where only qualitatively similar comparisons with experiment are demonstrated. An interesting point to note here is that this formulation does not allow

for a wall negative pressure drop. Finally, Berndt and Sörensén (1976) derived a boundary condition,

$$C_{P,w} - C_{P,s} = 2\left(\frac{\rho U}{\rho_\infty U_\infty}\right) aK \frac{\partial \theta_s}{\partial x} + \left(\frac{\rho}{\rho_\infty}\right)\theta_s^2 \quad (5)$$

by integrating the pressure along a path from the center of the slat through the slot and into the plenum. That analysis neglected shear stress contributions and estimated the value of K from an inviscid analysis in much the same way as the Davis and Moore theory did, but this time Berndt and Sörensén allowed for the effect of slot depth (wall thickness). This equation essentially combines the functional forms of equations (1) and (4) as the applicable wall-pressure-drop condition. In this and each of the previously cited forms of the boundary condition, the equations have been derived after the assumption of inviscid flow. A minor qualification of this statement is made for the development of equation (2) in which the viscous effects were empirically added after the fact.

Slotted-Wall Streamline-Curvature Coefficient

The inconsistencies in the slotted-wall boundary conditions presented earlier carry over into the values of the streamline-curvature coefficient K. The experimentally determined values of K obtained before this study and the theoretically developed variations of K with openness ratio do not agree. These differences and the reasons for the discrepancies are thoroughly discussed in Everhart (1988). Figure 2 shows the experimental variation of K with wall openness ratio (Barnwell 1976; and Baronti, Ferri, and Weeks 1973) compared with the theories of Davis and Moore (1953) and Chen and Mears (1957, as corrected by Barnwell (1976)). The three experimentally determined values of K are parametrically inconsistent because they were obtained for a speed range of 93 ft/sec to $M_\infty = 0.95$ and with the number of slots varying from 3 to 15. These comparisons show considerable disagreement between the experiment and the theory; they also reveal large discrepancies from two different theoretical models of the wall geometry. This disagreement occurs because the physics of the problem is not appropriately captured. Therein lies the impetus for the current studies. New extensions of the slotted-wall theory that yield improved correlations with experimental data and consistent, parametric variations of the slotted-wall boundary-condition coefficients have been presented by Everhart (1987, 1988). These extensions incorporate the experimental results of this report and will not be presented herein.

Analysis of Previous Experiment

Data from existing experiments are analyzed in this section and the physics of fluid motion near a slotted wall is explored. Several previous slot-flow–wall-interference studies are examined, including those of Chen and Mears (1957), Gardenier and Chew (see Goethert 1961), and Berndt and Sörensén (1976). Additionally, an analysis of some recently published data obtained in the diffuser flow apparatus (DFA) of the National Transonic Facility (NTF)(Everhart, Igoe, and Flechner 1991) is presented. Note that all these experiments assumed two-dimensional flow when in fact the tunnel sidewall boundary layer and corner vortices impose some degree of three-dimensional flow on the experiments.

Chen and Mears Experiment

Chen and Mears (1957) presented a theoretical and experimental study of the slotted-wall boundary condition. Three slot experiments (presented in fig. 3) were conducted in the Brown University 22 in. × 32 in. low-speed wind tunnel. In test 1, the upper half of a 24-in-chord Joukowsky airfoil was placed on a solid floor of the wind tunnel with its leading edge 12 in. downstream of the slot origin. In test 2, the same airfoil was moved so that its leading edge was 22 in. downstream of the slot origin. Finally, in test 3, a 12-in-chord Joukowsky airfoil was placed in the center of the tunnel between two slotted walls with its leading edge 17 in. downstream of the slot origin. Each slotted wall had nine 0.5-in-wide slots with an openness ratio of 14.1 percent. The slots originated 3 in. downstream of the beginning of the test section and terminated 47 in. downstream. In each case, the airfoil spanned the 32-in. width of the tunnel and had a chord-to-tunnel semiheight ratio of 1.09. This ratio is large compared with those of 0.3 to 0.6 typically used for conventional airfoil studies; the large airfoil size was chosen to accentuate the airfoil and wall interaction.

The test velocity for each experiment was 93 ft/sec. All pressure measurements were referenced to the atmospheric plenum pressure. Measurements of the pressure and flow angle were made in the test section over both the slot and the slat at a position 2 in. (4 slot widths) above the plane of the wall along its length with probes mounted in a slot in the sidewall of the tunnel. (See fig. 3.) All Chen and Mears data presented here have the axial coordinate referenced to the x station corresponding to the leading edge of the airfoil, then are normalized using airfoil chord length.

The Chen and Mears pressure measurements taken over the slot are presented in figure 4(a) with

the corresponding flow-angle measurements in figure 4(b). Here, the pressure coefficient is calculated by using the pressure drop across the wall because the reference pressure is the plenum pressure. The pressure coefficients for the 12- and 24-in. airfoils maximize at different upstream levels ahead of $x/c = -0.5$. This disagreement is possibly due to the differences in the growth of the tunnel-wall boundary layers but is more likely due to the finite tunnel effects manifested in the short slot length upstream of the airfoil leading edge. The short slot length would not allow the flow to become fully developed before airfoil-induced flow disturbances were imposed. Differences in the pressure drop downstream of the leading edge begin appearing immediately and are clearly evident in the data near and downstream of the point of maximum thickness ($x/c = 0.30$). For test 2, the trailing edge of the airfoil extended past the end of the slots, which gives a finite-tunnel effect that is evident in both the pressures and flow angles. (See fig. 4(b).)

The flow angles presented in figure 4(b) also show the effects of the finite length of the slots. Data from tests 1 and 2 are similar in their development upstream of the maximum airfoil thickness but diverge significantly downstream. Interestingly, the measurements on the small airfoil (test 3) compare very well with the test 1 results beginning at a point slightly upstream of the leading edge and continuing throughout the remaining measurement region.

The streamwise gradient of the flow angle was obtained by computing the differences in the measured values of the flow angle for each test and is presented in figure 4(c), which shows that ahead of the airfoil leading edge, all gradients are essentially the same. The data from tests 1 and 3 give similar results for the whole range of measurements; however, test 3 again shows significant finite-tunnel effects downstream of the maximum airfoil thickness.

Based on these observations, the test 3 measurements are believed more representative of the interactions between the airfoil flow field and the slotted-wall flow field in a typical airfoil wind tunnel, even though the chord-to-tunnel semiheight ratio is probably excessive. These data demonstrate the finite-tunnel effect on wall pressure data and the need to maintain enough upstream and downstream slot openness to allow the flow in the slot region to stabilize.

Chen and Mears (1957) made flow-angle measurements over both the slat and the slot; these are presented in figure 5(a) with the corresponding gradient presented in figure 5(b). The measurements for all the tests are "practically the same except in the rear portion," where a larger inflow angle can be observed over the slot as might be expected. They also had similar comparisons for pressure measurements but, "to avoid congestion of the graphs," they did not present them. The similarity of the streamwise variation of the flow angle and its gradient and the pressure over the slot and slat indicate a nearly homogeneous flow in the far-field region of the slots. Additionally, these data indicate that for many of the slots the rapidly varying portion of the slotted-wall flow field is constrained to a narrow region near the wall.

Berndt and Sörensén Experiment

Berndt and Sörensén (1976) conducted an experiment at a Mach number of 0.903 to evaluate the flow field near a slotted wall. A schematic of the test facility and wall configuration (taken from that reference) is shown in figure 6. Those authors had a wall with three slots 4 mm (0.156 in.) wide, a slot spacing of 80 mm (3.15 in.), and a ratio of $d/a = 0.05$. The slot depth was 6 mm (0.236 in.) and had a ratio of $t/d = 1.5$. A circular airfoil with a 90-mm chord (3.54 in.) positioned with the leading edge at tunnel station 0 mm was used as a disturbance model. The chord-to-tunnel semiheight ratio for the Berndt and Sörensén study was 0.72.

The Berndt and Sörensén wall-pressure drop measurements are presented in figure 7(a). Both model-in and tunnel-empty pressure data are presented along with the increment between the two conditions. An examination of the increment curve shows the airfoil to have two major effects on the wall-pressure drop. The first effect is global and is caused by the airfoil interaction with the tunnel and plenum system. For matched free-stream Mach numbers, the far-field upstream pressure in the tunnel with the model installed will be the same as that for the tunnel-empty case. However, the pressure increment equilibrates upstream at a constant value that differs from the tunnel-empty value which indicates a negative shift in the reference plenum pressure. Because of this shift, the plenum pressure is a very poor choice for calculating the test Mach number for transonic wind tunnels. The second major effect is a region of large local pressure variation 1 chord upstream of and behind the model leading and trailing edges. The term local is used to indicate the immediate vicinity of the model where large changes in some flow property (pressure in this instance) occur.

Flow-angle data measured in the slot are presented in figure 7(b). Approximately 0.5 chord upstream of the leading edge, the flow angle flattens and

becomes relatively insensitive to the airfoil model. Unfortunately, data are unavailable downstream of the station that corresponds to the airfoil trailing edge; also, the nature of the flow returning to the tunnel through the slot is unknown. Berndt and Sörensén state that the measurements downstream of station 80 mm (3.15 in., $x/c = 0.89$) are unreliable due to their low values. It is important to note the magnitude of the flow angles in the slot. At station -40 mm (-1.57 in., $x/c = -0.44$), the tunnel-empty values are about 13° whereas airfoil-in values are about 18°. The Berndt and Sörensén setup is such that large outflow occurs over most of the airfoil test region.

Figure 7(c) presents the computed streamwise gradient in the flow angle determined from the data presented in figure 7(b). The effect of the airfoil is clearly evident on both the streamwise gradient and the previously noted uncertainty in the flow-angle measurement. The airfoil effect on the gradient of the slot-flow angle occurs primarily in the region beginning approximately 0.5 chord length upstream of the airfoil leading edge.

Berndt and Sörensén measured the total pressure both along and through the slot on its centerplane. Those model-in results are reproduced here as figure 7(d). The total pressure of the slot-entry flow from a position 0.67 chord upstream of the airfoil leading edge to another position near the airfoil trailing edge is very near that of the free stream. Berndt and Sörensén state that "the slot flow under consideration is one with fairly small effects of inflow from the wall boundary layer and of viscous stress in the slot." However, contrary to that statement, the drop in the total pressure through the slot, particularly near the model, is an indication of the viscous shearing in the slot and the return of lower energy plenum air to the slot as the flow reverses direction. For the tunnel-empty data, Berndt and Sörensén state that "When there is no model present the level of the total pressures (not shown) is somewhat reduced, while the losses toward the rear are absent."

Wu, Collins, and Bhat Experiment

Wu, Collins, and Bhat (1983) and Bhat (1988) conducted flow-field survey experiments over a baffled slot. The wall contained a single centerline slot that was 0.36 m (14.2 in.) long by 6.6×10^{-3} m (0.26 in.) wide and had zigzag baffles that made a 14° angle normal to the wall. A schematic of the experiment taken from the Wu, Collins, and Bhat paper is shown in figure 8. The flow-field measurements were made normal to the wall at four spanwise stations and at various free-stream Mach numbers and amounts of plenum suction. The u, v, and w velocity components were obtained with a five-port flow-angle probe. Although the experimental setup did not have a true slot (because of the baffles), the data are nonetheless comparable to that obtained for flow over a slotted wall. Observations from these data are used later in the report to help explain trends in other data sets.

Figure 9 presents the Wu, Collins, and Bhat data for $M_\infty = 0.81$ at a spanwise station 1.27 cm from the slot. Examination of the normal component v/U_∞ shows that the flow accelerates toward the slot, reverses direction (i.e., goes negative), then reaccelerates toward the slot. Wu, Collins, and Bhat projected the v and w components from the four spanwise stations onto the transverse plane; the results are presented in figure 10 for a free-stream Mach number of 0.6 at two different levels of plenum suction. In figure 10(a) with no applied suction, an apparent vortex-like secondary motion exists. However, when suction is applied (fig. 10(b)), the vortex is apparently removed and the flow is directed strongly toward the slot.

Everhart, Igoe, and Flechner Experiment

Everhart, Igoe, and Flechner (1991) conducted a study of the flow near a slotted wall in the DFA. This facility, which is a small-scale version of the contraction, test section, and diffuser regions of the NTF, is described in detail by Gentry, Igoe, and Fuller (1981). The test section region of the tunnel is shown schematically in figure 11(a). The tunnel is 18.26 in. square with slotted upper and lower walls and with solid sidewalls. Each slotted wall was composed of six rectangular slots, each with a constant width of 0.25 in. and thickness of 0.0625 in. ($t/d = 0.25$). The slots originate at tunnel station 0 in. and terminate in the reentry region at tunnel station $\approx$45 in. The slot coordinate system and wall cross section shape are shown in figures 11(b) and 11(c).

During the experiment, flow angles were measured with a three-tube flow-angle probe. Measurements were made through the slot on the centerplane at a fixed longitudinal station and also along the slot at a fixed vertical distance from the slot. Test results were obtained at free-stream Mach numbers of 0.6, 0.725, and 0.85.

The test model used in the study was an NACA 0012-64 airfoil with a 5.4-in. chord, a leading edge at station 22.6 in., and a trailing edge at station 28 in. Maximum thickness of the airfoil is at $x/c = 0.40$, which corresponds to tunnel station 24.76 in. The

chord-to-tunnel semiheight ratio is 0.59, which is typical for two-dimensional airfoil testing. Only airfoil data at zero lift were obtained but not at all test conditions. Because problems were incurred during data acquisition and reduction, pressure data on the airfoil and on the slotted wall were not available for analysis.

The development of the tunnel-empty slot-flow variables both normal to and along the slot is shown in figure 12 for a free-stream Mach number of 0.6. In each part the local flow angle, measured in degrees, the local Mach number and the local total-pressure ratio are plotted versus y/d. Note that y/d is positive into the tunnel, that $y/d = 8$ corresponds to 2 in. into the free stream, and that $y/d = -4$ corresponds to 1 in. into the plenum. The flow angle is measured positive out of the tunnel into the plenum. In figure 12(a), the flow angle in the tunnel starts out small, increases rapidly as the slot is approached, and reaches a value of about 7° of outflow at the slot entrance (at $y/d = 0$). The flow angles increase almost linearly from $y/d = 0.4$ to the *vena contracta*, which occurs between $y/d = -0.3$ and $y/d = -0.5$ in all cases. Variations of the local Mach number (fig. 12(b)) and local total pressure (fig. 12(c)) show the expected decrease due to viscous shearing of the flow near the wall. At the slot entrance, the total pressure in the slot is about 91 percent of its free-stream value. As the flow develops along the slot, the fluid shearing increases, which indicates increased mixing of the lower energy plenum air with the high-energy tunnel free stream. Unfortunately, survey measurements were never conducted on the solid portion of the tunnel wall, which precludes accurate estimates of the effect of the boundary-layer growth on the mixing process.

The effects of a change in the free-stream Mach number on the slot-flow parameters are demonstrated in figure 13. In the three parts of this figure, the local flow angle, Mach number, and total-pressure ratio at tunnel station 24 in. are plotted versus y/d for free-stream Mach numbers of 0.6 and 0.85. Virtually no differences in the flow-angle results exist except between $y/d = 0.4$ to 4. Differences in the Mach number profiles shown in figure 13(b) are as expected and give an indication of the penetration depth of the tunnel flow into the plenum. The viscous slot flow is contained in a very narrow region near the wall. For the higher Mach number, the total-pressure ratio (fig. 12(c)) indicates a greater loss in the total head in the slot. Increasing the Mach number from 0.6 to 0.85 causes the total-pressure ratio in the slot to decrease from 0.91 to 0.82. A much thicker shear layer exists for the higher Mach number.

Comparison of the airfoil results with the tunnel-empty results at tunnel station 24 in. is shown in figure 14 for a free-stream Mach number of 0.6. At that station all the slot measurements with the airfoil installed are smaller than the corresponding tunnel-empty values. The difference occurs because this tunnel station is very near the station that corresponds to maximum airfoil thickness and, thus, is near the station where the flow angle around the airfoil reverses sign. This reversal of the flow brings the lower momentum air from the plenum further into the slot, which decreases the local Mach number (fig. 14(b)) and the local total pressure (fig. 14(c)). Similar results are evident in the Berndt and Sörensén (1976) total-pressure data presented in figure 7(d). Note that the *vena contracta* for the airfoil-installed data occurs at approximately the same location as for the tunnel-empty data.

An interesting phenomenon occurs in the flow-angle data (fig. 14(a)) between $y/d = 1$ to 2. In that region, the flow begins reversing direction and the flow angle approaches zero before it reaccelerates into the slot. Unfortunately, that tunnel station was the only one in which measurements were made normal to the wall through the slot with the airfoil installed so the exact reason for this occurrence is unknown. One plausible explanation is found in data presented by Wu, Collins, and Bhat (see fig. 9) where the measured transverse velocity component for their experiment exhibits the same qualitative characteristic. The reason is a vortical motion over the slot (see fig. 10(a)) for the case of no plenum suction. However, when suction is applied (fig. 10(b)), the vortex is apparently removed and the flow is directed strongly toward the slot. For the tunnel-empty DFA data, the pressure drop across the wall is strong enough for the normal velocity to increase through the slot to the *vena contracta*. However, when the airfoil is present, it acts as a sink and reduces the local wall-pressure drop. This effect would allow the formation of a vortex and would give the flow-angle results of figure 14(a) by analogy with the results of Wu, Collins, and Bhat.

Longitudinal measurements in the DFA were made along the slot at different heights (normalized by the slot width) and the results are shown in figure 15. On each part of the figure, data obtained inside the tunnel at 1 and 2 in. above the slot ($y/d = 4$ and 8, respectively) are shown, as are data in the slot ($y/d = 0$) and at a position on the plenum side of the *vena contracta* ($y/d = -0.9$). Note that the flow angles measured inside the tunnel gradually increase up to the leading edge of the model, whereas the flow angles measured in the slot are nearly constant

or slightly decreasing over a 2-chord region approximately 0.5 chord upstream of and in front of the airfoil leading edge. That is, the upstream trend in the flow-angle gradient in the slot is nearly opposite from that inside the tunnel. Excluding a large positive shift in the overall level of the slot-flow angle (a global effect), the airfoil does not appear to significantly interact with the slot except in a localized region near the airfoil (which agrees with previous observations of the data of Berndt and Sörensén). This effect is more apparent in the flow-angle gradient, which was computed from the data of figure 15(a) and is plotted for each measurement height in figure 15(d). Upstream, the large variations in the slot and plenum streamwise gradient are attributable to slot opening and stabilization of the flow after which the gradient has an approximately constant negative value. However, in the tunnel far from the slot, the gradient is approximately constant and positive except near the airfoil.

Gardenier and Chew Data

Data acquired by Gardenier and Chew and presented as "unpublished AEDC transonic model tunnel data" in Goethert (1961, fig. 11.25a) have been reproduced here as figure 16. These data were for a free-stream Mach number of 0.75 to 1.20 in the Arnold Engineering Development Center (AEDC) transonic model tunnel (1 ft) in which the wall had a single, sharp-edged longitudinal slot that was 1.3 in. wide (11 percent open) and 0.125 in. thick. In the figure, the wall-pressure drop is plotted versus the average transverse mass flux in the slot normalized by the longitudinal mass flux measured in the free stream. The figure shows that the Mach number has negligible (if any) influence on the results. Furthermore, Goethert states that

> Several tests (results unpublished) were conducted in the same model tunnel using a wall thickness increased considerably beyond the 1/8 in. of the wall presented in Fig. 11.25a [fig. 16]. Also, slots with the edges beveled to increase their sharpness and with rounded edges were studied. In all cases, basically similar characteristics were obtained, that is, a remarkable independence of Mach number existed as well as a predominantly linear characteristic of the cross-flow pressure drop.

For comparison, the following expression gives a good representation of the data shown in the figure:

$$\left(\frac{\Delta_p}{q_\infty}\right) = 0.2254\left(\frac{\rho_h v_h}{\rho_\infty U_\infty}\right) + 1.7460\left(\frac{\rho_h v_h}{\rho_\infty U_\infty}\right)^2 \quad \left(\frac{\rho_h v_h}{\rho_\infty U_\infty} \geq 0\right) \quad (6)$$

where the subscript h denotes the average. Note that this expression has a θ-like contribution similar to the formulation of Baldwin (eq. (2)) and also a θ^2-like contribution similar to that of Wood (eq. (4)) and Berndt and Sörensén (eq. (5)). The relationship between the inflow (negative) transverse mass flux and the pressure drop is consistent with that for outflow in that a nearly linear variation exists for small values of Δ_p/q_∞ for the thin wall boundary layers of this study. (See Goethert 1961.) Implications for the small inflow conditions are that the flow returned smoothly to the test section with little (if any) separation on the slotted wall internal to the test section.

Spanwise velocity distributions presented by Goethert (1961, fig. 11.25(b)) indicate that the average velocity in the slot is approximately 90 percent of that in the center. Therefore,

$$\left(\frac{\rho_h v_h}{\rho_\infty U_\infty}\right) = 0.90\left(\frac{\rho_s v_s}{\rho_\infty U_\infty}\right) = 0.90\epsilon\left(\frac{\rho_{vc} v_{vc}}{\rho_\infty U_\infty}\right) \quad (7)$$

where ϵ is the orifice coefficient required to achieve the plenum conditions imposed at the minimum flow area represented by the *vena contracta*. The reduction in the effective slot width represented by equation (7) when substituted into equation (6) yields a modified Gardenier and Chew equation for the pressure drop across the slotted wall with no streamline curvature. This expression is

$$\left(\frac{\Delta_p}{q_\infty}\right) = 0.203\epsilon\left(\frac{\rho_{vc} v_{vc}}{\rho_\infty U_\infty}\right) + 1.571\epsilon^2\left(\frac{\rho_{vc} v_{vc}}{\rho_\infty U_\infty}\right)^2 z \quad \left(\frac{\rho_{vc} v_{vc}}{\rho_\infty U_\infty} \geq 0\right) \quad (8)$$

Equation (8) is used later for comparison with other data.

Summary of Previous Experiments

A summary of the results obtained from these data sets follows. First, the Chen and Mears low-speed, incompressible data indicate that sufficient slot length should be both ahead of and behind the model for the slot flow to become fully developed. Otherwise, the effect of finite-length slots will become an important consideration. For wind tunnel walls with many slots, when measurements are made sufficiently far from the wall, the flow angles and pressures over the slot are very close to those measured over the slat. Thus, in the far field of the slot the average of the spanwise flow across the tunnel would be predicted by slender-body theory. Furthermore, a comparison of the longitudinal flow-angle gradients

(computed from the data) over the slot with those over the slat shows that nearly the same values were obtained. Therefore, sidewall measurements of the pressure should yield sufficiently representative values of the average pressure level and gradients across the slotted wall.

A reexamination of the Berndt and Sörensén high-transonic data strongly suggests that the effect of the airfoil is that of a perturbation on the existing tunnel-empty pressure distribution. The model had only a small effect on the pressure drop across the wall in the test region approximately 1 chord or more upstream of the leading edge, which indicated a localized effect of the model on the slot-flow field. Strong variations in the flow-angle gradients with the model installed were even more localized than the wall-pressure-drop variations in that the major influence extended only 0.5 chord upstream of the model leading edge. However, the airfoil appears to decrease the plenum pressure below the tunnel-empty value, which indicates a global shift in the undisturbed pressure drop over the entire extent of the slotted wall. Measurements of the total pressure of the flow entering the slot were very near the free-stream total pressure, particularly with the airfoil installed. A large drop in the slot total pressure occurs when the fluid passes through the slot, which indicates that strong viscous shearing occurs in the slot.

Analysis of recently published subsonic and low-transonic slotted-wall flow-field survey results obtained in the DFA revealed several significant points. Tunnel-empty slot-flow angles were large (as were those measured in the Berndt and Sörensén study) and insensitive to changes in free-stream Mach number. This insensitivity implies a global dominance of the tunnel geometry and its wall boundary layer on the slot-flow field. A comparison of the tunnel-empty *vena contracta* position with the airfoil-installed position showed it to be insensitive to the presence of the model for the given test conditions and tunnel geometry. The "fixed" location of the *vena contracta* in the slot implies that the interface between the high-energy tunnel flow and the low-energy plenum flow remains at the wall for outflow; corresponding data for inflow conditions were not available. When the airfoil was installed, the slot-flow angle upstream of about 0.5 chord ahead of the airfoil leading edge was not significantly affected (again in agreement with Berndt and Sörensén); however, the flow-angle measurements in the slot had different characteristics from those in the tunnel away from the slot as evidenced by a sign change in the flow-angle gradients. This sign change is another manifestation of the dominance of the wall boundary layer away from the local region of airfoil influence.

Finally, the Gardenier and Chew (Goethert 1961) data obtained at high-transonic and low-supersonic conditions show a definite quadratic trend with increasing transverse mass flow. This trend when combined with the large slot-flow angles measured in both the Berndt and Sörensén and the DFA experiments, negates the assumption that the square of the crossflow velocity component is negligible as was assumed in the classic ideal-slot theories.

Present Experiments

Facility Description

The present experiments were conducted in the Langley 6- by 19-Inch Transonic Tunnel (6 × 19 Tunnel) (Ladson 1973). Details of the plenum chamber and model service area surrounding the test section of the 6 × 19 Tunnel are shown in figure 17. The test section has slotted top and bottom walls and solid sidewalls and is shown with the near slotted wall removed. Each sidewall has movable turntables for installing the airfoil models and changing the airfoil angle of attack. Cross-sectional dimensions of the test section are 6 in. wide by 19 in. high with a length of about 50 in. A schematic of the facility is given in figure 18(a) and the test section is in figure 18(b).

Operational control of the Mach number is done hydraulically by either manual or automatic adjustment of the total pressure in the settling chamber. (See fig. 18(a).) The operating Mach number is computed from the measured free-stream total pressure and the reference static pressure that is measured in the plenum chamber. The test Mach number is computed from the measured free-stream total pressure and an upstream reference static pressure at the −30-in. station. (See fig. 18(b).) This is an atmospheric facility, so the reference static pressure is not too different from that measured in the plenum chamber. The tunnel reference static pressure port was used because of its insensitivity to the model, to changes in model attitude, and to the tunnel-wall geometry. The operating Mach number range is from about 0.1 to 1.2 and the unit Reynolds number varies to about 9×10^6 ft^{-1} at the highest Mach numbers. Typical operational characteristics of the 6 × 19 Tunnel are shown in figure 19.

Models

Airfoil model. A 6-in-chord NACA 0012 airfoil (fig. 20) was used as the disturbance model in the 6 × 19 Tunnel experiments. This airfoil was instrumented chordwise with 47 (23 upper surface, 23 lower

surface, and 1 leading edge) 0.0137-in-id pressure orifices along the midspan of the airfoil. Pressure data were integrated to give normal force and pitching moment. No drag measurements were made. All data were acquired while allowing free transition of the model boundary layer. Coordinates of the model taken at the orifice locations are given in table I. The tunnel-spanning model was mounted in the center of the tunnel on turntables in the tunnel sidewalls. Station $x = 0$ in. is at the model midchord.

Wall configurations. Because many geometrical variations are possible, a baseline slot configuration was established. This configuration was rectangular in cross section, had a constant openness ratio, and a constant thickness (or slot depth). Figure 21 shows the variation in the number of slots tested versus the wall openness ratio. The slotted walls spanned the range slot widths from 0.90 in. for the 15-percent-open wall with one slot to 0.09 in. for the 6-percent-open wall with four slots. The wall slats were 0.125 in. thick and had sharp edges. A solid wall was also tested and is indicated in the figure by the solid symbol at the origin. Note that in the subsequent discussions the wall-symbol notation used in this figure is strictly adhered to (for instance, open circles correspond to one-slot configurations).

The three 15-percent-open wall configurations, which were constructed with one, two, and four slots, are shown in figure 22. The two- and four-slot configurations each have half a slot on each side at the theoretical reflection plane formed by the sidewall of the tunnel. These walls are installed in the tunnel between stations -29 and 19.5 in. All walls were constructed such that the slots opened linearly from 0-percent openness at station -23 in. to full openness at -17 in. Constant slot width (openness ratio) was maintained to the 19.5-in. tunnel station where the flow enters the diffuser. (See fig. 18(b).)

Orifices for slot-flow pressure measurements were installed on one slat from each wall configuration. Each slat had 15 0.020-in-id orifices placed on the centerline of the slat sidewall. The orifices were more closely spaced in the region directly below the position of the airfoil. A few slats had orifices installed both on the top (tunnel side) centerline of the slat and on the bottom (plenum side) of the slat. The longitudinal location of each slat orifice is tabulated in table II.

In subsequent sections it is necessary to refer repeatedly to the different wall configurations being considered. For the sake of brevity, a shorthand notation has been established consisting of the slot openness ratio followed by the number of slots, with a hyphen separating the two. For example, a 15-percent-open wall with four slots is denoted 15-4. Likewise, a 7.5-percent-open wall with two slots is denoted 7.5-2.

Sidewall Pressure Orifices

The sidewall of the wind tunnel test section is shown in figure 23. This view gives an indication of the number and general location of the pressure measurements made on the tunnel sidewall. The top tunnel wall is defined as the left slotted wall and the flow direction is from the bottom of the figure to the top. The circular region in the center of the sidewall is the airfoil turntable; however, it has been replaced with a blank that is instrumented for wind tunnel calibration. A 6-in. ruler is at the top of the turntable for reference. Centerline calibration orifices are visible upstream and downstream of the model location, as are three streamwise rows of pressure orifices on the left of the turntable near the slotted wall. The three rows of slot-flow pressure orifices each contain 21 0.020-in-id orifices and are at stations 8.5, 8.0, and 7.5 in. from the tunnel centerline. The orifices are located so that the closest spacing is in the region directly above the model. Table III gives the location of the sidewall pressure orifices near the slotted wall. Pressures obtained from these orifices were used for the near-field analysis of the slot flow. At the extreme left of the sidewall are two brackets; the upper one is for installing the slotted wall and the lower one is for mounting the slot flow-angle probe.

Instrumentation

A detailed schematic of the data acquisition system (DAS) and of the instrumentation hookup is shown in figure 24. The individual components are described in subsequent paragraphs.

Data acquisition system. The DAS is composed of two major pieces of hardware: the Hewlett Packard (HP) 9845B computer and the Innovative Data Technologies (IDT) GPIB 1050 nine-track tape drive. The HP computer was used to acquire the data from all associated instrumentation during testing and to process the data to obtain engineering units. Only a limited capability to do postrun data analysis was available on the system so the major portion of the data reduction and analysis was done at the Langley central computing facilities. All the data were recorded on the nine-track tape drive for postrun processing.

Pressure instrumentation. The data acquired during the tests were obtained by using several different types of pressure instrumentation. Absolute readings for the tunnel reference conditions of

total and plenum chamber pressures were made with 30-psi differential Datametrics pressure transducers in which the reference side of the gauge was reduced to vacuum. These instruments have a quoted accuracy of 0.25 percent of reading. Two Datametrics 1085A Electronic Manometers were used to condition the signals before sending the information to the DAS. The total pressure was measured in the tunnel settling chamber; the plenum static pressure was the far-field pressure measured in the plenum chamber. The latter pressure was hydraulically averaged in the plenum with a large-diameter (0.25-in-id) tube that was vented at several places around the interior plenum chamber wall before the pressure gauge measurement. This near-atmospheric pressure was used as the reference for all the differential measurements. As a consistency check on the other measurements, the difference between the total and plenum pressures was measured with a Datametrics gauge rated at 30 psi and was continuously monitored on an HP 3478A Multimeter.

All measurements on the airfoil surface, along the tunnel sidewall, and on the flow angle probes were acquired as differential pressures with an electronically scanned pressure (ESP) system manufactured by Pressure Systems Incorporated. The instruments have a quoted accuracy of 0.07 percent of full scale. The gauges are highly accurate because of their capability for on-line, anytime calibration. This feature was used before each run to minimize errors. The ESP system included two pressure modules rated at 10 psi and three at 5 psi (each with 32 pressure ports for a total of 160 differential pressure measurements), the 780B pressure calibrator unit (PCU), and the 780B data acquisition and control unit (DACU). A 780B system is capable of acquiring up to 20 000 samples per second.

Temperature instrumentation. Total temperature was obtained from the Type K thermocouple in the settling chamber. Temperature was displayed on a Fluke, John Manufacturing Company, Inc. 2190A Digital Thermocouple, measured with an HP 3478A Multimeter, and recorded by the DAS.

Flow-angle probes. The flow angle was measured with three-tube flow-angle probes manufactured by United Sensor, Incorporated; these are shown schematically in figure 25. The probes have 0.015-in-id orifices and the outer tubes are chamfered to give an included angle of 90° on the probe head. The probe tip is approximately 0.030 in. wide by 0.090 in. high; the total probe length is 4 in. from tip to base. The probe dimensions were selected to minimize probe-slot interference. The probe orifices were sized to reduce the response time associated with making pressure measurements through a small-volume system according to the method of Sinclair and Robins (1952).

The probes were calibrated in the 6 × 19 Tunnel for a Mach number of 0.1 to 0.95 and for a pitch of −15° to 15°, although the more detailed calibration data were acquired between −5° and 5°. When the probes were in use, a preliminary measurement was made at the expected slot-flow angle for a zero airfoil angle of attack. The probe axis was then adjusted close to this measured angle. This procedure gives a quasi-nulling effect on the probe and may keep the succeeding measurements within the higher resolution portion of the probe-calibration table.

Accuracy and repeatability of the probe measurements were primary concerns during this study. Ten wind tunnel runs were made to determine how well the flow angle and Mach number could be determined. Each run covered the entire Mach number range and, based on these measurements, the measured flow angles have a maximum standard deviation of less than 0.1°. Likewise, the maximum standard deviation of the local Mach number as determined from the probe measurements is less than 0.0026.

Test Conditions

Mach and Reynolds numbers. The plenum reference Mach number is computed from the total pressure measured in the settling chamber and the plenum reference static pressure. The plenum pressure is obtained by hydraulically averaging the pressure measured in a large-volume tube (0.25-in. id) that has been vented at several places around the interior of the plenum chamber. Based on this value of Mach number, the tunnel-empty Mach number at the model station is adjusted to the required free-stream Mach number. The free-stream Mach number at the model station with the model installed is taken as the tunnel-empty model station calibrated value versus the upstream Mach number at the −30-in. tunnel station. Previous experience has shown this upstream Mach number to be insensitive both to the model and to changes in wind tunnel wall geometry over the entire Mach number range. Because the 6 × 19 Tunnel is an atmospheric wind tunnel, Mach number cannot be varied independently of the Reynolds number. The relationship between the two is shown in figure 19. For a free-stream Mach number of 0.7, the chord Reynolds number is about 3.25×10^6 ft^{-1} for the 6-in-chord NACA 0012.

As part of the study, multiple tunnel runs were necessary with and without the flow-angle probe in place because of probe interference in the measured wall- and slot-pressure data. To determine the repeatability of the test conditions, the standard deviation of the tunnel Mach number was determined from the same consecutive repeat runs used for the probe analysis. The standard deviation of the free-stream Mach number was typically less than 0.0017; for free-stream Mach numbers around 0.7, the standard deviation of the free-stream Mach number is about 0.0010. Both repeatability values are considered good for transonic wind tunnels.

Mach number calibrations. Typical tunnel-empty centerline values of the local Mach number plotted versus tunnel station for the 15-1 wall configuration are shown in figure 26. In each case, the data indicate flow acceleration to the test-section Mach number far upstream in the converging portion of the nozzle, a plateau between stations -36 and -30 in., acceleration through the slot-development region between stations -23 and -17 in., and, thereafter, the data remain essentially flat through the rest of the tunnel. When installed, the model is between stations -3 and 3 in. The diffuser section appeared to have little effect on the centerline data downstream of the model except possibly for some of the smaller openness-ratio walls at the higher Mach numbers. In all cases, the Mach number distribution is flat near the model station except, again, at the very highest Mach numbers. Because the upstream Mach number consistently plateaus at the same location and because prior experience in this facility has shown this region to be insensitive to the model, measurements made at tunnel station -30 in. have been chosen as the upstream reference position.

Based on the preceding conclusions, the subsequent calibration procedure was applied to each wall configuration. At each setting of the reference Mach number, a least-squares fit of the data between stations -6 and 6 in. was made and evaluated at station 0 in. to give a calibration Mach number. The calibration value was then plotted versus the reference value and the least-squares coefficients of the parabolic curve to determine

$$M_{\text{cal}} = A_{ls} + B_{ls} M_{\text{ref}} + C_{ls} M_{\text{ref}}^2 \qquad (9)$$

Typical results are as shown in figure 27 for the 15-1 wall. Only those data between free-stream Mach numbers 0.1 and 0.9 were analyzed; therefore, any deviations from the curve fit outside this range were inconsequential. The least-squares coefficients for each wall are shown in table IV.

Angle of attack. The model angle of attack is set manually by rotating the turntables to the desired pitch. This angle is determined from inclinometer readings on a reference surface attached to the model turntable. During the experiment, data were acquired at 0°, ±0.5°, ±1°, and ±2° on all wall configurations. Data were acquired at ±4° on some configurations. The angles were generally set to within ±3 min of arc (±0.05°).

Wall-Pressure Data

General observations. Typical wall-pressure data from the 6 × 19 Tunnel experiment are shown in figure 28. The tunnel-empty (fig. 28(a)) and airfoil-installed (fig. 28(b)) wall-pressure coefficients are shown for the 6-4 wall configuration at a free-stream Mach number of 0.7. These data are plotted versus tunnel station with an expanded pressure scale to accentuate the differences between the rows of sidewall pressures. In figures 28(a) and 28(b), the pressures measured on the slat ($y\prime = 9.5$, $y = 0$) and along sidewall rows 1 ($y\prime = 8.5$, $y = 1.0$), 2 ($y\prime = 8.0$, $y = 1.5$), and 3 ($y\prime = 7.5$, $y = 2.0$) are presented. The far-field measurement of the plenum pressure coefficient $C_{P,p}$ is also shown. Data along row 1 for the tunnel-empty configurations were not acquired because the instrumentation was used to measure the tunnel-empty centerline pressures. For all walls, the slots open linearly beginning at $x = -23$ in. and reach constant width at $x = -17$ in. In each figure, the pressure changes due to the opening of the slots are evident downstream of $x = -23$ in. The downward spike in the data for $x \geq 5$ is caused by a flow-angle probe (probe tip at $x = 6$ in.) and its support ($x = 10$ in.) mounted inside the tunnel 2 in. above the wall over the center slot.

The pressure data for the tunnel-empty case (fig. 28(a)) show virtually no difference between rows 2 and 3. For the airfoil-installed cases (fig. 28(b)), a significant shift in the level of the measurements is evident along row 1 relative to that of rows 2 and 3. This shift indicates that row 1 (which is closest to the slotted wall) is highly affected by the slot and the large flow gradients there. Rows 2 and 3, therefore, are better indicators of the inviscid, far-field (or average) wall-pressure field. Berndt (1982) and Kemp (1986) each have made analyses that indicate flow-field measurements should be made at $y/a \geq 0.75$ to ensure that flow-field measurements are not adversely affected by the rapidly varying flow in the slot. The data obtained along row 1 do not generally meet this requirement.

Airfoil effect. The effect of the airfoil on the pressure data measured along the tunnel sidewall is

shown in figure 29 for a free-stream Mach number of 0.7. (Recall that the airfoil extends from x = −3 to 3 in.) To enable correlation between the different wall configurations, the pressure scale has been chosen to permit comparisons with the wall that has the largest pressure variations—that is, the solid-wall configuration. For clarity, only those data along row 3 are plotted. Note that, given a symmetrical airfoil, an indication of both the top and bottom wall-pressure distributions is available by combining the positive and negative angle-of-attack data. Additionally, note that open symbols represent data acquired at a positive airfoil angle of attack, whereas filled symbols represent the corresponding data at negative angles.

In figure 29(a), the tunnel-empty solid wall is compared with that for the airfoil at $\alpha = -4°$ to 4°. These data indicate that even for the larger lift values (for the solid wall), the major deviation from the undisturbed-tunnel flow is contained within approximately ±3 chords of the airfoil. The upstream pressure levels quickly approach that of the undisturbed-tunnel level and the downstream level appears to approach that of no lift. The lack of pressure recovery is an indication of the large blockage caused by the airfoil wake in a solid-wall wind tunnel, even at small values of lift.

When the walls are opened (figs. 29(b)–29(g), the tunnel blockage is greatly reduced. The zero-lift minimum pressure coefficient changes from $C_P \approx -0.08$ for solid walls to $C_P \approx -0.025$ for the 15-4 slot configuration. The major deviation from the undisturbed tunnel flow is also reduced to within ±2 chords of the airfoil. The flow in the tunnel with the airfoil installed appears as a perturbation about the well-established tunnel-empty flow. This perturbation is especially evident when the pressures around the downstream probe are considered. Here, the probe support and its wake create a blockage; the pressure signature reacts by moving as a reference shift in the data when changing the model pitch angle is changed.

Slot-Pressure Data

Slotted-wall theories show that the pressure drop across the slot is a required parameter for determining wall characteristics. This requirement poses the dilemma of where the slot pressure should be measured. To resolve the question, all slotted walls were equipped with pressure orifices in the middle of the slat sidewall and several wall configurations were equipped with orifices on the slat back in the plenum Tunnel-empty pressures from these orifices are compared with a far-field measurement of the plenum pressure coefficient $C_{P,p}$ in figure 30 for three different slotted walls at $M_\infty = 0.7$. In each case, the slat-back (plenum-side) pressure results are very near those measured in the far field of the plenum whereas the slat-sidewall measurements are significantly different. Also, the greater the number of slots (compare fig. 30(b) with fig. 30(c)), apparently the better the agreement between the slat back and the far-field plenum. This large disagreement between the slat sidewall and the far field is most likely the result of large gradients caused by flow acceleration in the slot. In general, the pressures measured on the slat sidewall do not equal those measured either in the tunnel above the slots or in the far field of the plenum. However, the far-field measurement of the plenum pressure is a sufficient representation of that measured on the slat back. Therefore, to determine the wall-pressure drop $C_{P,p}$ should be used as the local slot pressure coefficient.

Airfoil Effect on Plenum Pressure

The effect of the zero-lift airfoil on the pressure drop coefficient $\Delta C_{P,ff}$ across the wall as determined by the far-field reference pressure upstream of the slots ($x = -30$ in.) and by the average far-field pressure in the plenum chamber is compared in figure 31 for a free-stream Mach number of 0.7. This pressure drop coefficient $\Delta C_{P,ff}$ is plotted versus the wall openness ratio. For matched free-stream Mach numbers, the airfoil causes the plenum pressure to drop globally relative to the corresponding tunnel-empty case. This effect is present for all slot geometries tested; however, the difference decreases with increasing openness ratio. For openness values greater than 10 percent, the difference in the measurements is negligible. This phenomenon indicates that the tunnel is approaching open-jet conditions in which the free-stream static pressure is equal to that of the surrounding plenum. These observations are consistent with those of Berndt and Sörensén (1976). (See also fig. 7(a).)

Slot-Flow Measurements

Flow-field measurements for the 15-1 wall were made on the slot centerplane normal to the wall for both tunnel-empty and zero-lift airfoil conditions. This wall was chosen because of the large slot-to-probe-width ratio that reduces the probe to wall interference. Because an automatic probe-traversing mechanism was available and because substantial time and effort would be required to make these measurements, only this wall configuration underwent detailed slot-flow measurements. Measurements were made in the slot at approximately 0.5 chord upstream of the airfoil leading edge for all wall configurations.

Although slot data were obtained for all openness ratios, the data may be suspect for the smallest values of openness for two reasons: first, as the slot-to-probe-width ratio becomes small, the possibility of large measurement errors due to blockage at the higher Mach numbers increases; second and more importantly, because the *vena contracta* of the flow occurs 0.3 to 0.5 slot widths into the plenum (fig. 12(a)), the probe (from the top tube to the bottom tube) spans an increasingly significant portion of the measurement region. For the 15-1 slot configuration, the *vena contracta* should occur around 0.45 in. into the plenum; for the 5-2 slot configuration, the *vena contracta* should occur around 0.08 in. into the plenum. If the flow separates at the slot-entry edge for walls that are 0.125 in. thick, the *vena contracta* will be in the plenum for the 15-1 slots, but it will be in the slot for the 5-2 slots. Because the flow angle and its gradient undergo large changes near the *vena contracta,* small errors in probe positioning are critical and much care is required to prevent error.

Flow-angle measurements. Flow-angle measurements from the 6 × 19 Tunnel are shown in figure 32 for free-stream Mach numbers of 0.3 and 0.7. These measurements were made at $x = -6$ in., which corresponds to a tunnel station 3 in. (0.5 chord) upstream of the airfoil leading edge. The flow angle θ, which is measured positive out of the tunnel, is plotted versus the normalized distance from the wall y/d, which is measured positive into the tunnel. The data show the flow angles to be somewhat insensitive to changes in the free-stream Mach number. For the zero-lift airfoil and tunnel-empty cases, the value of the flow angle in the slot is $\approx 7°$ and the maximum is $\approx 12°$. The airfoil only slightly increases the maximum angle achieved, which is not too different from the tunnel-empty case. Comparison of the total pressure ratios (fig. 33) indicates that the airfoil reduces the total head losses in the middle of the slot by forcing higher energy fluid through the slot. For the zero-lift airfoil case, the fuller total pressure ratio indicates a thinner shear layer. This effect is again obvious in figure 34 in which the local Mach numbers are higher for the airfoil case.

Flow angles measured in the slot of the different wall configurations are shown in figure 35 for $M_\infty = 0.7$. These measurements were again made at tunnel station $x = -6$ in. The generally decreasing angle with increasing wall openness and decreasing slot number is intuitively correct. Lower values of openness at constant slot number would have higher values of normal crossflow velocity for constant normal mass flux due to the reduced slot area. Likewise, a greater number of slots at constant openness ratio would decrease the crossflow area.

The increasing uncertainty in the measurements is evident for the smaller openness ratios, particularly for the 5-2 and 6-4 walls. Interestingly, the difference between the airfoil and tunnel-empty measurements for each openness ratio is very small across the range of openness ratios considered, which again is an indication of dominant tunnel-empty crossflow attributable to tunnel configuration and to the growth of the wall boundary layer.

Total pressure measurements. The ratio of the slot to free-stream total pressures for the different slotted walls is shown in figure 36 for $M_\infty = 0.4$ and 0.7. For the tunnel-empty case (fig. 36(a)), the higher Mach number increases the shear in the slot, which generally results in larger total head losses at the wall. For the airfoil case (fig. 36(b)), the increased Mach number has little impact on the total pressure losses in the slot. The airfoil decreases the slot losses upstream of the airfoil leading-edge station due to the reduction in the plenum pressure (thereby increasing the wall-pressure drop) over that for the corresponding tunnel-empty case. The larger wall-pressure drop forces more and higher energy mass flow through the slot.

Slot Viscous Effects

Viscous effects in slots manifest themselves by narrowing the effective slot and are traditionally handled by the use of an orifice (or discharge) coefficient ϵ. Outwardly directed flow passing through the slot will (for the present case) separate from the sharp edges of the slat and narrow until the minimum width is reached at the *vena contracta.* (See fig. 1(b).) The transverse velocity (or flow angle) will increase because of area reduction until the *vena contracta* is reached. It will then decrease to the zero-velocity (or flow-angle) condition of the plenum chamber. This effect is evident in the data presented in figures 12(a), 13(a), 14(a), and 32, which were obtained by traversing the probe on the centerline of the slot normal to the tunnel wall. An estimate of the value of ϵ for the sharp-edged slots of this study is obtained as follows. Crossflow continuity in the slot region can be written $(\rho v d)_s = (\rho v d)_{vc} = (\rho v)_{vc}(\epsilon d_s)$. Therefore,

$$\epsilon = \frac{(\rho v)_s}{(\rho v)_{vc}} \tag{10}$$

Precise mass-flux variations with Mach number were obtained as follows: the longitudinal and transverse mass-flux quantities were determined from the tunnel-empty flow-field measurements on the largest

openness ratio and, hence, most interference-free wall configurations. For the 15-1 configuration in which detailed measurements were made, these quantities were also determined at the *vena contracta* that is located at the maximum of the ρv curves shown in figure 37(a). Longitudinal mass flux ρU (fig. 37(b)) at this location was then computed.

The results for the 15-1 walls are plotted versus M_∞ in figure 38. A first-order least-squares fit of the data (solid lines in fig. 38) was then made. The results for the 15-1 slot are

$$(\rho U)_\infty = 2.644 M_\infty \text{ slug/ft} \tag{11a}$$

$$(\rho U)_s = 2.215 M_\infty \text{ slug/ft} \tag{11b}$$

$$(\rho U)_{vc} = 1.914 M_\infty \text{ slug/ft} \tag{11c}$$

$$(\rho v)_\infty = 0.263 M_\infty \text{ slug/ft} \tag{11d}$$

$$(\rho v)_s = 0.263 M_\infty \text{ slug/ft} \tag{11e}$$

$$(\rho v)_{vc} = 0.358 M_\infty \text{ slug/ft} \tag{11f}$$

Equations (10) and (11) result in

$$\epsilon = 0.74 \tag{12}$$

for the 15-1 wall, which is consistent with published values (Anon. 1978) of $\epsilon = 0.61$ to 0.90, depending on the sharpness (cross-sectional geometry) of the opening. That value is also consistent with empirical values that Sedin and Sörensén (1984) used to match theoretical computations with experimental measurements. Note for the present study that the shop fabrication instructions were to break the edges with a radius of 0.005 in., but the actual slot-entry radius is unknown. All the walls in this study are assumed to have "sharp" edges with $\epsilon = 0.74$.

The Mach number insensitivity of the flow angles in the slot and at the *vena contracta* is also clearly demonstrated in equations (11a–f). The angles are given by

$$\theta_s = \frac{v_s}{U_s} = \frac{(\rho v)_s}{(\rho U)_s} = 0.119 \text{ rad} = 6.80° \tag{13a}$$

and

$$\theta_{vc} = \frac{v_{vc}}{U_{vc}} = \frac{(\rho v)_{vc}}{(\rho U)_{vc}} = 0.187 \text{ rad} = 10.72° \tag{13b}$$

This Mach number insensitivity was just as obvious in the slot measurements made on other wall configurations used in the present study, in the previously presented Gardenier and Chew data (fig. 16), and in the Everhart, Igoe, and Flechner data (fig. 13(a)). Based on earlier discussions, the measurements for θ_s should be more representative of θ_{vc} for smaller slots due to considerations of probe-height-to-slot-depth ratio.

Slotted-Wall Pressure Drop

The pressure drop across the wall at the probe measurement station was determined by taking the average of the pressure coefficient obtained on rows 2 and 3 and subtracting the far-field measurement of the plenum pressure coefficient. The pressure drop was constant with the free-stream Mach number except for the very wide 15-1 wall where it decreased slightly at the higher Mach numbers. The average value of the pressure drop coefficient $\Delta C_{P,w}$ obtained for the 15-1 wall is

$$\Delta_{CP,w} = C_{P,w} - C_{P,p} = 0.0188 \tag{14}$$

The plenum flow angle for the 15-1 wall using equations (11a–f) is

$$\theta_p = \frac{\rho_{vc} v_{vc}}{\rho_\infty U_\infty} = 0.135 \text{ rad} \tag{15}$$

The plenum flow angle from equation (15) and $\Delta C_{P,w}$ from equation (14) have been plotted in figure 39 along with results from other 6 × 19 Tunnel measurements, from data acquired by Berndt and Sörensén (1976), and from results of the Everhart, Igoe, and Flechner (1991) experiment. Additionally, because the exact value of ϵ and the sensitivity of the measurements to variations in this parameter are unknown, two dashed curves representing modified versions of the Gardenier and Chew data (eq. (8)) are also presented. These two curves were obtained by using typical ϵ values of 0.74 and 0.64. A theoretically based estimate is obtained by neglecting the streamline curvature term in equation (5) and is shown as the solid line. The experiments agree well with the theoretically based estimate, which indicates a valid correlation for the assumption of no streamline curvature.

Boundary-Layer Growth

Flexible-wall experiment. An estimate of the velocity at the wall from the tunnel-empty boundary-layer growth can be obtained from the results of an earlier adaptive, solid, flexible-wall experiment (Everhart 1983) conducted in the 6 × 19 Tunnel. The boundary-layer growth in the 6 × 19 Tunnel grew as defined by $\delta^*/x = 0.0643 R_x^{-1/5}$ with a virtual origin of −48 in. At $M_\infty = 0.7$, the 6 × 19 Tunnel has a

unit Reynolds number of about 6.6×10^6 ft^{-1}. Thus, at the measurement station, the boundary layer has grown such that the effective normal velocity at the wall is given by

$$\frac{v_w}{U_\infty} = \frac{d\delta^*}{dx} = \frac{0.0514}{(2.3 \times 10^7)^{1/5}} = 0.0017 \qquad (16)$$

6 × 19 Tunnel slot experiment. By assuming that the boundary layer grows equally on all walls but recognizing the thickening in the slot region due to shear, we can use continuity to write

$$a\left(\frac{v_w}{U_\infty}\right) \approx d\epsilon\left(\frac{\rho_s v_s}{\rho_\infty U_\infty}\right) \qquad (17)$$

For the 15-1 tunnel-empty case, $a = 9.5 + 6 + 9.5$ in. $= 25$ in. and $d = 0.9$ in. From the tunnel-empty measurements (eqs. (11a–f)), $\rho_s v_s / \rho_\infty U_\infty = 0.099$. As was previously shown in equation (12), the orifice coefficient for these sharp-edged slots is $\epsilon = 0.74$. Substitution in equation (17) yields

$$\frac{v_w}{U_\infty} = \frac{d\delta^*}{dx} = \frac{(0.74)(0.9)(0.099)}{25} = 0.0026 \qquad (18)$$

The growth of the tunnel-empty boundary layer (for this case) produces about 65 percent of the outflow through the slots (compare eqs. (16) and (18)); the rest is produced by the geometry of the tunnel and plenum.

Some indication of the magnitude of the boundary-layer thickness can be obtained from an experiment conducted in the 6 × 19 Tunnel by Sewall (1982) to study the sidewall boundary-layer effects on transonic airfoil data. The following values of sidewall boundary-layer thickness at the model station were measured for $M_\infty = 0.50$, $\delta = 0.661$ and $\delta^* = 0.087$ in.; for $M_\infty = 0.94$, $\delta = 0.622$ and $\delta^* = 0.083$ in. If δ^* is assumed constant on each wall, the boundary layer is found to reduce the effective cross-sectional area of the tunnel by 3.8 percent at $M_\infty = 0.5$. To maintain a constant centerline Mach number distribution when the tunnel walls are parallel, the mass corresponding to this area deficit would have to be removed from the test section through the slots. A more rational and common approach is to adjust the wall divergence angle to accommodate this reduced area.

As a final indication of the viscous effects on the slot flow, the above values of the boundary-layer thickness yield $\delta/d \approx 0.71$, which is near the position where the local total pressure ratio asymptotes to 1 at $x = -6$ in. (0.5 chord upstream of the model leading-edge position). If the boundary-layer thickness is assumed to remain approximately constant with slot width changes, then the boundary-layer thickness will be about twice the slot width for the 5-percent-open wall.

Summary of Experiment

Detailed, experimental studies of the wall flow field of a longitudinally slotted transonic wind tunnel have been presented. Available data have been reevaluated and new data have been presented and analyzed. The present experiments, when combined with those of previous investigators, give a more complete (although not conclusive) physical characterization of the flow near and through the slotted wall of a transonic wind tunnel.

From the analysis of the different data sets, several groups of observations can be made as follows. The first observation concerns the influence of the wall geometry on the measurements. The data indicate that sufficient slot length should be both ahead of and behind the model for the flow in the slot to become fully developed. Otherwise, the influence of finite-length slots will become an important consideration. For "larger" numbers of slots when "sufficiently" far from the wall, the flow angles and pressures measured over the slot are very close to those measured over the slat. Thus, in the far field of the slot, a spanwise averaging of the longitudinal flow exists as would be predicted by slender-body theory and is known as a homogeneous-wall flow field. A comparison of the computed flow-angle gradients over the slot with those over the slat shows that nearly the same values were obtained. Therefore, tunnel sidewall measurements of the longitudinal pressure variation and its resulting gradients along and over the slotted wall should yield a sufficient representation of the average pressure level and gradients across the slotted wall.

For the range of conditions considered in this study, the effect of the airfoil on the wall pressures appears as a perturbation on the existing, well-established, tunnel-empty pressure distribution provided that the sidewall boundary layer is unseparated. When the global effect of lift is present, the "reference" level of the downstream wall-pressure distribution changes almost as a zero shift with changes in airfoil angle of attack. Aside from this global effect, the model had only a small effect on the wall pressure ahead of approximately 1 chord upstream of the leading edge, which indicates a combined localized and global effect of the model on the slot flow.

The slot-flow characteristics are affected by the airfoil in two major ways. First, a global interaction of the airfoil, tunnel, and plenum extends over the entire length of the slotted wall that establishes the far-field flow development in the slot and in the tunnel and that decreases the plenum pressure compared with the corresponding tunnel-empty plenum pressure for matched free-stream Mach numbers. This interaction determines the first-order mass flux through the wall and also the undisturbed, far-field pressure drop across the wall. The interaction is diminished with increasing openness ratio, which indicates a more open-jet performance as would be expected. The small, almost constant airfoil-induced, adverse pressure gradient in the upstream portion of the tunnel thickens the wall boundary layer and in turn increases the mass flux through the wall in the regions where streamline curvature is negligible. When the global effect upstream of about 0.5 chord ahead of the leading edge of the airfoil and downstream of the slot development region is accounted for, the flow angle in the slot appears to be nearly independent of the model and is almost completely dominated by the growth of the boundary layer and other tunnel geometry effects. As a result, the flow-angle gradients upstream in the slot may have different characteristics from those inside the tunnel; those differences are caused by model-induced changes in the streamline curvature. (For instance, the far-field streamwise flow-angle gradient may have a different sign inside the slot from that inside the tunnel away from the slot.) The other interaction is a local phenomenon in the near region approximately 0.5 chord both upstream and downstream of the model. In this region, the flow is driven by the inviscid pressure imposed on the wall by the airfoil and is highly dependent on the strong variations in streamline curvature. The limits of this flow region are determined by the onset of large changes in the wall flow-angle gradients.

Measurements of the pressures in the slot region indicate that the local variation on the back (or plenum) side of the slat is not significantly different from that measured in the far field of the plenum. The larger the number of slots, the closer is the correlation between those measurements made on the back of the slat and those made in the far field of the surrounding plenum.

Viscous effects on the slot flow field were significant. Measurements of the total pressure of the flow entering the slot show it to be near the free-stream total pressure, particularly with the airfoil installed. A large drop in the slot total pressure occurs while the fluid passes through the slot, which is indicative of strong viscous shearing. Large experimental values of the tunnel-empty slot-flow angle were measured ($\approx 7^\circ$ outflow in the 6 $\times$ 19 Tunnel studies), and about 65 percent of this can be attributed to the growth of the tunnel-wall boundary layers. These large angles violate the assumption that the square of the crossflow-velocity component is negligible as prescribed in the first-order, classic ideal-slot theory. For the present 6 $\times$ 19 Tunnel studies, the slot width was reduced by 26 percent because of separation from the sharp entry edge of the slot lip. A reduction in the geometric slot width by 26 percent allowed the tunnel-empty wall pressure drop (i.e., that measured in the absence of free-stream curvature) to be correlated with the square of the slot-flow angle in accordance with higher order slotted-wall theory and leads to the conclusion that the effective slot is located at the *vena contracta*. Available data for slots with sharp entry edges indicate that the *vena contracta* occurs about 0.4 slot widths into the plenum for outflow conditions. Tunnel-empty *vena contracta* flow angles in the 6 $\times$ 19 Tunnel experiment were approximately 12°. The location of the *vena contracta* with and without the airfoil appears almost fixed, which indicates only a small deviation of the interface between the tunnel and plenum flows from the plane of the slotted wall. A lack of information regarding inflow to the tunnel does not allow similar definitive conclusions regarding the inflow *vena contracta*; however, for mild inflow (based on results presented by Goethert (1957)), valid assumptions can be made that the effective slot will be at the *vena contracta* and that the *vena contracta* will occur within the slot.

Finally, flow angles measured in the slot were found to be insensitive to variations in Mach number, which agrees with previously published AEDC results. Slotted-wall flow-field measurements acquired with a model installed reveal anomalies that can presently be explained only by the presence of a vortex originating at the slot-entry edge of the slat near the point of zero-slot flow angle near the maximum airfoil model thickness. Conclusive statements will require further experiments.

Concluding Remarks

An experiment has been conducted on the near-wall flow field of a longitudinally slotted transonic wind tunnel and the results are presented in this paper. This study is a precursor to a theoretical effort designed to improve the slotted-wall boundary condition and is designed to provide an appropriate database to evaluate the resulting coefficients in the boundary condition for a range of slotted-wall

geometries, wind tunnel test conditions, and test model attitudes. This study has been divided into two major parts—a survey of previous experiments and a reexamination of the published data; and the presentation of a new experiment, some of the resulting data, and the major findings. The present experiment, when combined with those of previous investigators, yields a more complete (although not conclusive) physical characterization of the flow in, around, and through the slotted wall of a transonic wind tunnel. Additionally, the concise compilation of the experiments and the results presented herein highlight deficiencies in the current database and indicate the need for new experiments.

NASA Langley Research Center
Hampton, VA 23681-0001
December 18, 1993

References

Anon. 1978: *Marks' Standard Handbook for Mechanical Engineers.* Eighth Ed., McGraw-Hill, Inc.

Allen, H. Julian; and Vincenti, Walter G. 1944: *Wall Interference in a Two-Dimensional-Flow Wind Tunnel, With Consideration of the Effect of Compressibility.* NACA Report 782. (Supersedes NACA WR A-63.)

Baldwin, Barrett S., Jr.; Turner, John B.; and Knechtel, Earl D. 1954: *Wall Interference in Wind Tunnels With Slotted and Porous Boundaries at Subsonic Speeds.* NACA TN 3176.

Barnwell, Richard W. 1976: Improvements in the Slotted-Wall Boundary Condition. *Proceedings—AIAA 9th Aerodynamic Testing Conference,* pp. 21–30.

Baronti, P.; Ferri, A.; and Weeks, T. 1973: *Analysis of Wall Modification in a Transonic Wind Tunnel.* AFOSR-TR-733-1900, U.S. Air Force. (Available from DTIC as AD 767 629.)

Berndt, Sune B. 1982: *Measuring the Flow Properties of Slotted Test-Section Walls.* FAA Rep. 135, Aeronautical Research Inst. of Sweden.

Berndt, Sune B.; and Sörensén, Hans 1976: Flow Properties of Slotted Walls for Transonic Test Sections. *Windtunnel Design and Testing Techniques,* AGARD-CP-174, pp. 17-1–17-10.

Bhat, Maharaj Krishen 1988: On Transonic Flow Over Segmented Slotted Wind Tunnel Wall With Mass Transfer. Ph.D Diss., Univ. of Tennessee.

Chen, C. F.; and Mears, J. W. 1957: *Experimental and Theoretical Study of Mean Boundary Conditions at Perforated and Longitudinally Slotted Wind Tunnel Walls.* AEDC-TR-57-20, U.S. Air Force. (Available from DTIC as AD 144 320.)

Davis, Don D., Jr.; and Moore, Dewey 1953: *Analytical Study of Blockage- and Lift-Interference Corrections for Slotted Tunnels Obtained by the Substitution of an Equivalent Homogeneous Boundary for the Discrete Slots.* NACA RM L53E07b.

Everhart, Joel L. 1983: *A Method for Modifying Two-Dimensional Adaptive Wind-Tunnel Walls Including Analytical and Experimental Verification.* NASA TP-2081.

Everhart, Joel L. 1987: Theoretical and Experimental Analysis of the Slotted-Wall Flow Field in a Transonic Wind Tunnel. SAE Tech. Paper Ser. 871757.

Everhart, Joel Lee 1988: Theoretical and Experimental Studies of the Transonic Flow Field and Associated Boundary Conditions Near a Longitudinally-Slotted Wind-Tunnel Wall. D.Sci. Diss., George Washington Univ. (Available as NASA TM-103381.)

Everhart, Joel L.; Igoe, William B.; and Flechner, Stuart G. 1991: *Slotted-Wall Flow-Field Measurements in a Transonic Wind Tunnel.* NASA TM-4280.

Garner, H. C.; Rogers, E. W. E.; Acum, W. E. A.; and Maskell, E. C. 1966: *Subsonic Wind Tunnel Wall Corrections.* AGARD-AG-109.

Gentry, Garl L., Jr.; Igoe, William B.; and Fuller, Dennis E. 1981: *Description of 0.186-Scale Model of High-Speed Duct of National Transonic Facility.* NASA TM-81949.

Glauert, H. 1947: *The Elements of Aerofoil and Airscrew Theory.* 2nd ed., Cambridge University Press.

Goethert, Bernhard H. 1957: *Properties of Test Section Walls With Longitudinal Slots in Curved Flow for Subsonic and Supersonic Velocities (Theoretical Investigations).* AEDC-TN-55-56, U.S. Air Force. (Available from DTIC as AD 131 406.)

Goethert, Bernhard H. 1961: *Transonic Wind Tunnel Testing.* AGARDograph No. 49, Pergamon Press.

Hansen, James R. 1987: *Engineer in Charge—A History of the Langley Aeronautical Laboratory, 1917–1958.* NASA SP-4305.

Kemp, William B., Jr. 1986: *Computer Simulation of a Wind Tunnel Test Section With Discrete Finite-Length Wall Slots.* NASA CR-3948.

Ladson, Charles L. 1973: *Description and Calibration of the Langley 6- by 19-Inch Transonic Tunnel.* NASA TN D-7182.

Pankhurst, R. C.; and Holder, D. W. 1965: *Wind-Tunnel Technique.* Sir Isaac Pitman & Sons Ltd. (London).

Pindzola, M.; and Lo, C. F. 1969: *Boundary Interference at Subsonic Speeds in Wind Tunnels With Ventilated Walls.* AEDC-TR-69-47, U.S. Air Force. (Available from DTIC as AD 687 440.)

Pope, Alan; and Harper, John J. 1966: *Low-Speed Wind Tunnel Testing.* John Wiley & Sons, Inc.

Sedin, Y. C.-J.; and Sörensén, H. 1984: Computed and Measured Wall Interference in a Slotted Transonic Test Section. AIAA-84-0243.

Sewall, William Grier 1982: Application of a Transonic Similarity Rule To Correct the Effects of Sidewall Boundary Layers in Two-Dimensional Transonic Wind Tunnels. M.S. Thesis, George Washington Univ. (Available as NASA TM-84847.)

Sinclair, Archibald R.; and Robins, A. Warner 1952: *A Method for the Determination of the Time Lag in Pressure Measuring Systems Incorporating Capillaries.* NACA TN2793.

Theodorsen, Theodore 1931: *The Theory of Wind-Tunnel Wall Interference.* NACA Rep. 4100.

Wood, W. W. 1964: Tunnel Interference From Slotted Walls. *Australia Q. J. Mech. & Applied Math.,* vol. 17, pp. 125–140.

Wright, Ray H.; and Ward, Vernon G. 1955: *NACA Transonic Wind-Tunnel Test Sections*. NACA Rep. 1231. (Supersedes NACA RM L8J06.)

Wu, J. M.; Collins, F. G.; and Bhat, M. K. 1983: Three-Dimensional Flow Studies on a Slotted Transonic Wind Tunnel Wall. *AIAA J.,* vol. 21, no. 7, pp. 999–1005.

Table I. NACA 0012 Airfoil Orifice Ordinates

Lower surface			Upper surface		
Orifice	x, in.	y, in.	Orifice	x, in.	y, in.
801	0	−0.0002	825	0.0733	0.1110
802	.0719	−.1127	826	.1533	.1582
803	.1490	−.1584	827	.2958	.2121
804	.2980	−.2149	828	.4535	.2529
805	.4514	−.2539	829	.6085	.2835
806	.6022	−.2829	830	.9008	.3222
807	.9048	−.3226	831	1.1971	.3445
808	1.2018	−.3450	832	1.4959	.3562
809	1.5000	−.3568	833	1.7961	.3598
810	1.7992	−.3602	834	2.0980	.3577
811	2.0981	−.3579	835	2.3693	.3498
812	2.3969	−.3495	836	2.6967	.3364
813	2.6983	−.3361	837	2.9965	.3191
814	2.9949	−.3190	838	3.2963	.2985
815	3.2939	−.2984	839	3.5946	.2754
816	3.5932	−.2745	840	3.8925	.2500
817	3.8928	−.2476	841	4.1951	.2215
818	4.1919	−.2188	842	4.4934	.1911
819	4.4939	−.1879	843	4.7940	.1586
820	4.7924	−.1560	844	5.0937	.1247
821	5.0893	−.1231	845	5.3911	.0896
822	5.3899	−.0884	846	5.6880	.0527
823	5.6881	−.0501	847	5.8332	.0330
824	5.8428	−.0293			

Table II. Slot and Slat Orifices

Side orifice	x, in.	y, in.	Top orifice	x, in.	y, in.	Bottom orifice	x, in.	y, in.
001	−16.0	9.5	016	−16.0	9.437	031	−16.0	9.563
002	−13.0	↓	017	−13.0	↓	032	−13.0	↓
003	−10.0		018	−10.0		033	−10.0	
004	−8.0		019	−8.0		034	−8.0	
005	−6.0		020	−6.0		035	−6.0	
006	−4.5		021	−4.5		036	−4.5	
007	−3.0		022	−3.0		037	−3.0	
008	−1.5		023	−1.5		038	−1.5	
009	0		024	0		039	0	
010	1.5		025	1.5		040	1.5	
011	3.0		026	3.0		041	3.0	
012	5.0		027	5.0		042	5.0	
013	7.5		028	7.5		043	7.5	
014	10.5		029	10.5		044	10.5	
015	14.0	↓	030	14.0	↓	045	14.0	↓

Table III. Sidewall Orifices

Row 1 orifice	x, in.	y, in.	Row 2 orifice	x, in.	y, in.	Row 3 orifice	x, in.	y, in.
101	−22.002	8.482	201	−22.020	7.955	301	−22.019	7.454
102	−18.996	8.475	202	−19.020	7.955	302	−19.017	7.460
103	−16.002	8.500	203	−16.018	7.967	303	−16.017	7.464
104	−13.012	8.489	204	−13.017	7.972	304	−13.016	7.474
105	−9.998	8.498	205	−10.017	7.980	305	−10.013	7.479
106	−7.999	8.497	206	−8.018	7.984	306	−8.016	7.485
107	−6.007	8.493	207	−6.007	7.994	307	−6.006	7.493
108	−5.007	8.493	208	−5.007	7.994	308	−5.006	7.494
109	−4.007	8.493	209	−4.007	7.995	309	−4.006	7.496
110	−3.007	8.494	210	−3.006	7.995	310	−3.006	7.497
111	−2.007	8.494	211	−2.007	7.997	311	−2.006	7.497
112	−1.005	8.495	212	−1.006	7.997	312	−1.006	7.497
113	−.006	8.496	213	−.006	7.997	313	−.008	7.491
114	.994	8.497	214	.992	7.997	314	.994	7.500
115	1.995	8.497	215	1.995	7.999	315	1.995	7.500
116	2.993	8.498	216	2.994	7.999	316	2.995	7.501
117	4.995	8.501	217	4.995	8.000	317	4.995	7.501
118	6.995	8.502	218	6.996	8.002	318	6.995	7.501
119	8.993	8.502	219	8.995	8.004	319	8.997	7.504
120	10.985	8.508	220	11.001	8.009	320	10.987	7.505
121	12.987	8.513	221	12.974	8.005	321	12.996	7.503

Table IV. Wind Tunnel Wall Mach Number Calibration Coefficients

[See equation (9)]

Wall	A_{ls}	B_{ls}	C_{ls}
15-1	0.000688	0.970948	0.076716
15-2	.000997	.965892	.090900
7.5-1	.000398	.975668	.078477
Solid	.000208	.989451	.079178
15-4	.000650	.976335	.060428
7.5-2	.000427	.992203	.033086
3.75-1	.000090	1.006190	.011167
10-4	.000531	.983785	.047933
5-2	.000604	.990582	.053354
6-4	.000789	.987352	.056231
3-2	.000299	1.008190	.030300
10-2	.000692	.976066	.069774

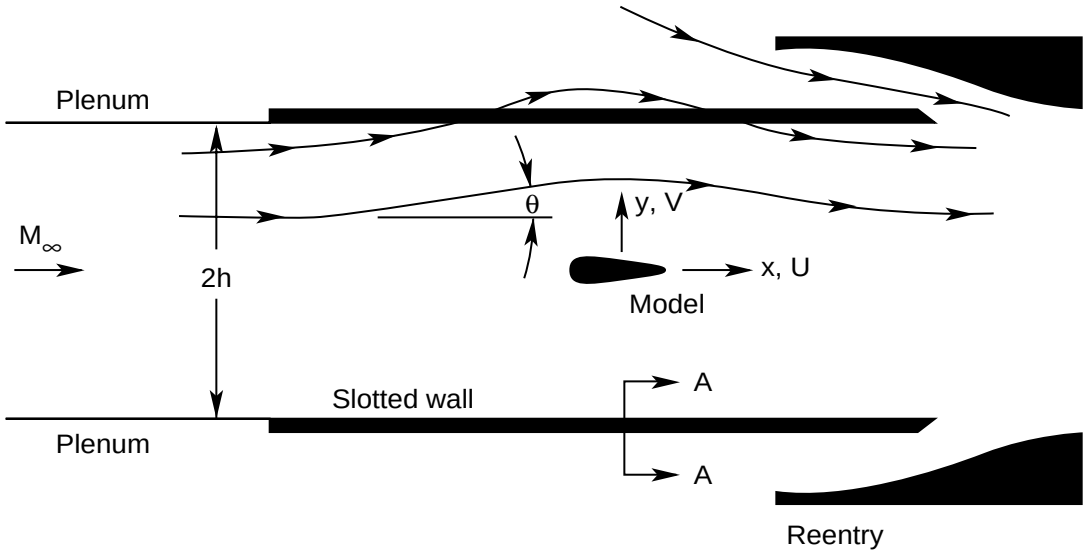

(a) Tunnel cross section.

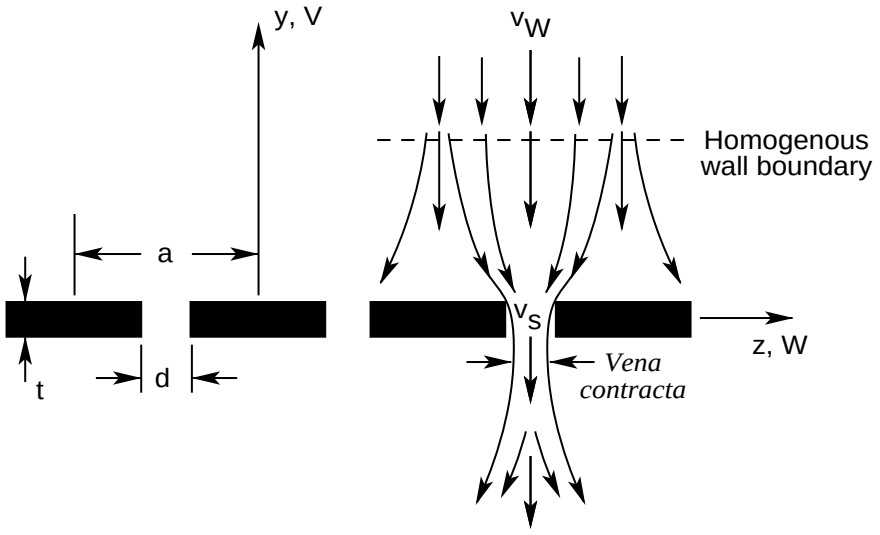

(b) Section A-A.

Figure 1. Typical slotted-wall wind tunnel.

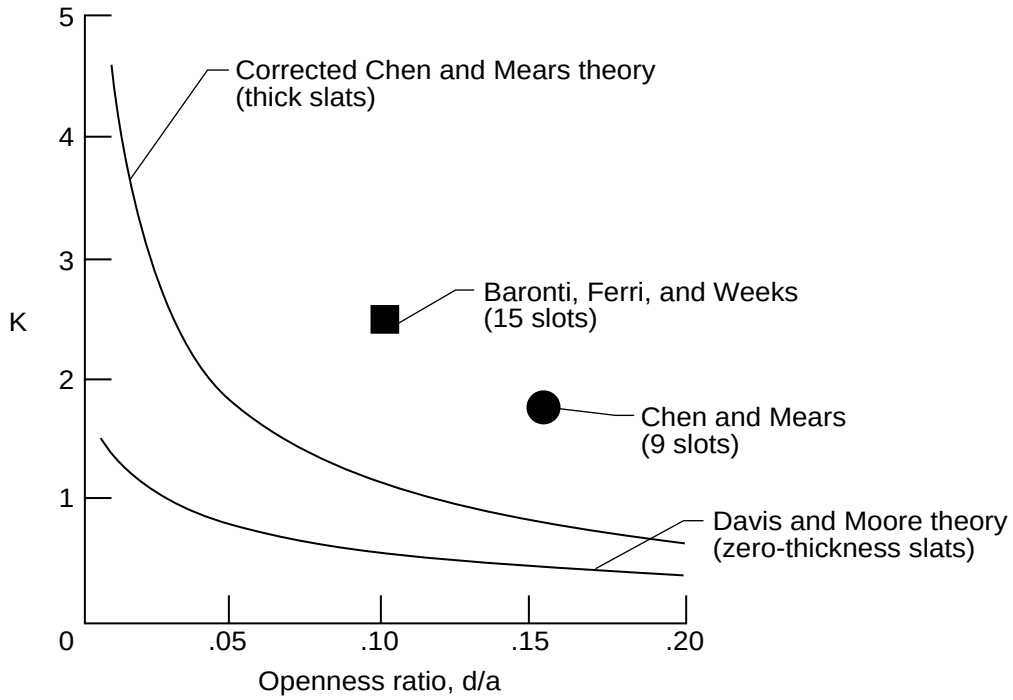

Figure 2. Published values of K.

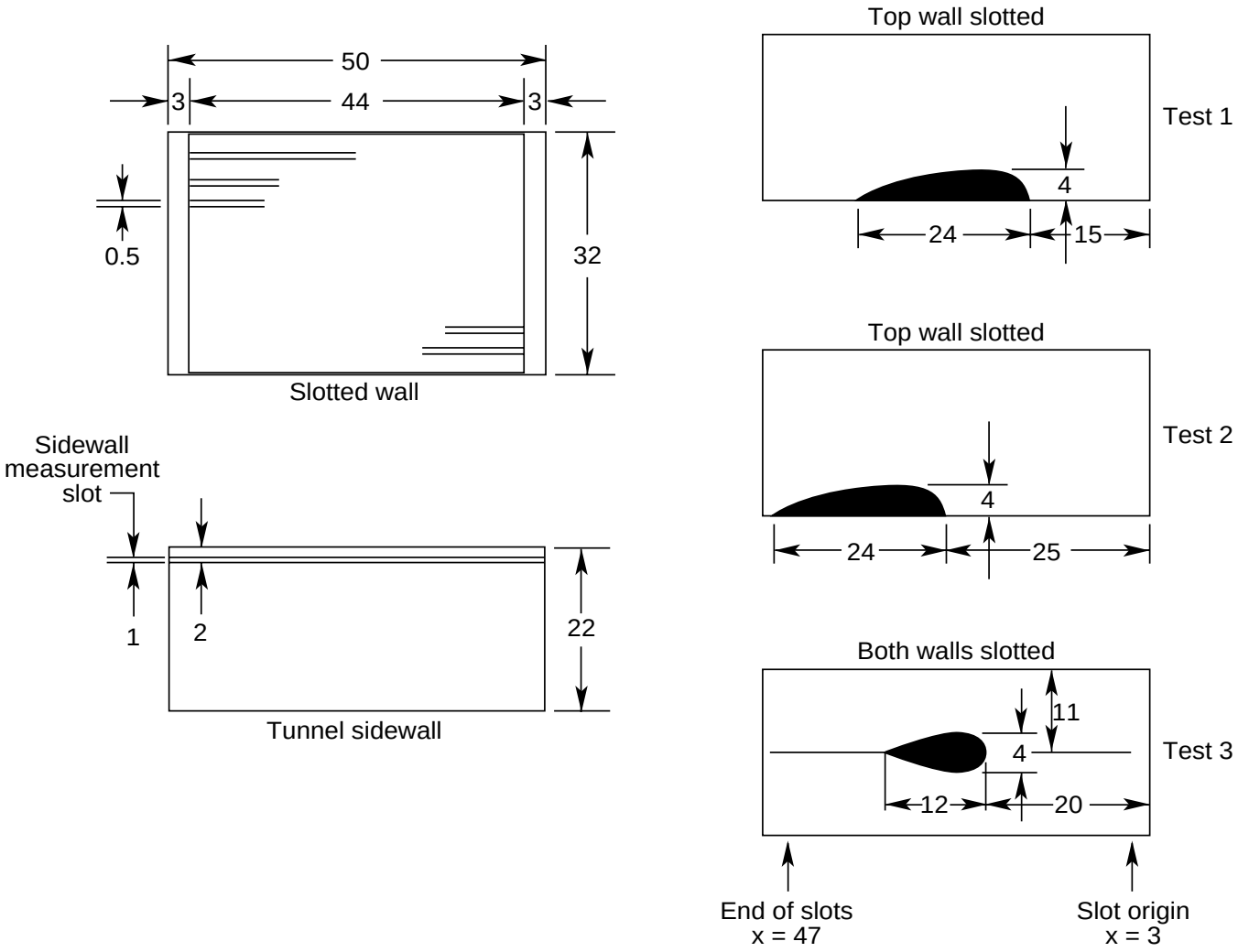

Figure 3. Chen and Mears experiment (1957). All dimensions are in inches.

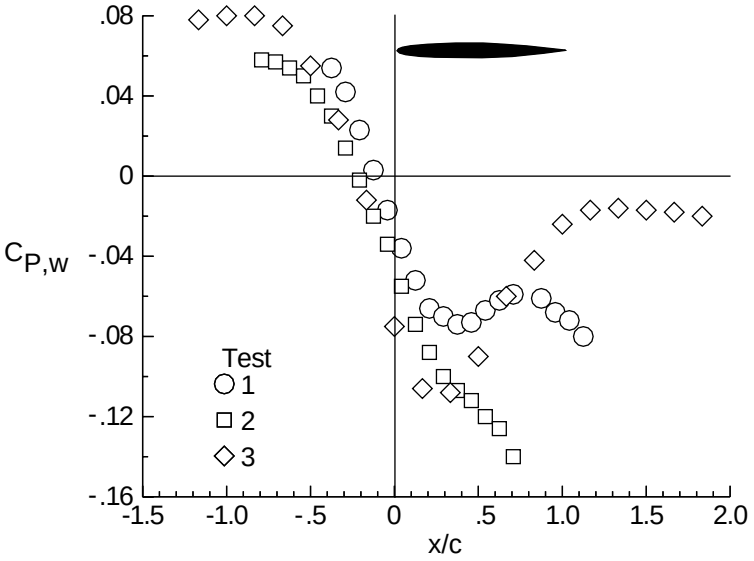

(a) Measured wall-pressure coefficient over slot.

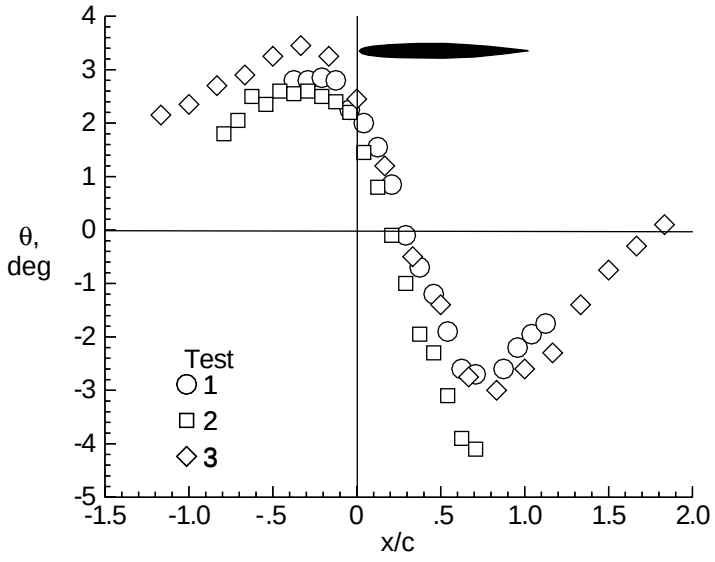

(b) Measured flow angle over slot.

Figure 4. Chen and Mears (1957) over slot data for all tests.

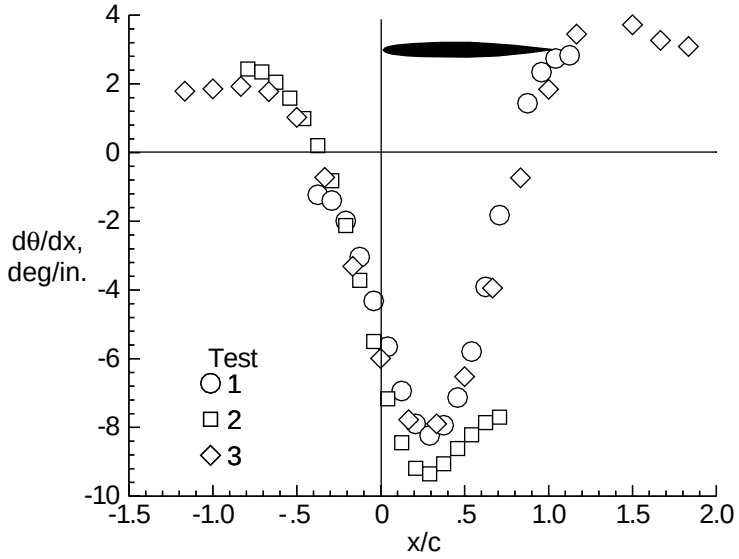

(c) Computed flow-angle gradient over slot.

Figure 4. Concluded.

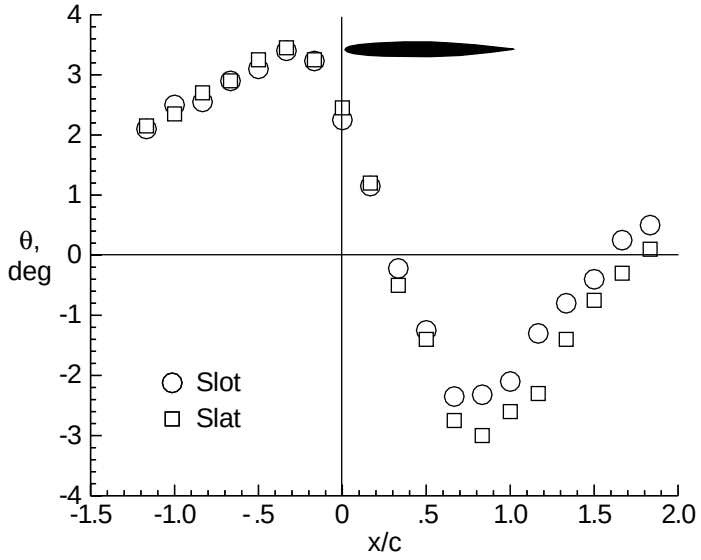

(a) Measured flow angles.

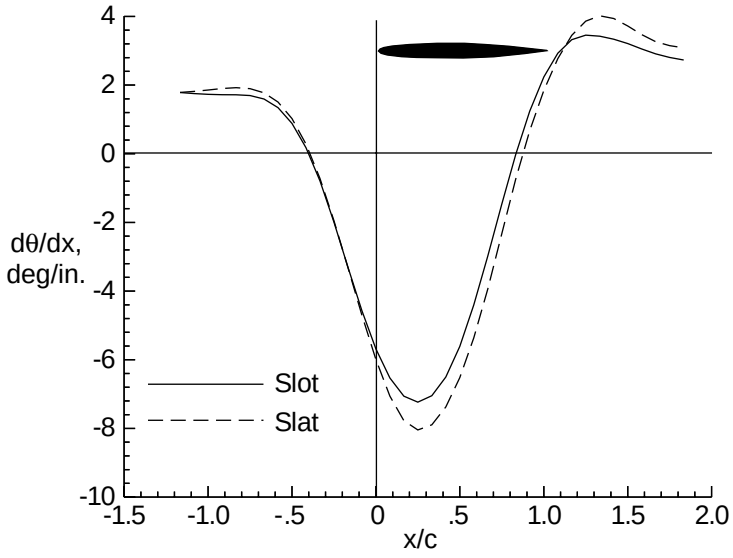

(b) Computed flow-angle gradient.

Figure 5. Chen and Mears (1957) test 3 data over slot and slat.

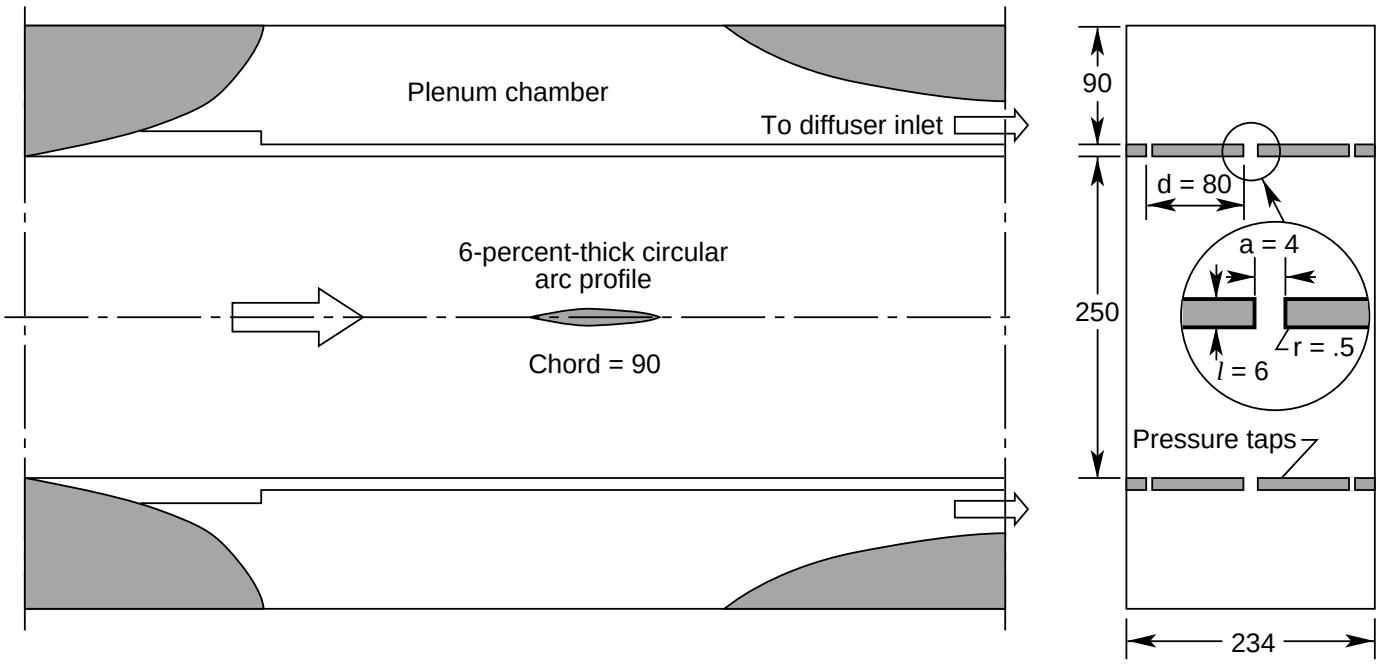

Figure 6. Berndt and Sörensén (1976). All linear dimensions are in millimeters.

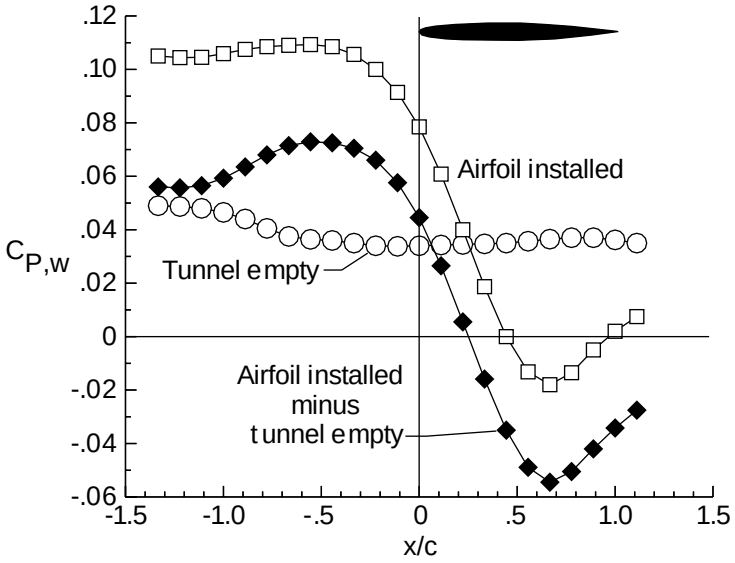

(a) Wall-pressure coefficient.

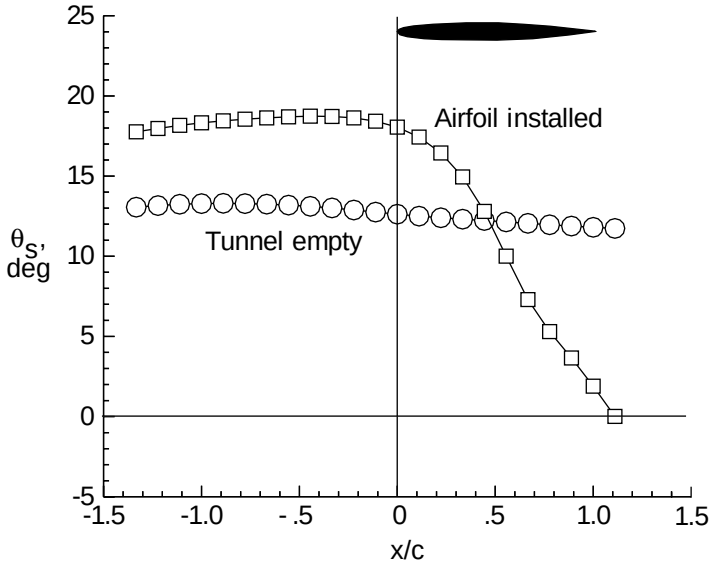

(b) Slot-flow angle.

Figure 7. Berndt and Sörensén data (1976).

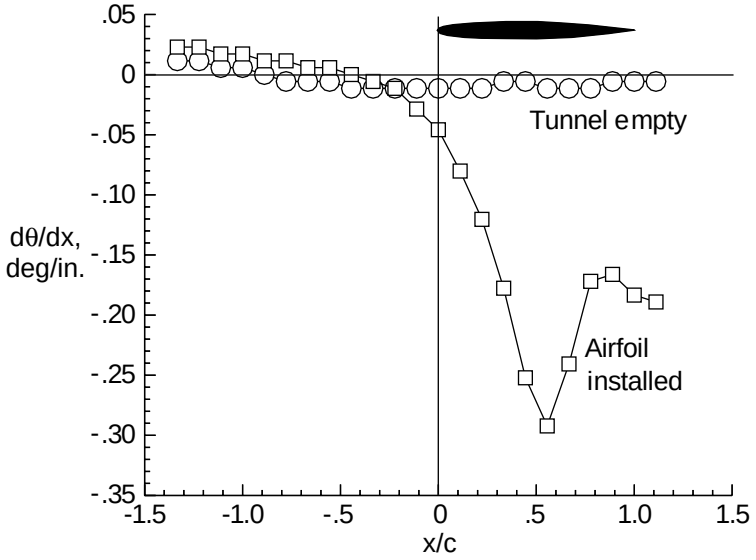

(c) Computed slot-flow angle gradient.

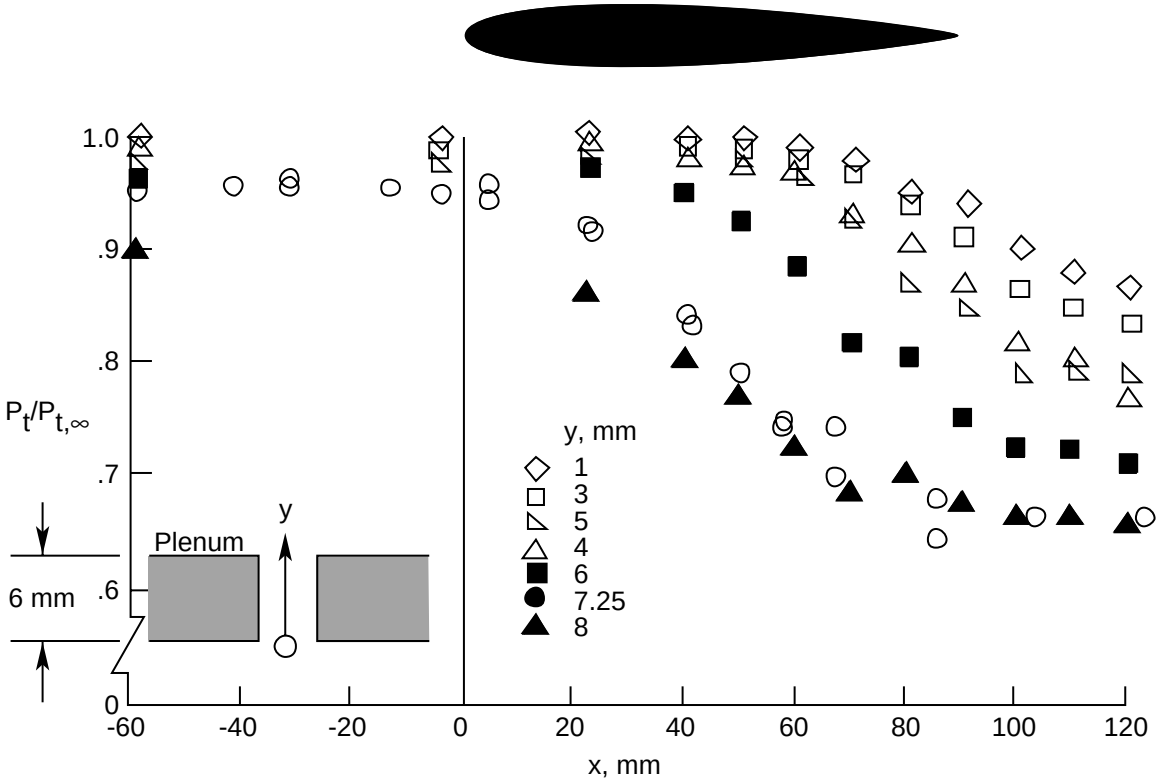

(d) Measured total-pressure distribution in slot.

Figure 7. Concluded.

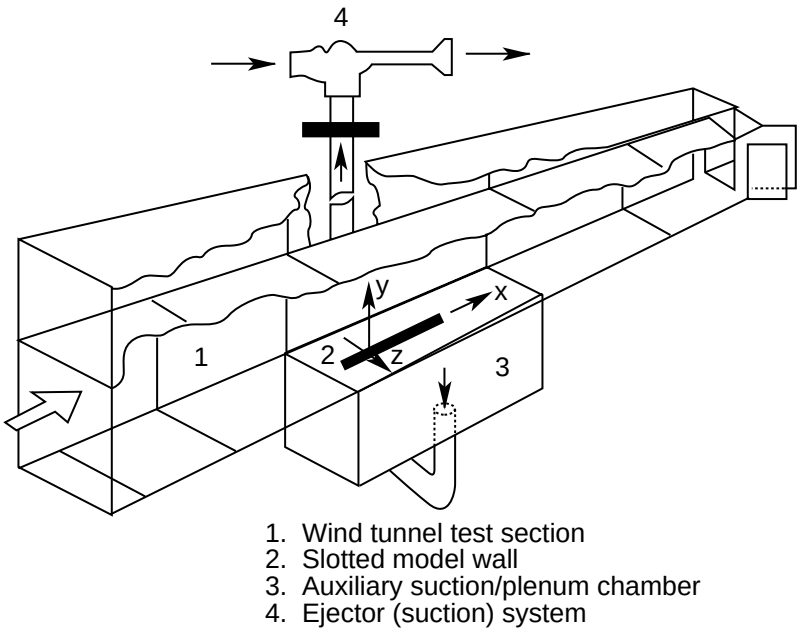

(a) Schematic of model mounting on tunnel floor.

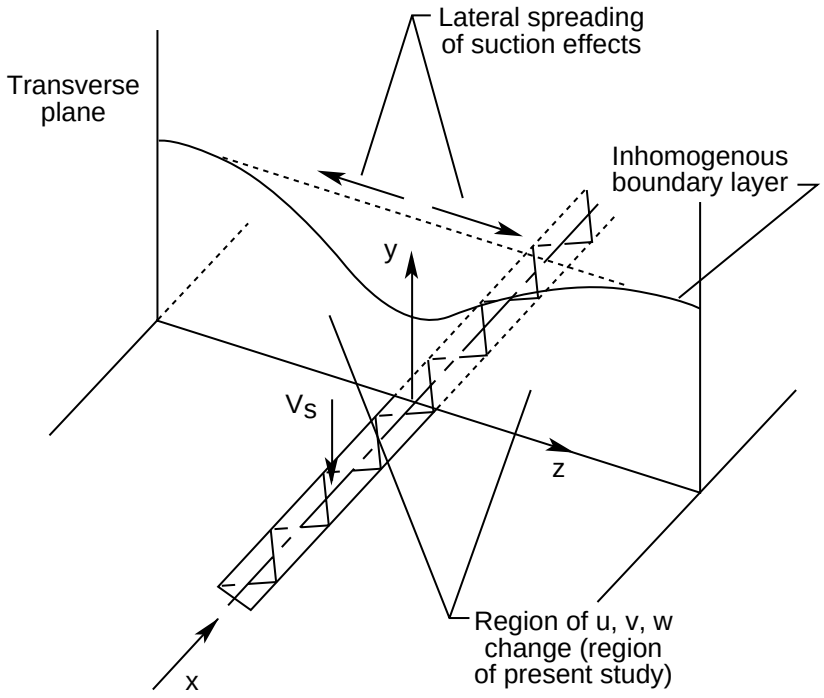

(b) Schematic of wall flow and measurement plane.

Figure 8. Wu, Collins, and Bhat (1983) experiment.

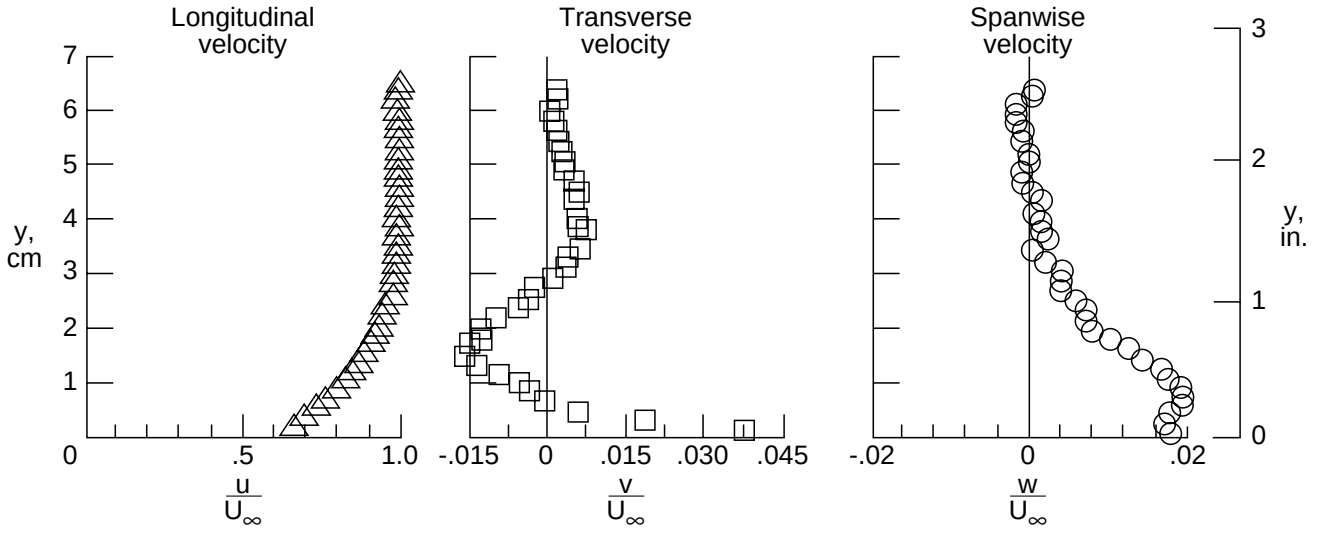

Figure 9. Velocity component distribution on single slotted-wall model. $M_\infty = 0.81$; $R = 8.14 \times 10^6$; $Q = 0.047$ ft^3/min; $z = 0.5$ in. (taken from Wu, Collins, and Bhat (1983)).

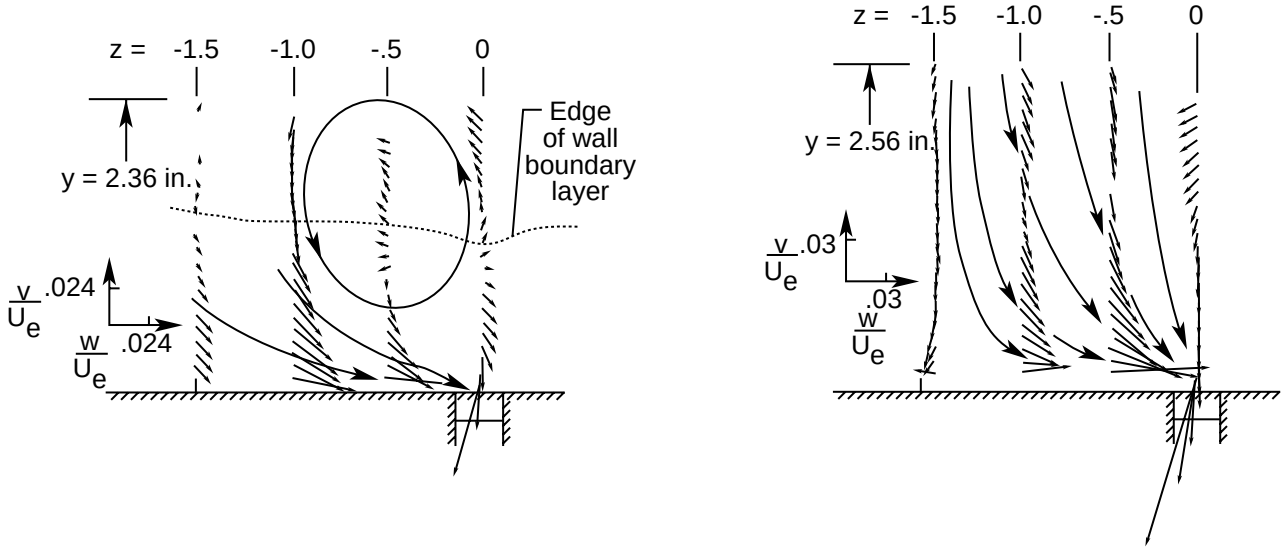

(a) $R = 7.32 \times 10^6$; $Q = 0$.

(b) $R = 5.43 \times 10^6$; $Q = 0.20$ ft^3/min.

Figure 10. Velocity vectors projected on crossflow plane and schematic of streamline patterns at $M_\infty = 0.6$ (Wu, Collins, and Bhat (1983)). All linear dimensions are in inches.

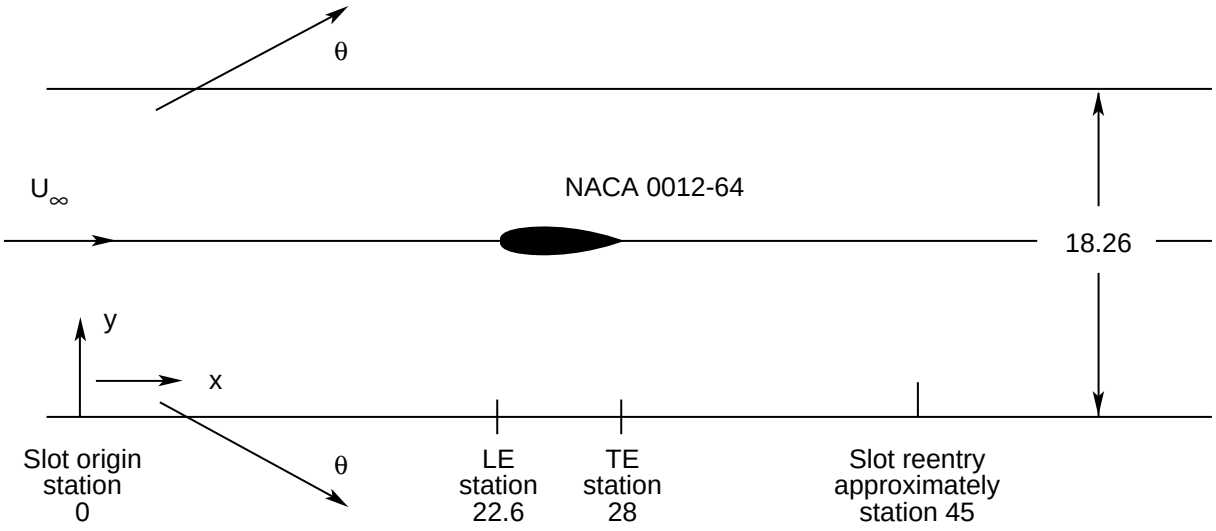

(a) Test cross section.

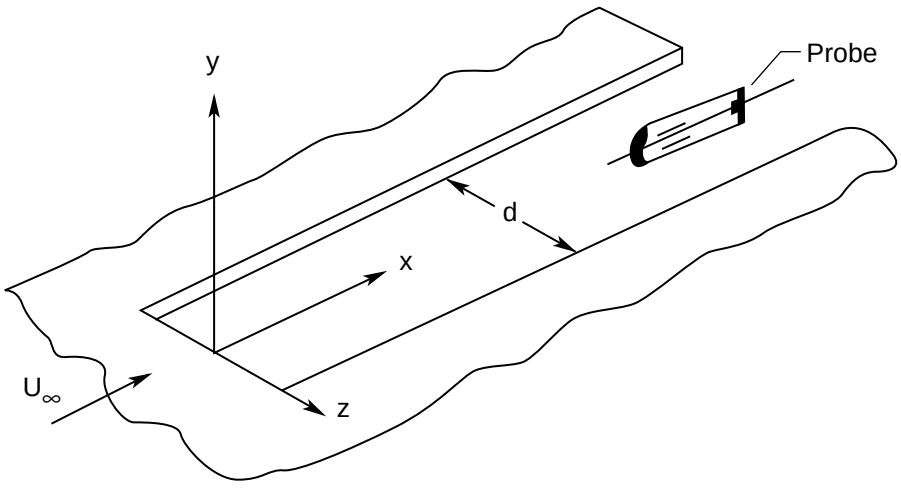

(b) Slot coordinate system.

Figure 11. Everhart, Igoe, and Flechner (1991) experiment. All linear dimensions are in inches.

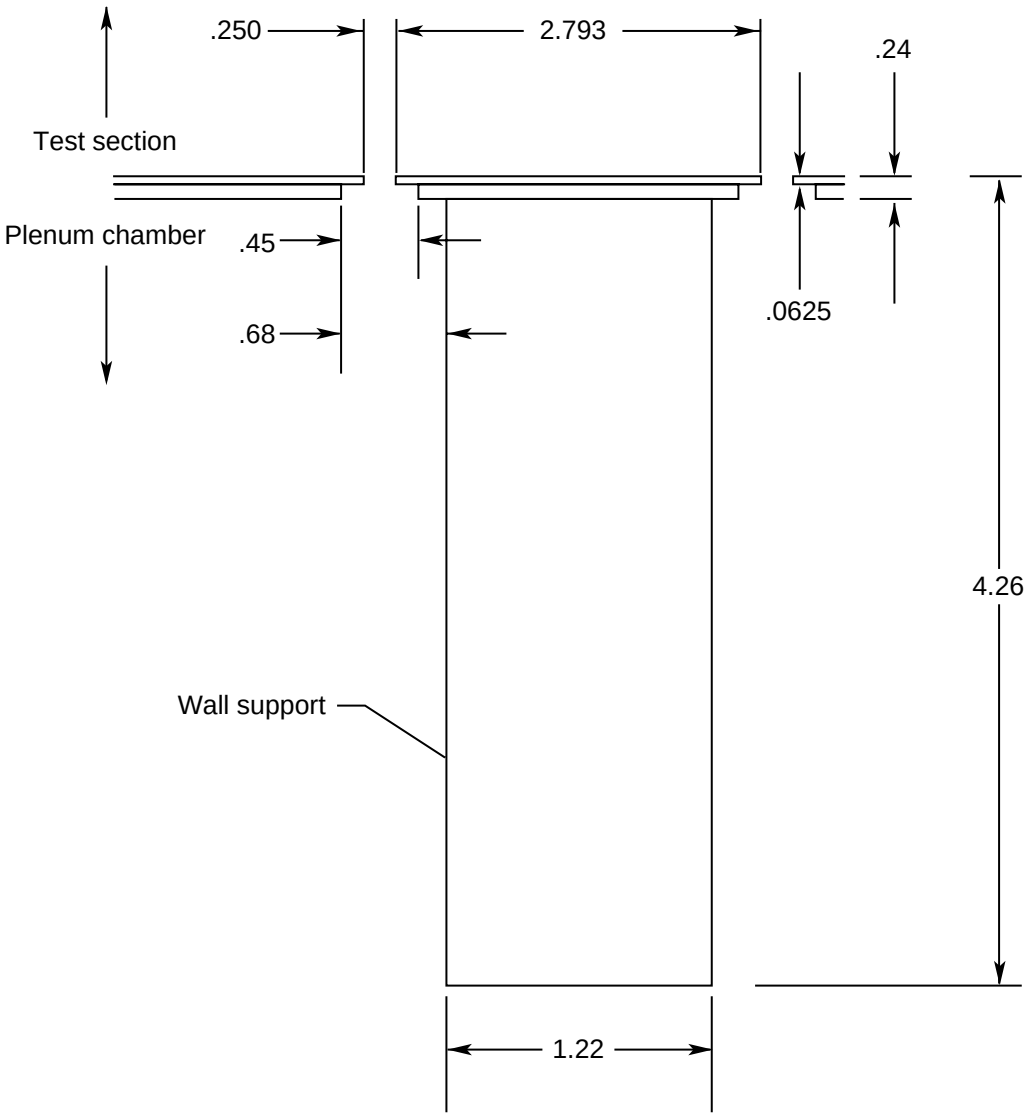

(c) Wall cross section.

Figure 11. Concluded.

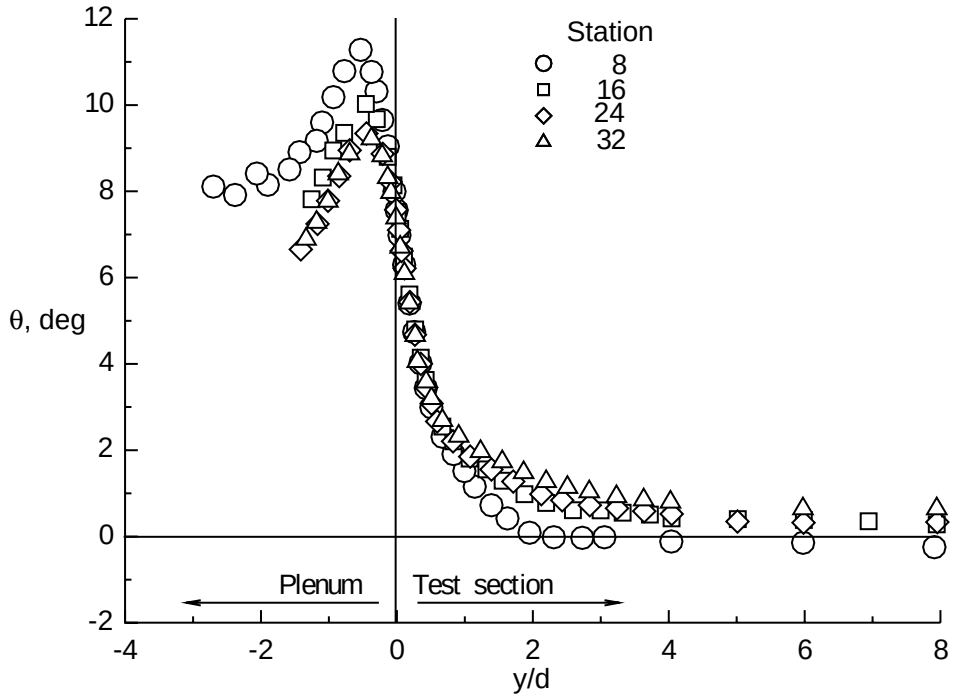

(a) Flow angle.

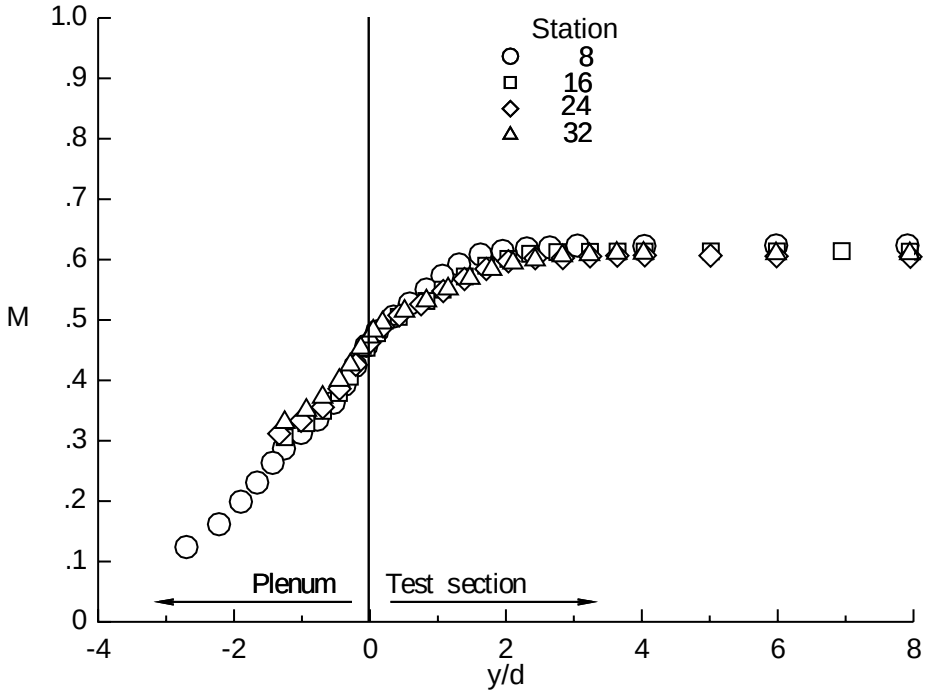

(b) Mach number.

Figure 12. Variation of DFA-probe measurements with tunnel station. $M_\infty = 0.6$.

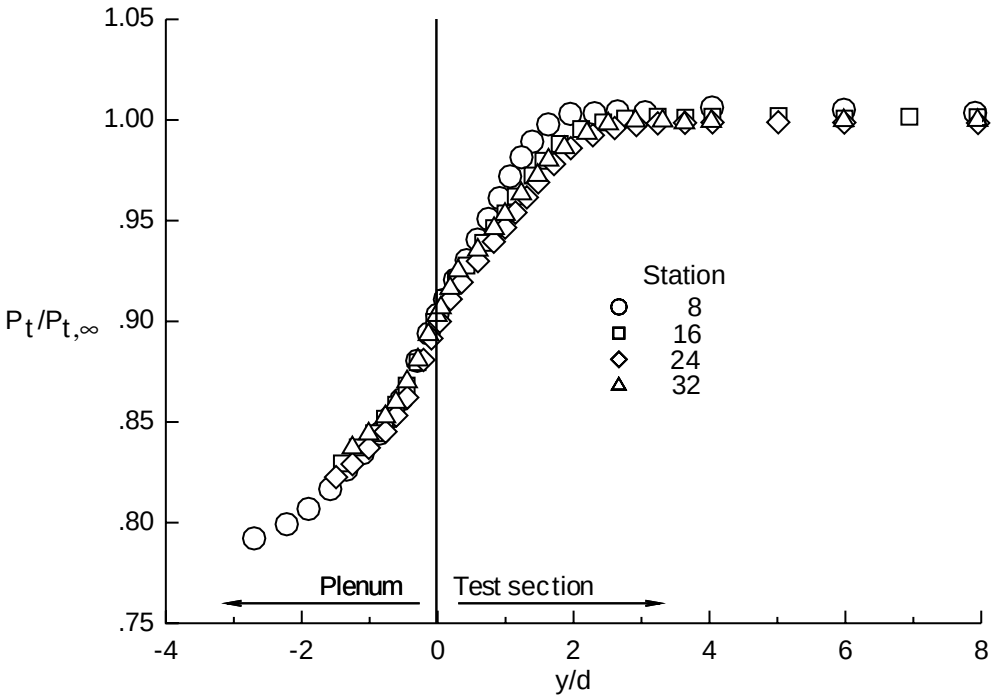

(c) Total pressure ratio.

Figure 12. Concluded.

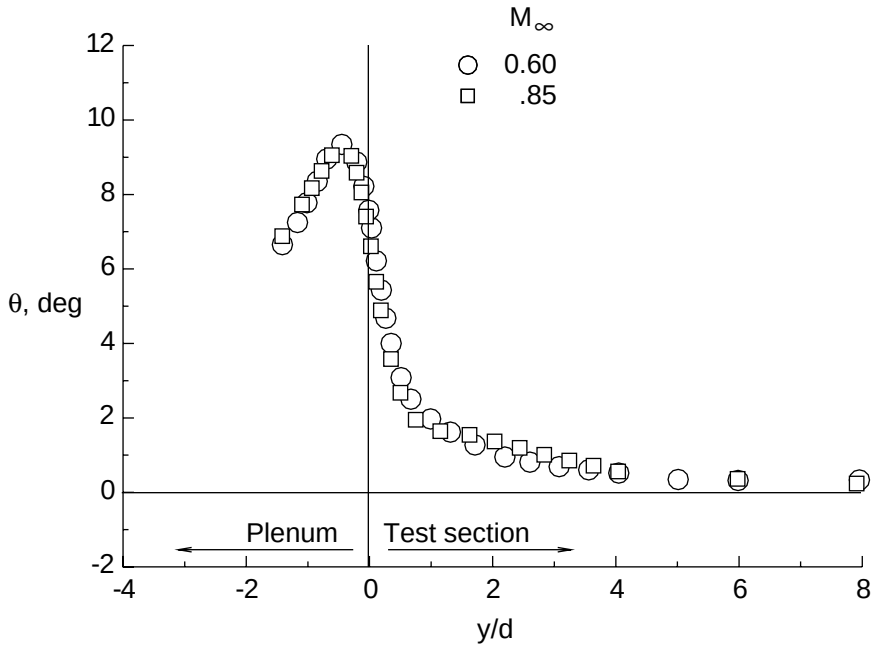

(a) Flow angle.

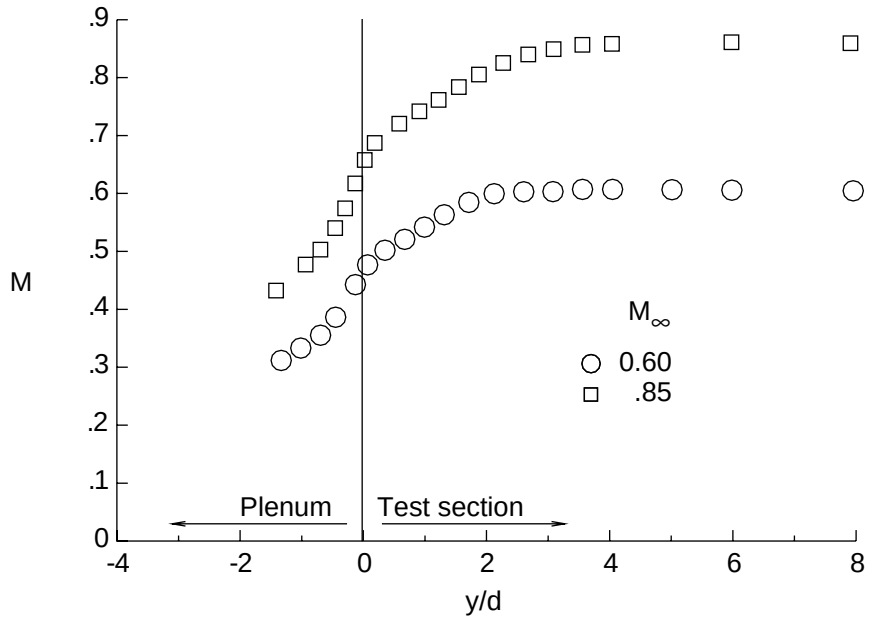

(b) Mach number.

Figure 13. Effect of tunnel-empty free-stream Mach number on local slot-flow properties measured in DFA at tunnel station 24 in.

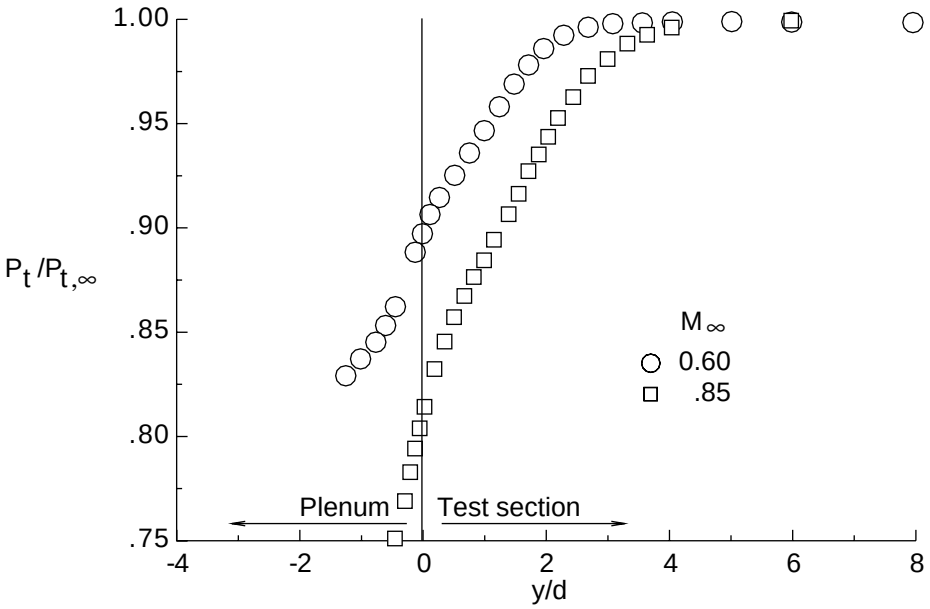

(c) Total pressure ratio.

Figure 13. Concluded.

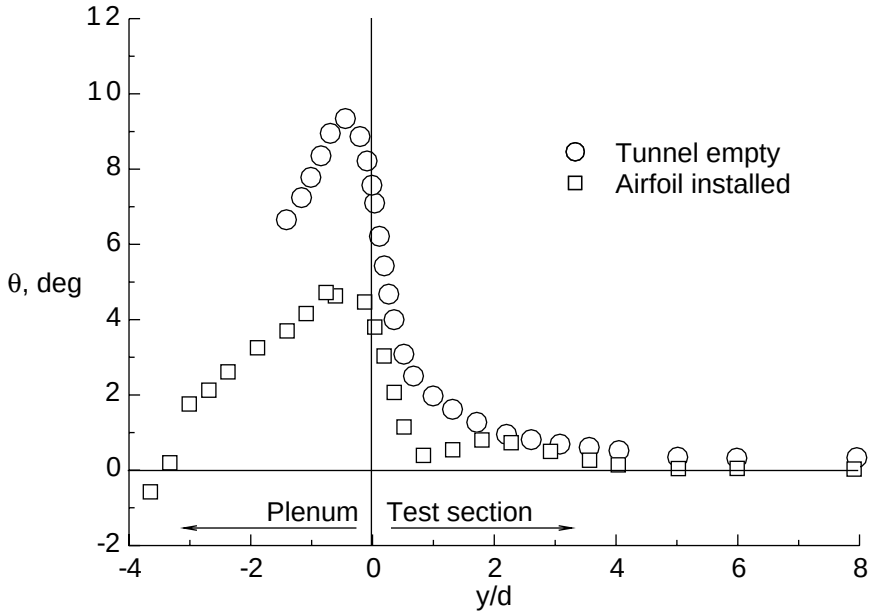

(a) Flow angle.

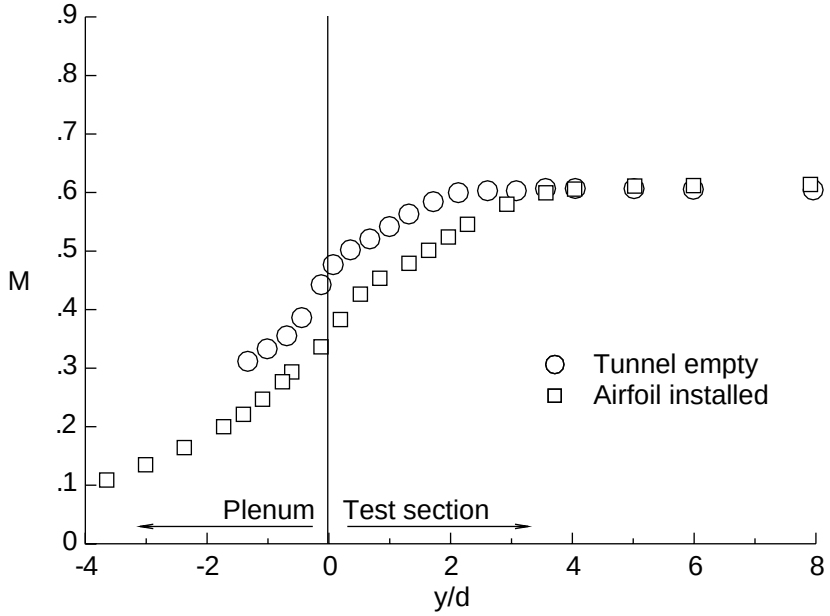

(b) Mach number.

Figure 14. Influence of airfoil-induced curvature on local slot-flow properties measured in DFA at tunnel station 24 in. $M_\infty = 0.6$.

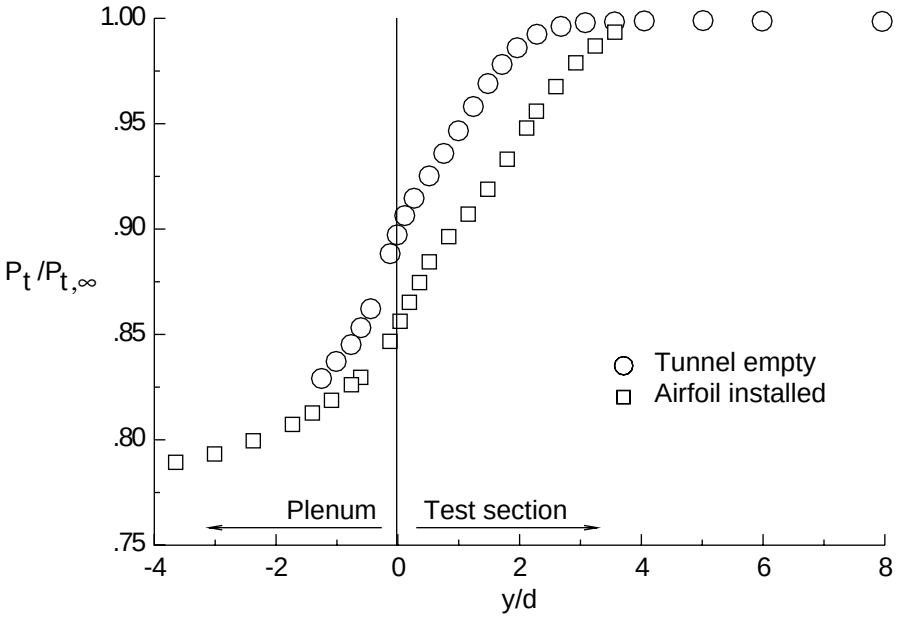

(c) Total pressure ratio.

Figure 14. Concluded.

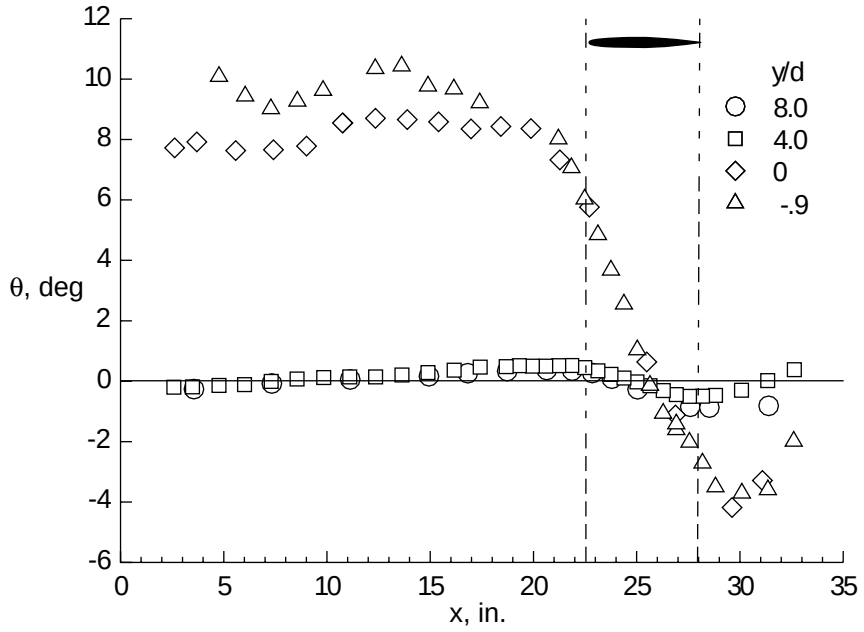

(a) Flow angle.

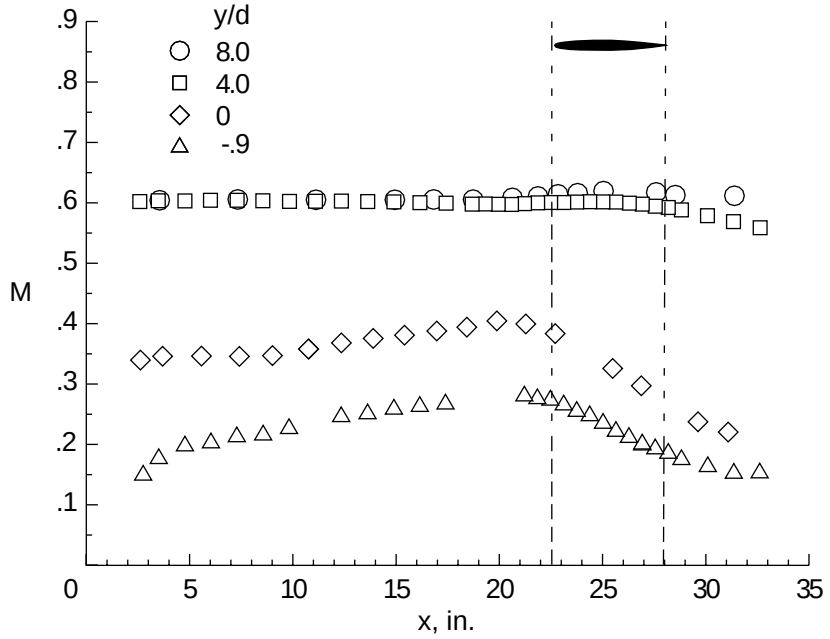

(b) Mach number.

Figure 15. Longitudinal probe measuements in DFA at various distances from slot. $M_\infty = 0.6$.

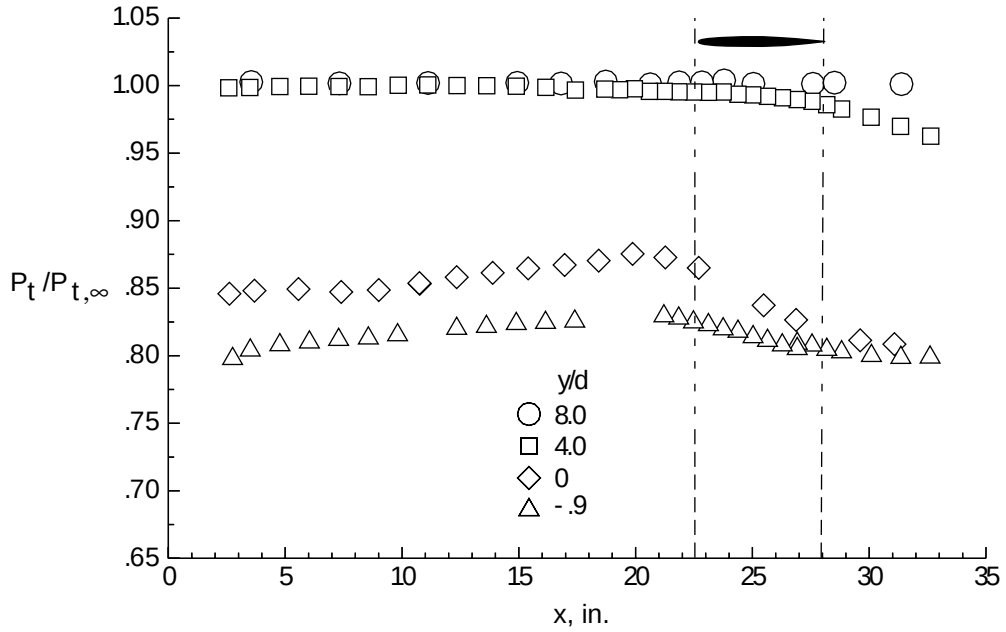

(c) Total pressure ratio.

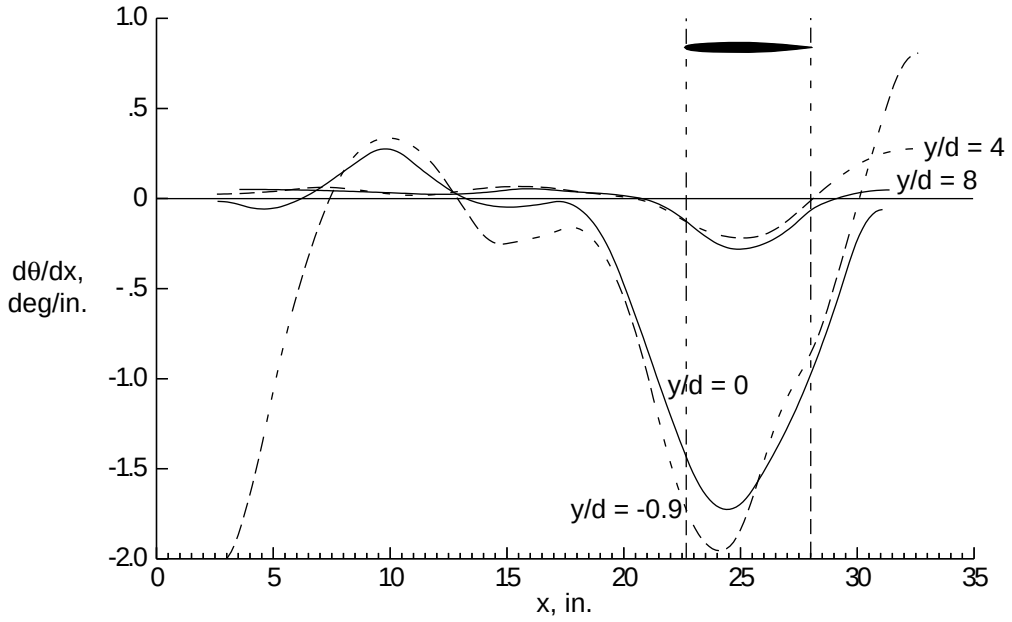

(d) Computed flow-angle gradient.

Figure 15. Concluded.

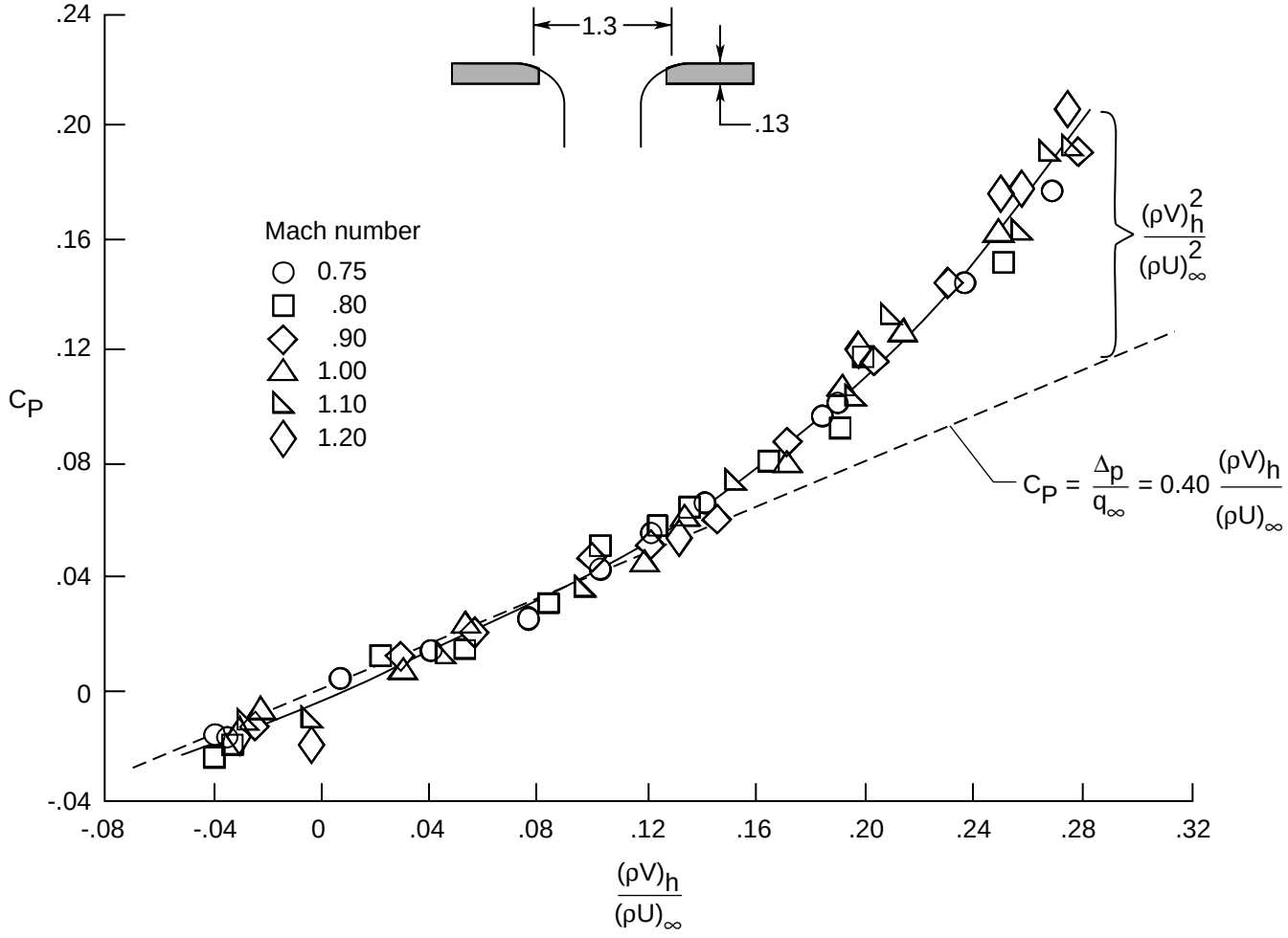

Figure 16. Gardenier and Chew data (Goethert (1961)). Mach number dependence of slotted-wall pressure drop.

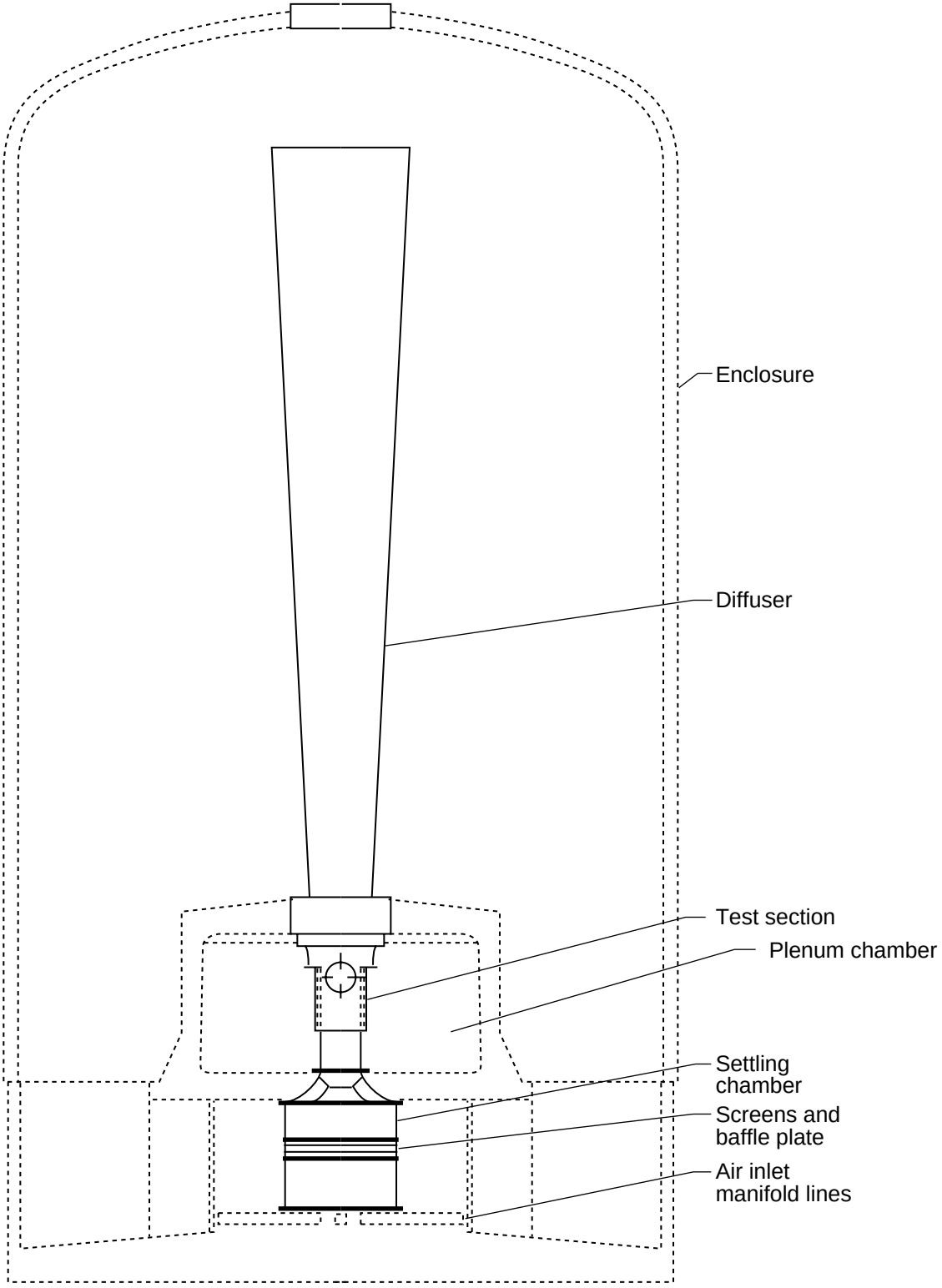

(a) Overall view.

Figure 18. Schematic of 6- by 19-Inch Transonic Tunnel.

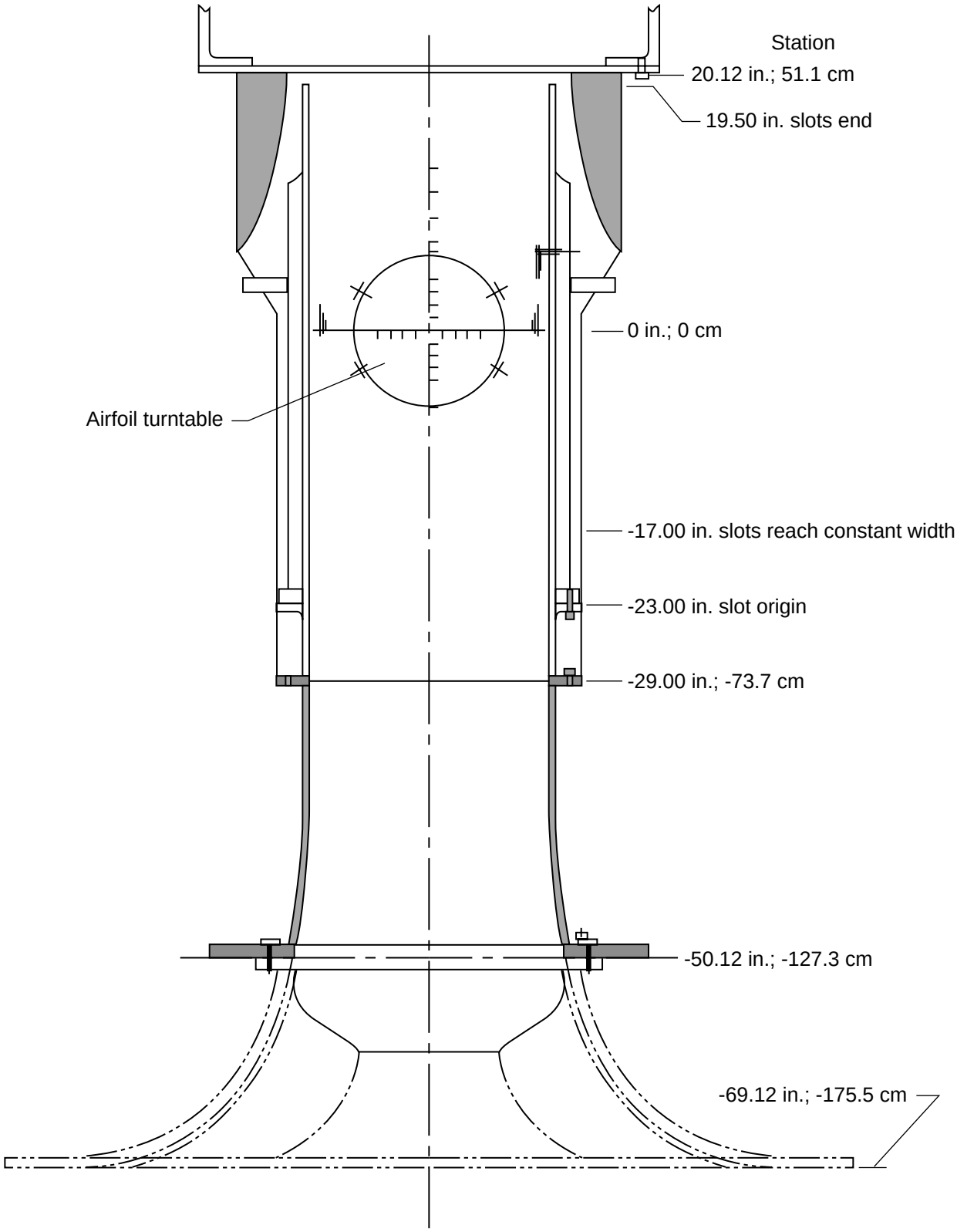

(b) Test-section details.

Figure 18. Concluded.

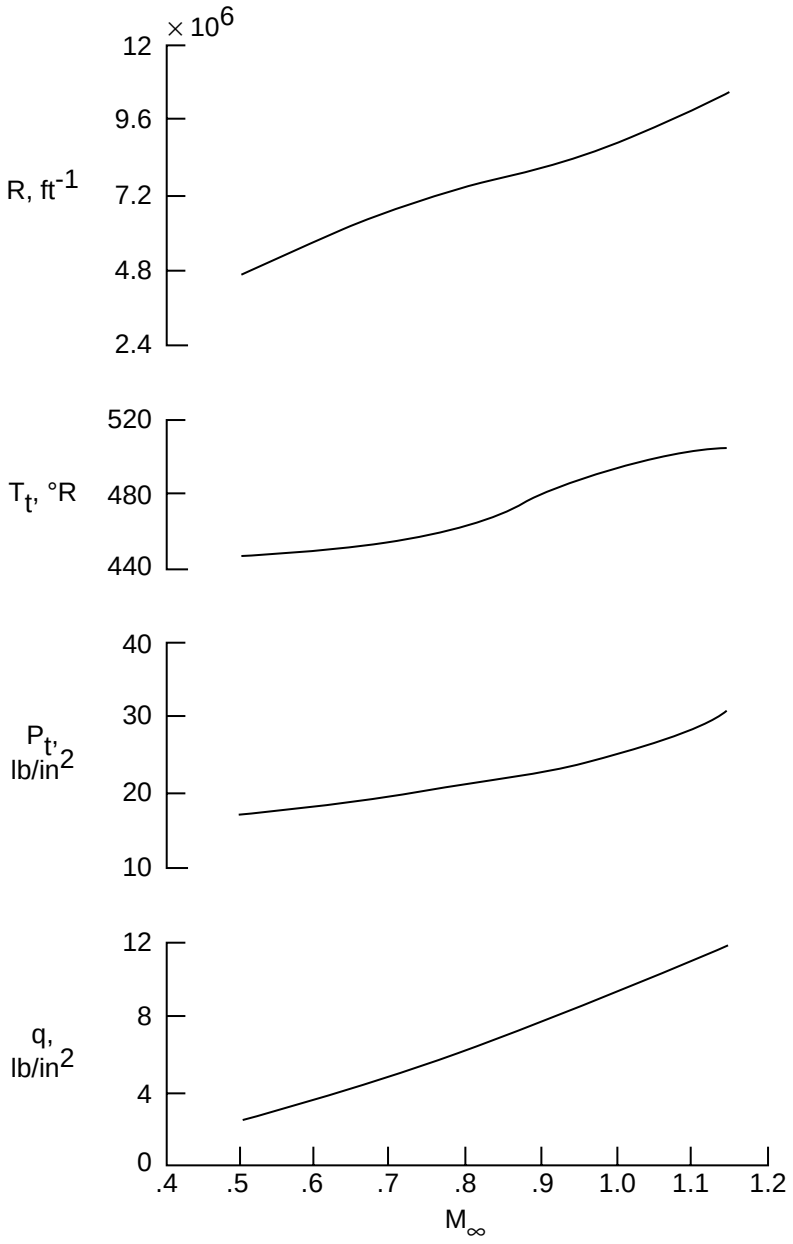

Figure 19. Typical operational characteristics of 6- by 19-Inch Transonic Tunnel.

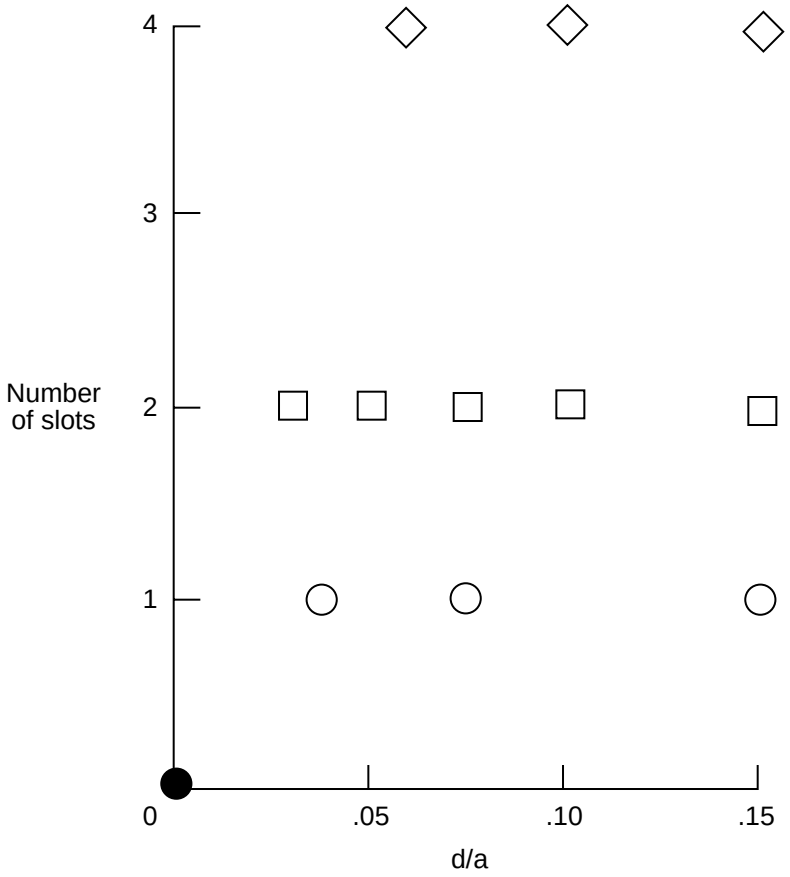

Figure 21. Wall-geometry test matrix.

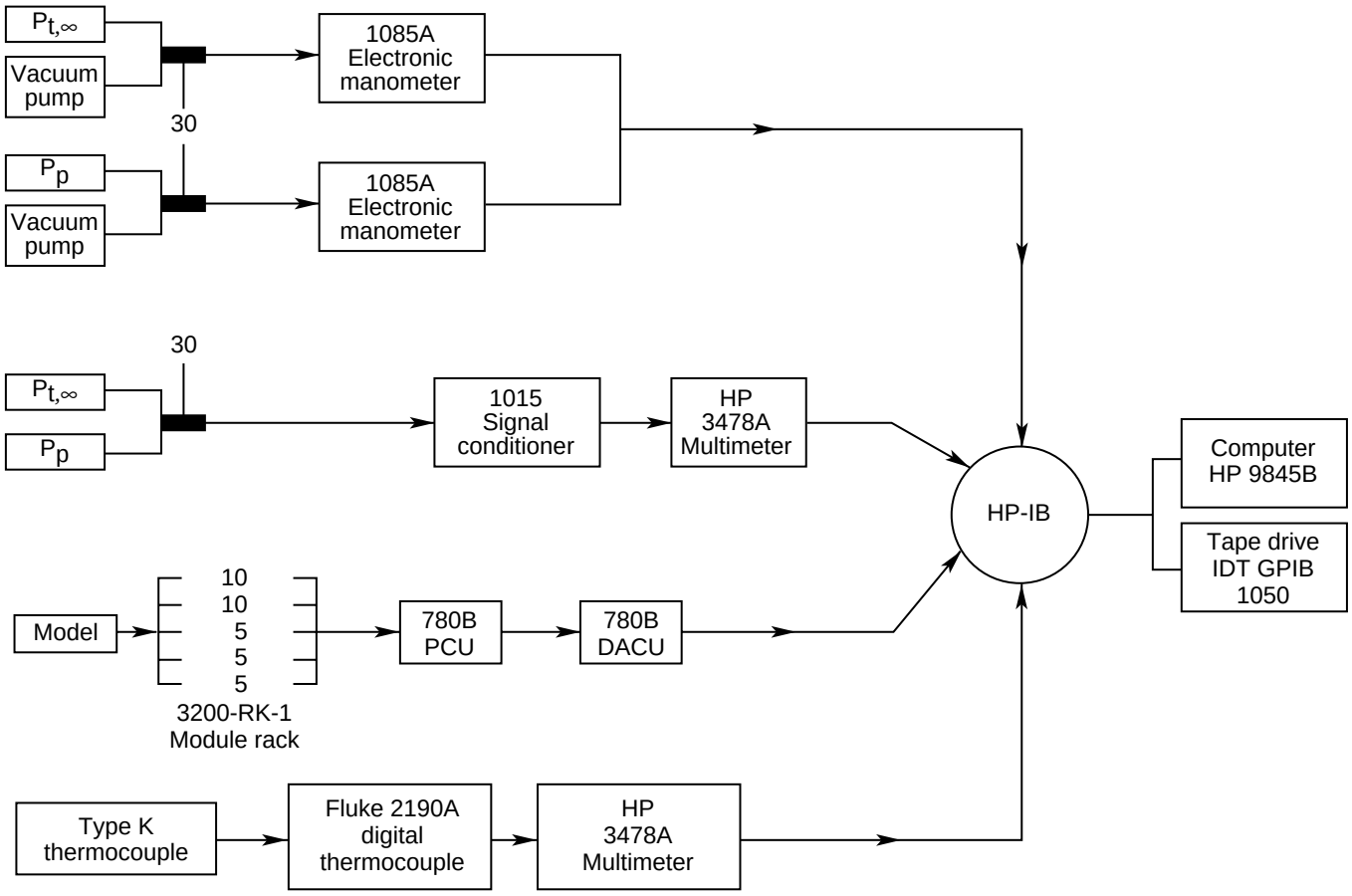

Figure 24. Schematic of data system and instrumentation. All pressure measurements are in pounds per square inch.

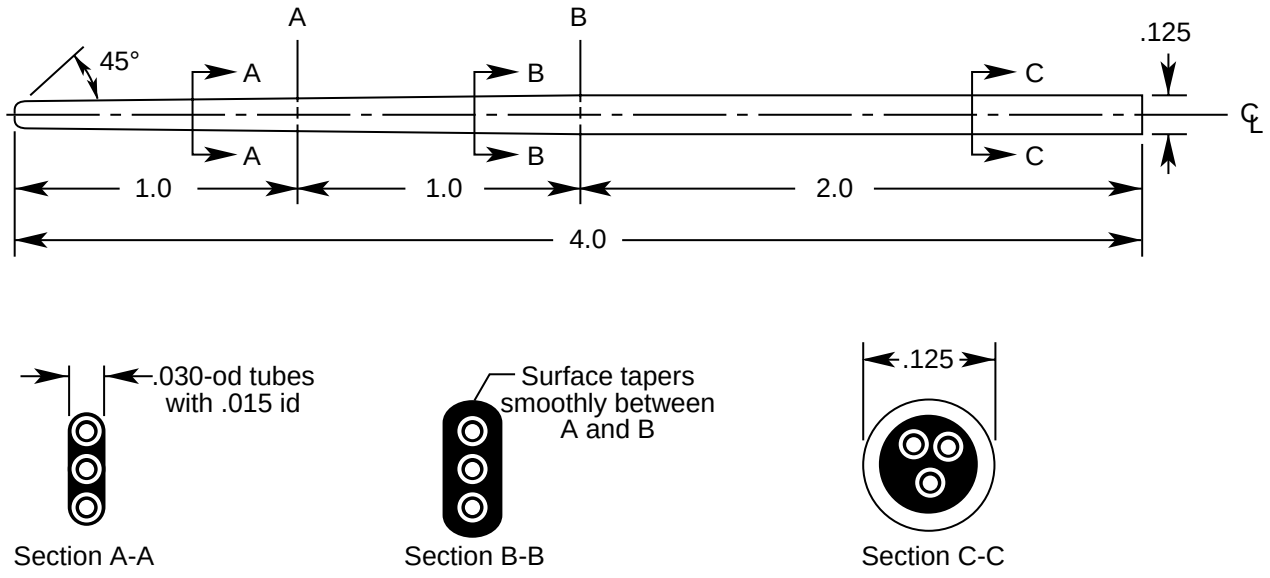

Figure 25. Schematic of 6- by 19-Inch Tunnel flow-angle probe. All linear dimensions are in inches.

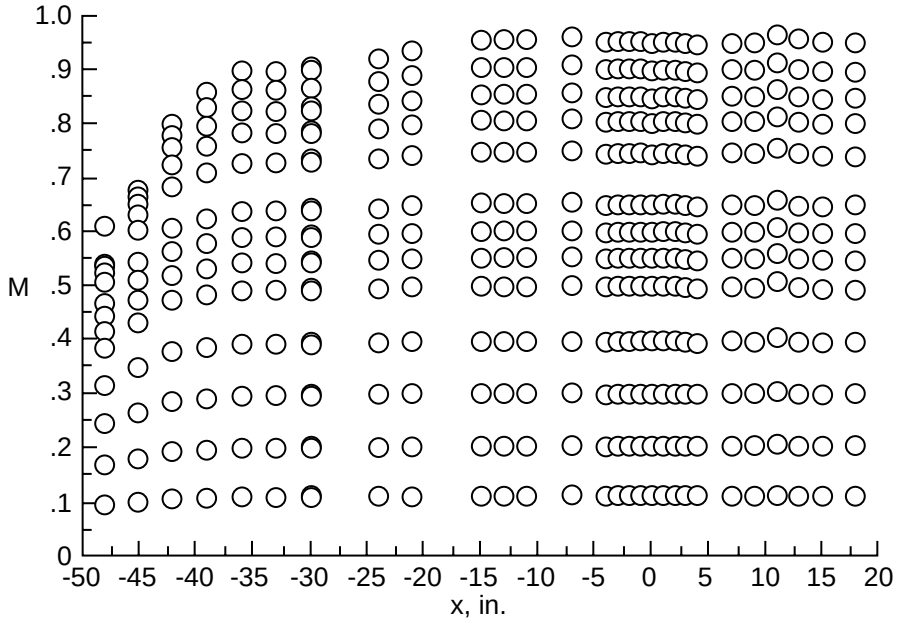

Figure 26. Centerline Mach number calibration for 15-1 wall.

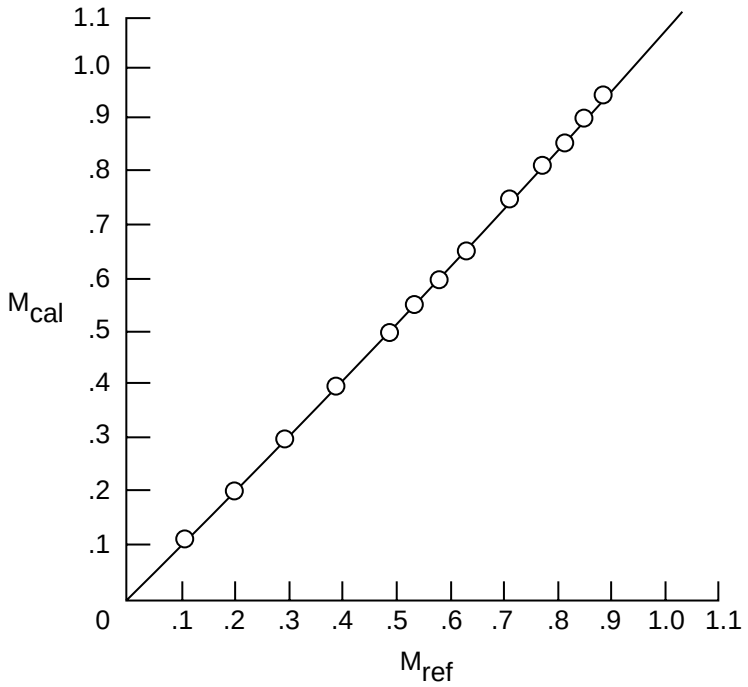

Figure 27. Wind tunnel wall calibration for 15-1 wall.

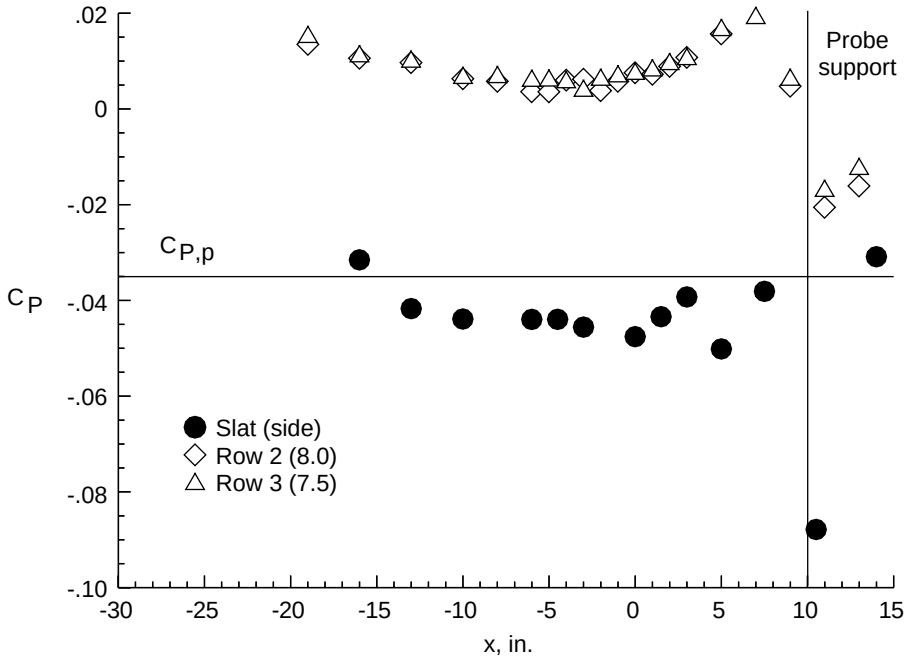

(a) Tunnel empty.

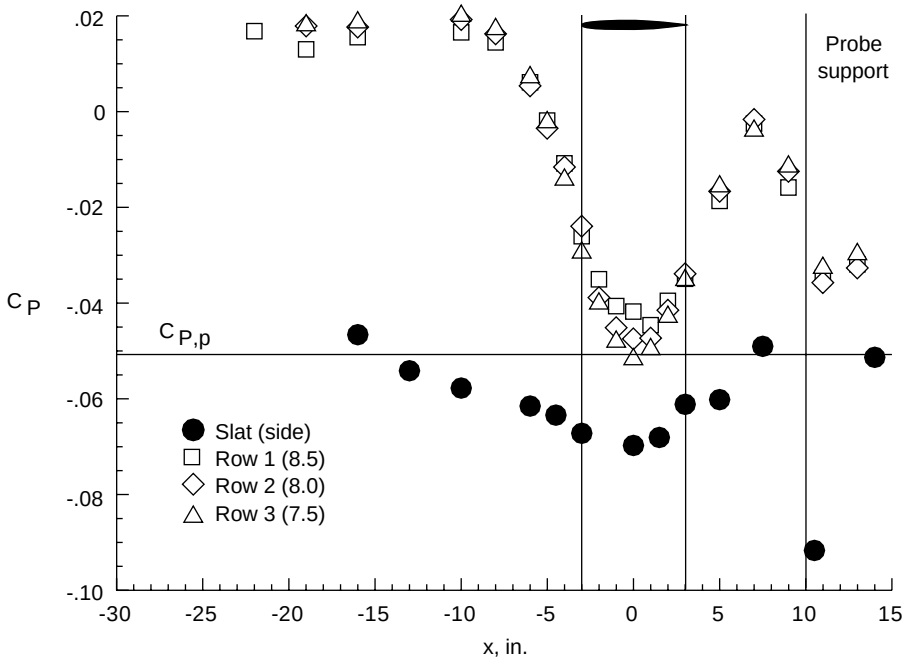

(b) Airfoil installed.

Figure 28. Pressure distributions near 6-4 slotted wall. $M_\infty = 0.7$.

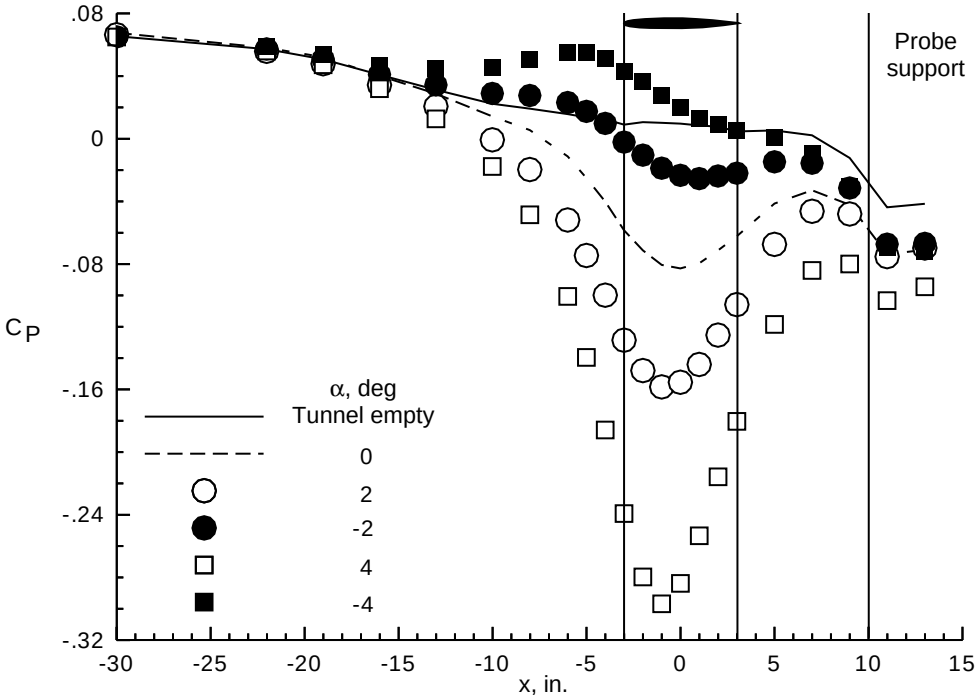

(a) Solid wall.

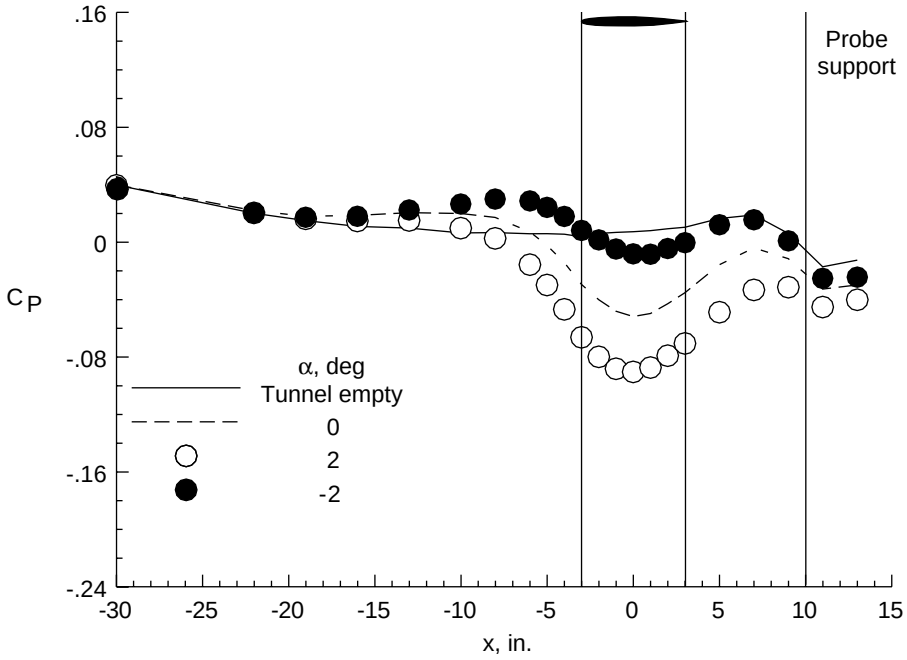

(b) 6-4 wall.

Figure 29. Airfoil influence on pressure distributions along row 3. $M_\infty = 0.7$.

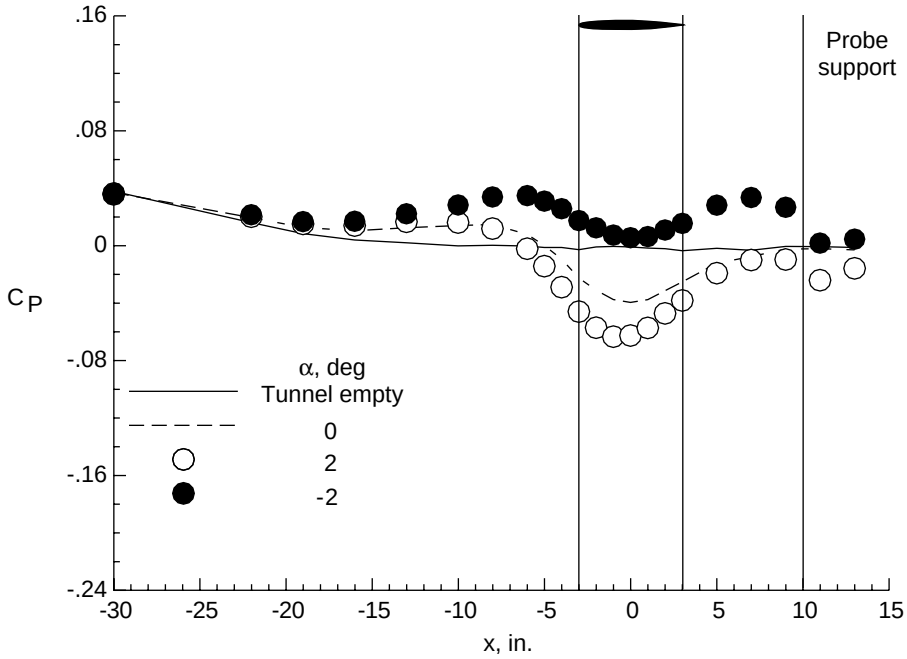

(c) 10-2 wall.

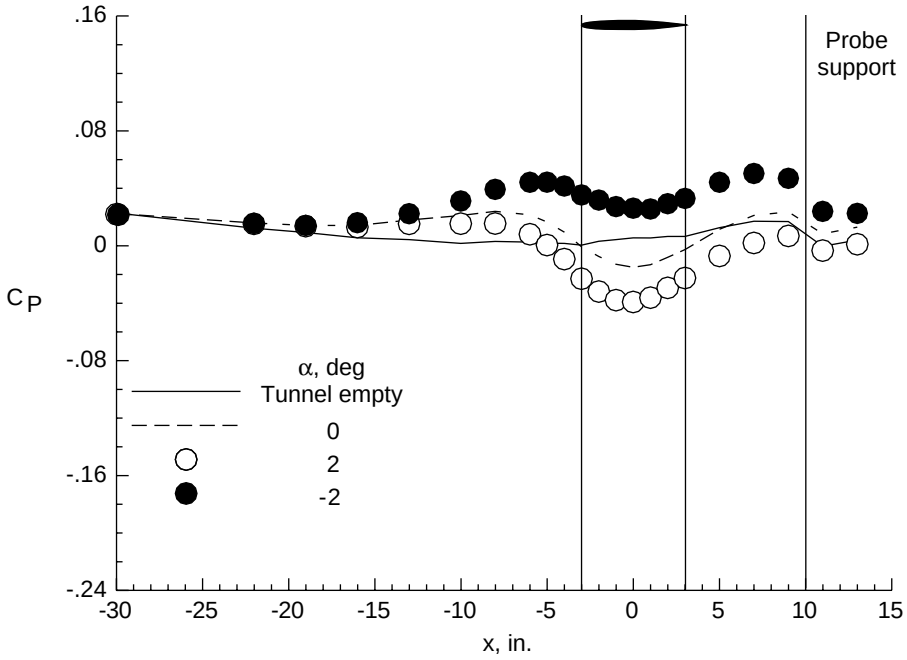

(d) 10-4 wall.

Figure 29. Continued.

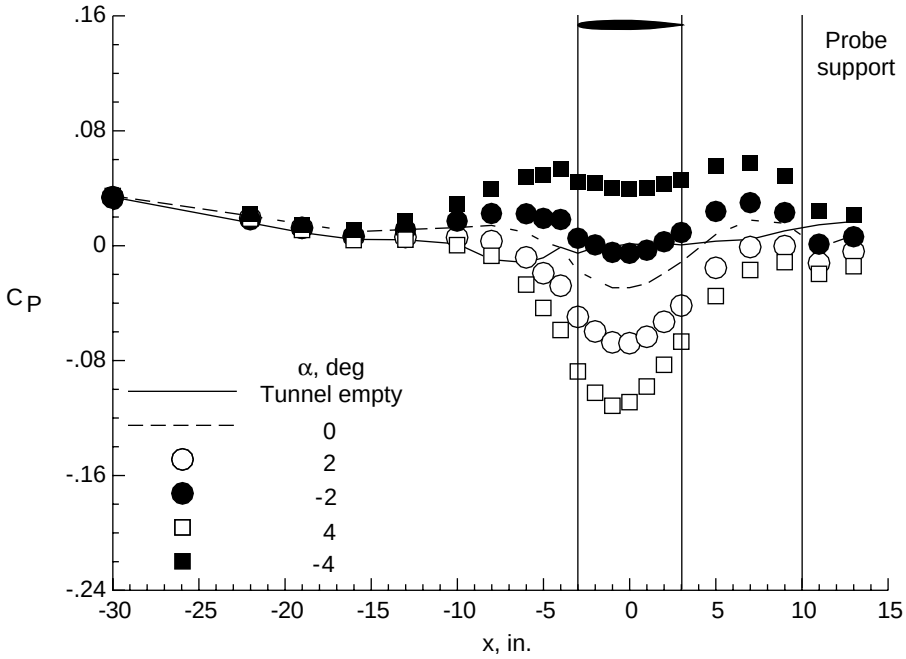

(e) 15-1 wall.

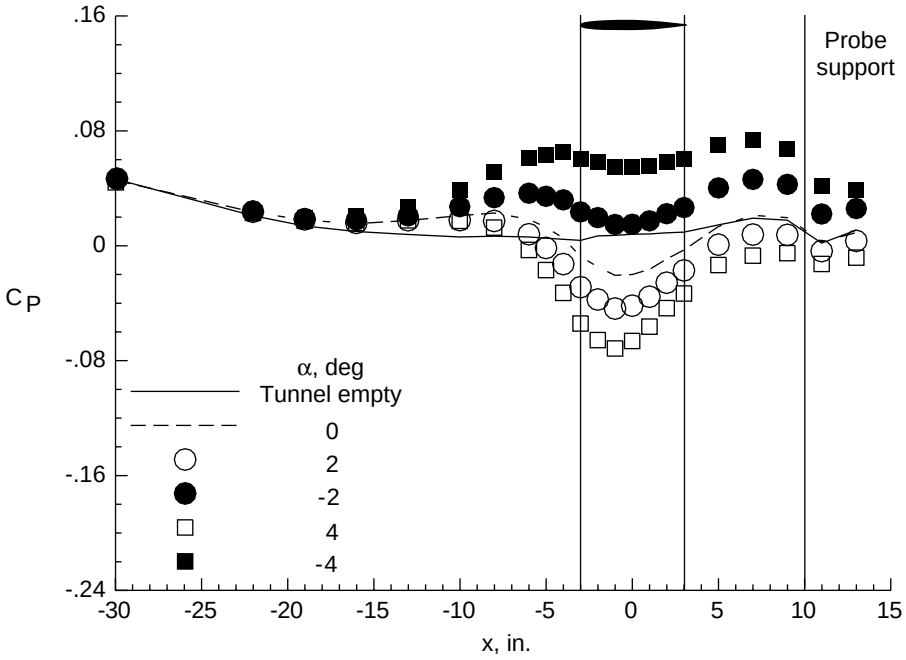

(f) 15-2 wall.

Figure 29. Continued.

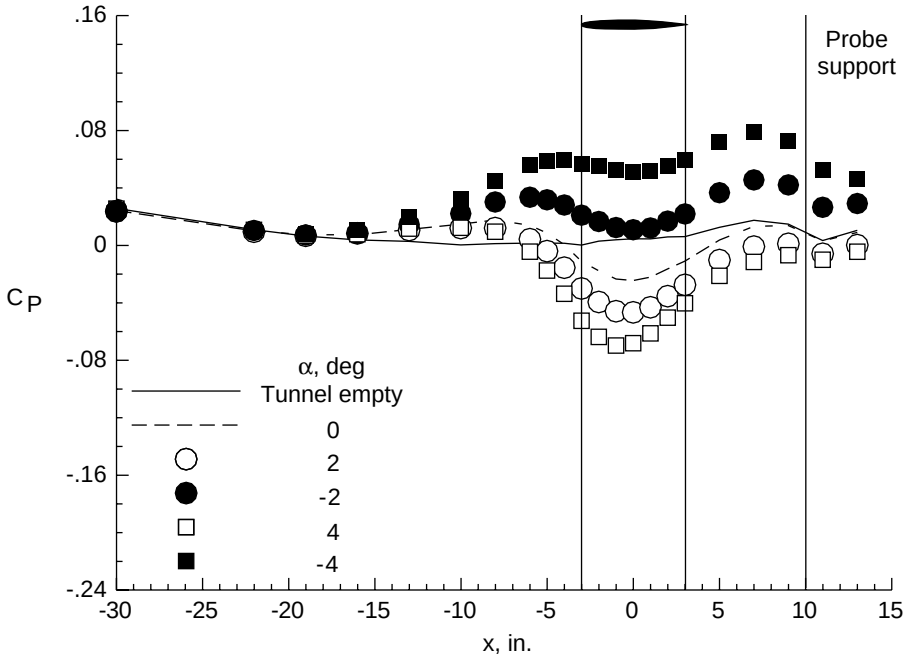

(g) 15-4 wall.

Figure 29. Concluded.

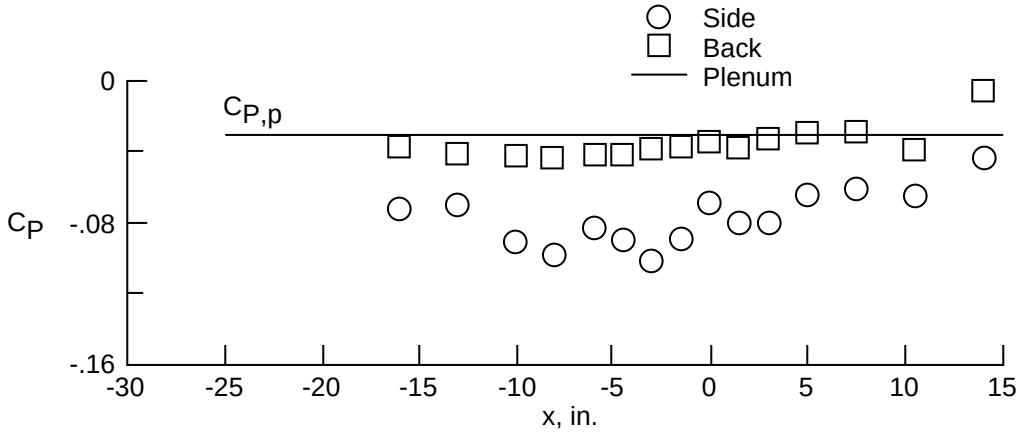

(a) 10-2 wall.

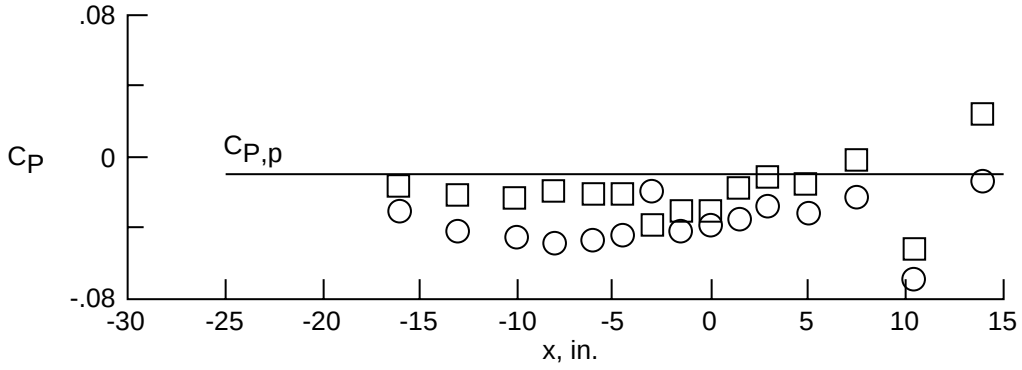

(b) 15-2 wall.

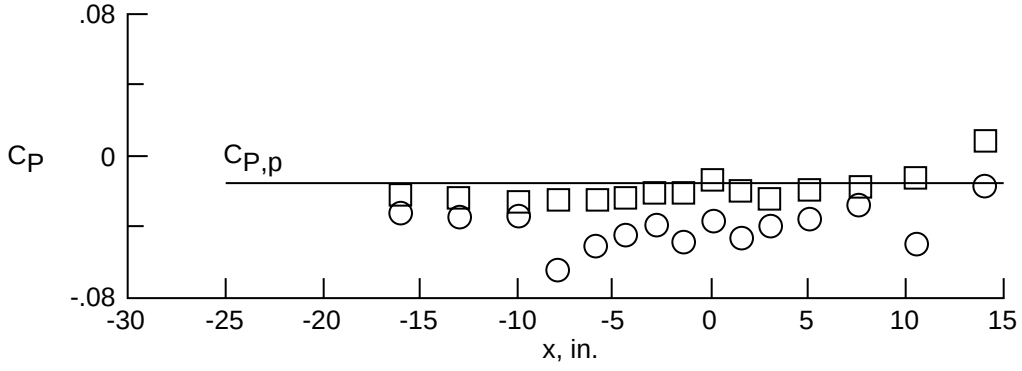

(c) 15-4 wall.

Figure 30. Tunnel-empty pressure measurements in slot region. $M_\infty = 0.7$.

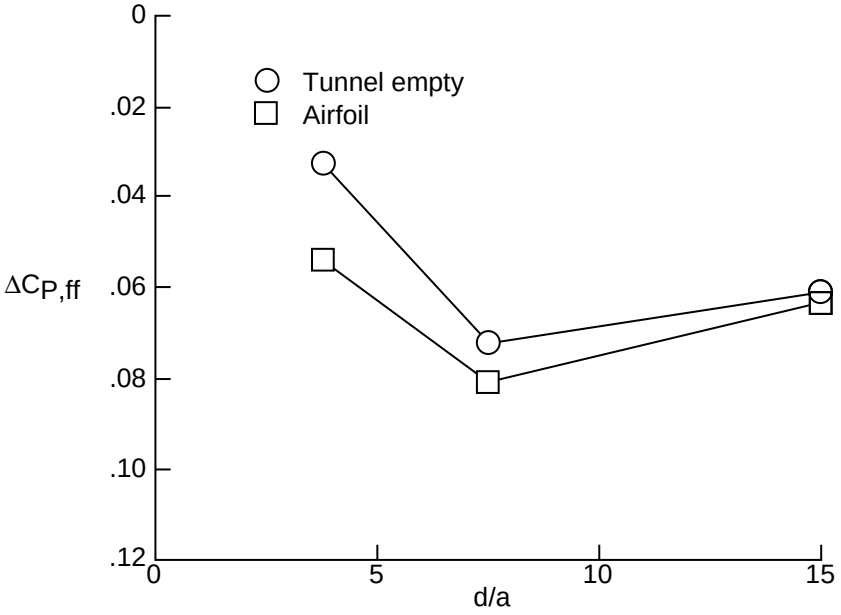

(a) One-slot walls.

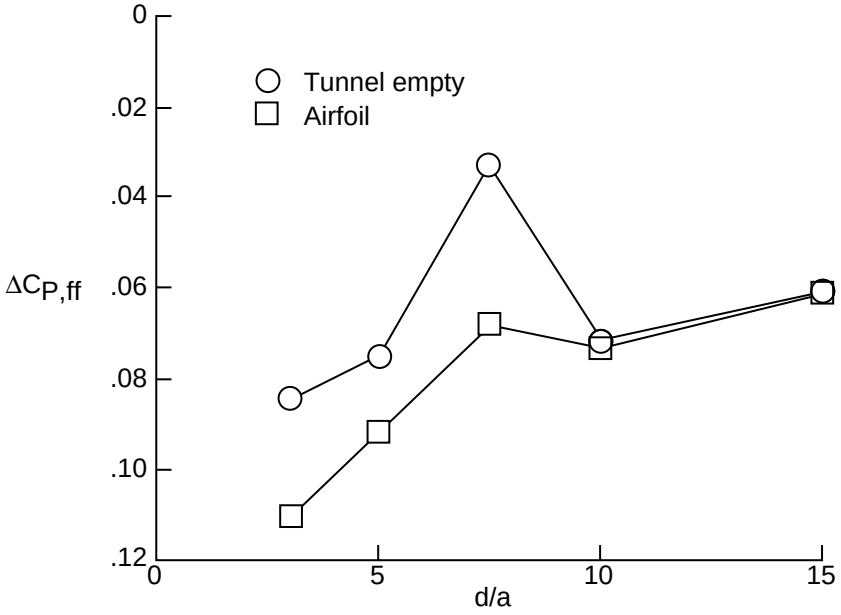

(b) Two-slot walls.

Figure 31. Far-field wall-pressure drop. $M_\infty = 0.7$.

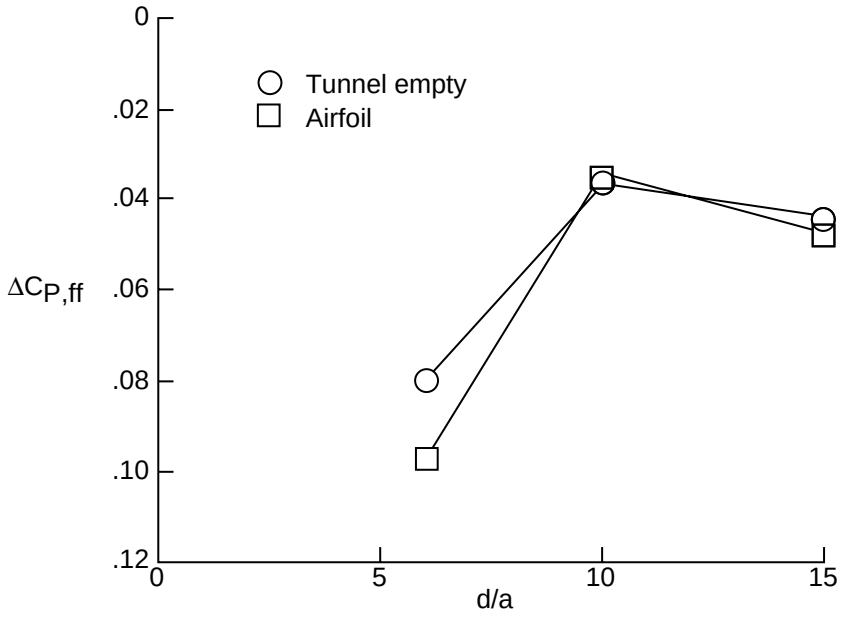

(c) Four-slot walls.

Figure 31. Concluded.

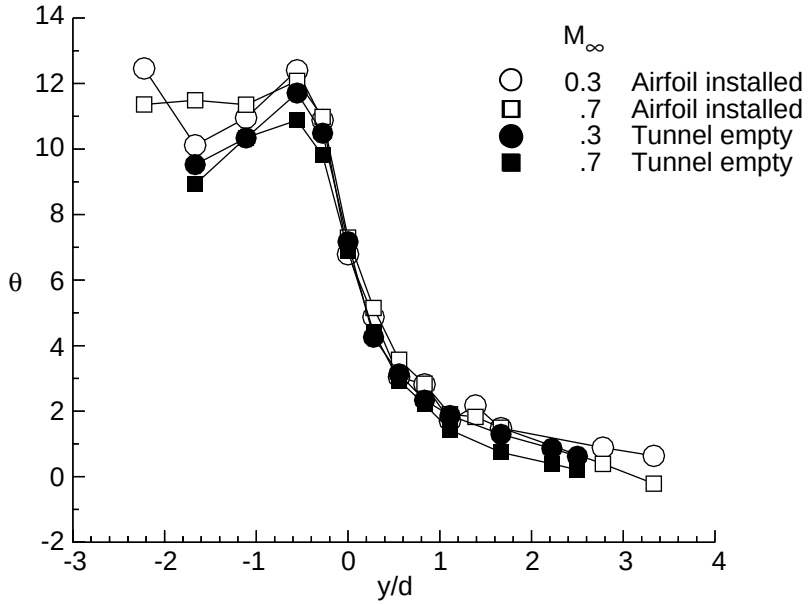

Figure 32. Comparison of tunnel-empty and airfoil-installed flow angles measured through 15-1 slot in 6- by 19-Inch Tunnel. $x = -6$ in.; $M_\infty = 0.3$ and 0.7.

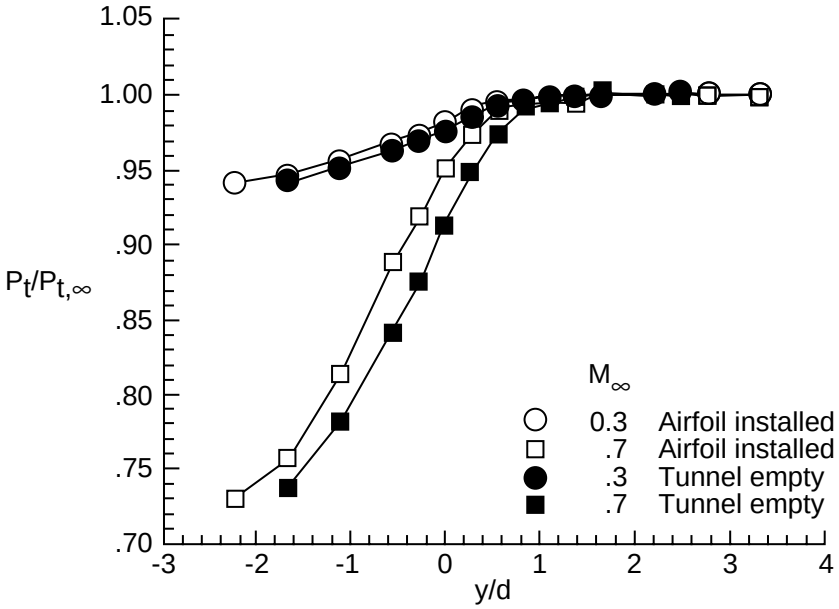

Figure 33. Comparison of tunnel-empty and airfoil-installed total pressures measured through 15-1 slot in 6- by 19-Inch Tunnel. $x = -6$ in.; $M_\infty = 0.3$ and 0.7.

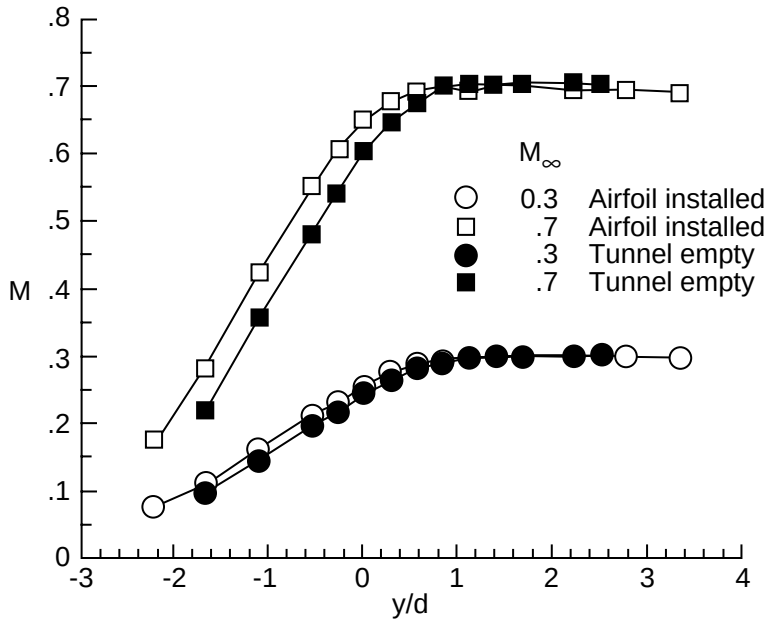

Figure 34. Comparison of tunnel-empty and airfoil-installed Mach numbers measured through 15-1 slot in 6- by 19-Inch Tunnel. $x = -6$ in.; $M_\infty = 0.3$ and 0.7.

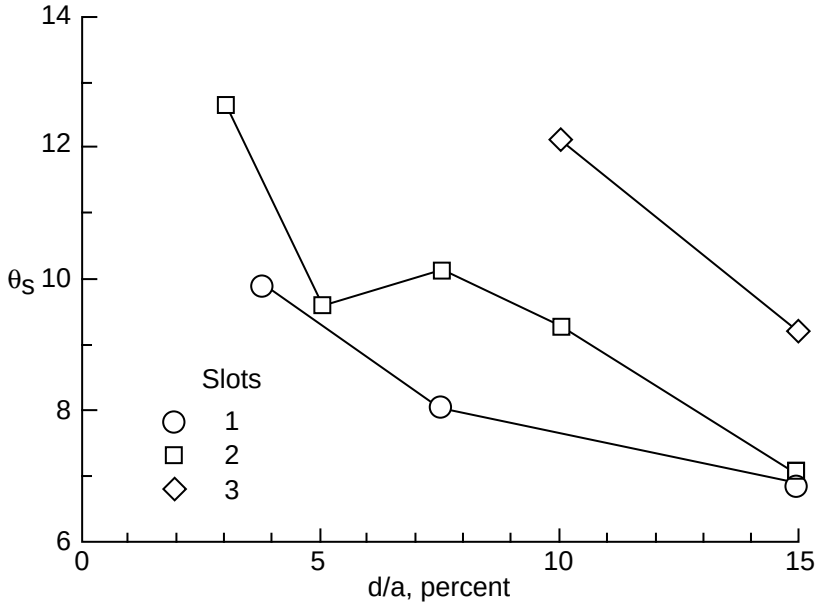

(a) Tunnel empty.

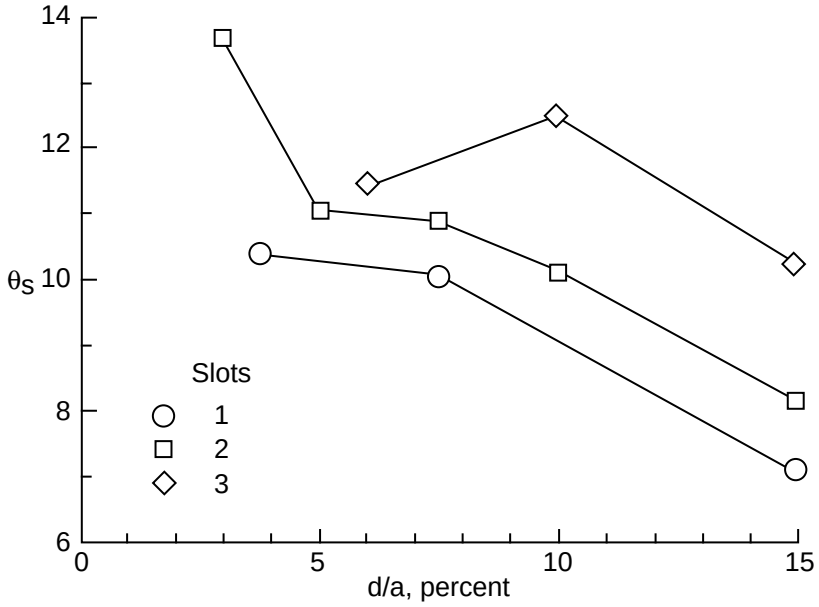

(b) Airfoil.

Figure 35. Summary of measured flow angles in slot. $x = -6$ in.; $M_\infty = 0.7$.

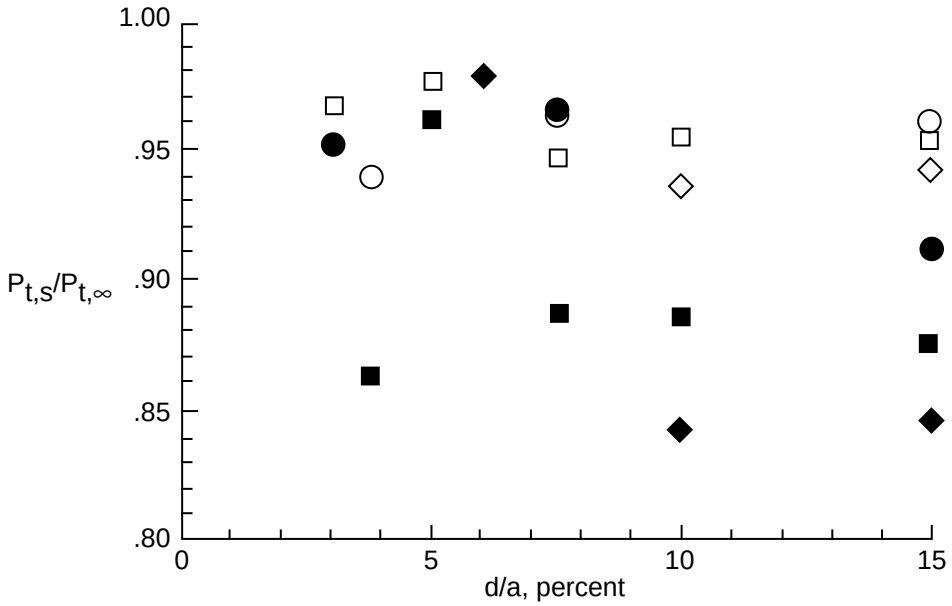

(a) Tunnel empty.

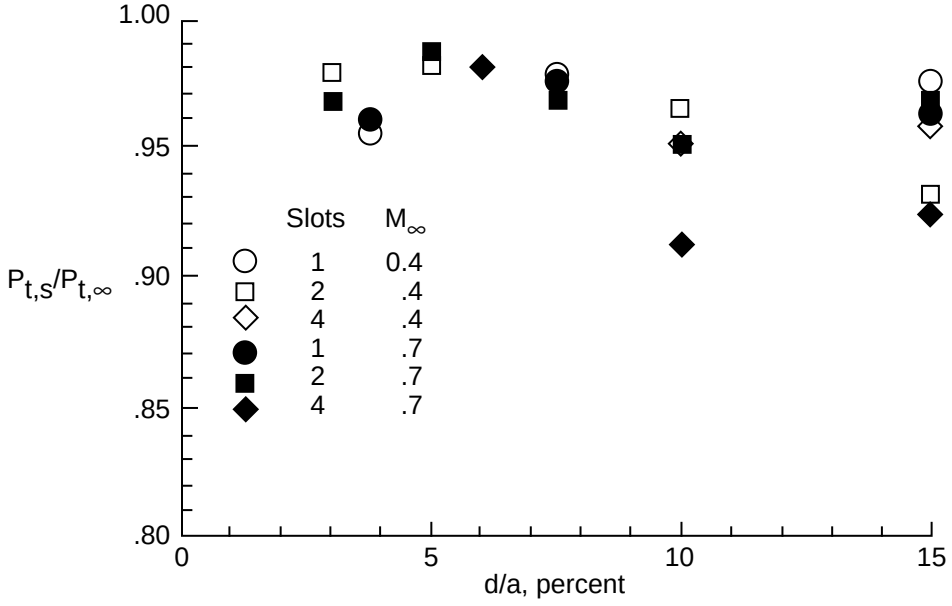

(b) Airfoil.

Figure 36. Summary of measured total pressures in slot. $x = -6$ in.

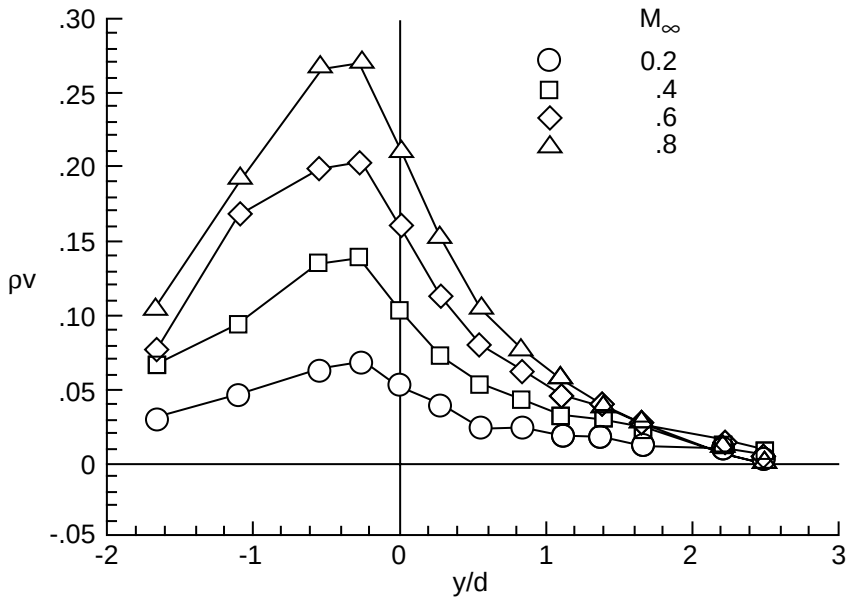

(a) Transverse mass flux.

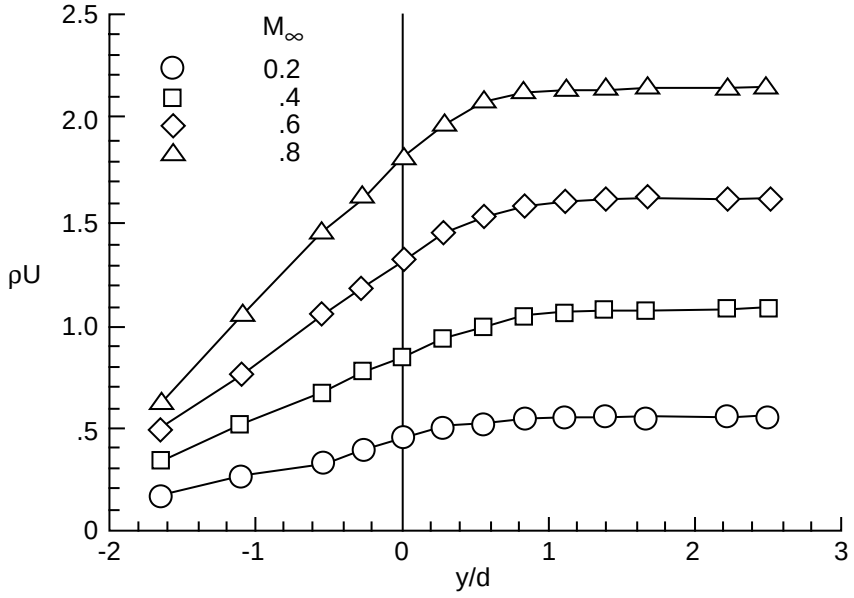

(b) Longitudinal mass flux.

Figure 37. Effect of Mach number on variation of tunnel-empty mass flux through 15-1 slot. $x = -6$ in.

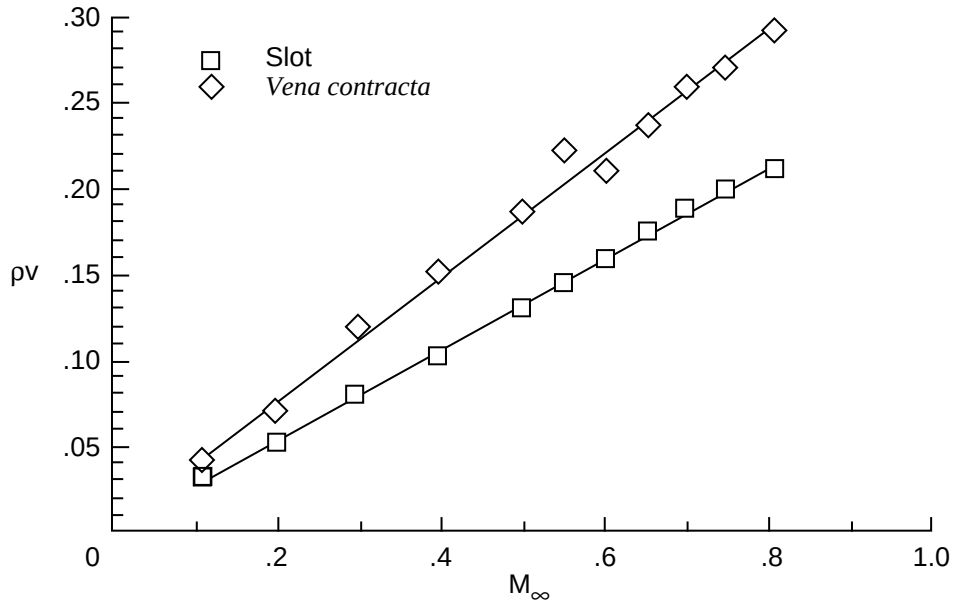

(a) Transverse mass flux.

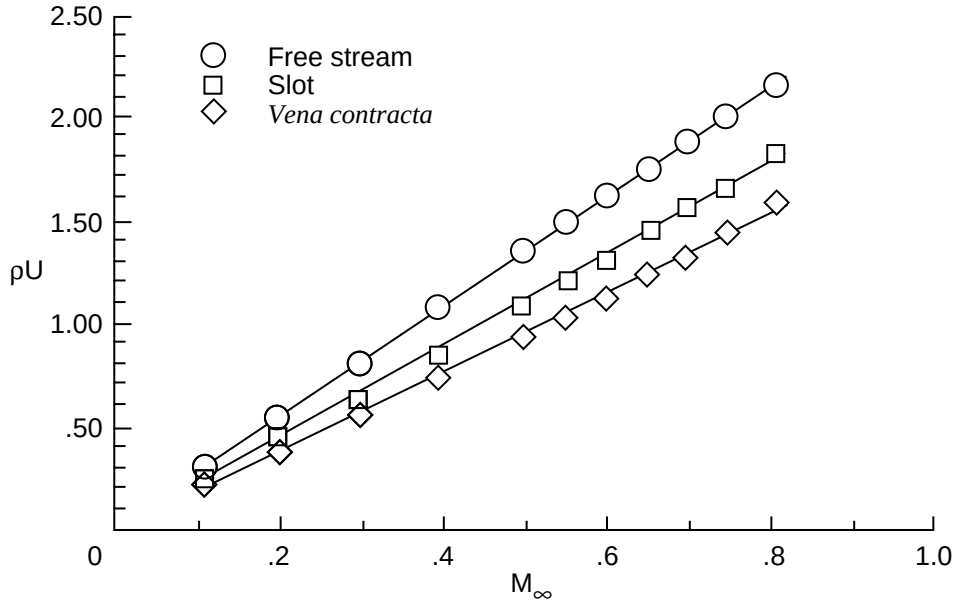

(b) Longitudinal mass flux.

Figure 38. Tunnel-empty mass flux variation for 15-1 wall. $x = -6$ in.

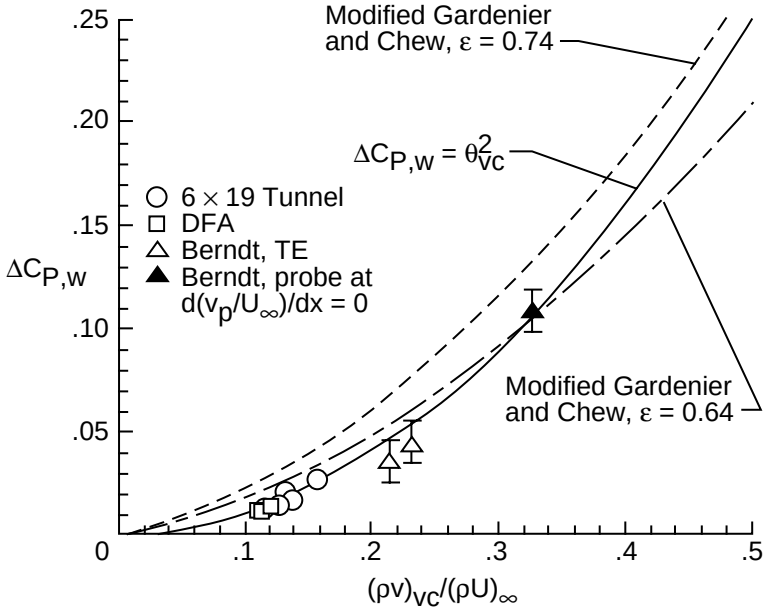

Figure 39. Correlation of tunnel-empty wall-pressuree drop with slot-flow angle.

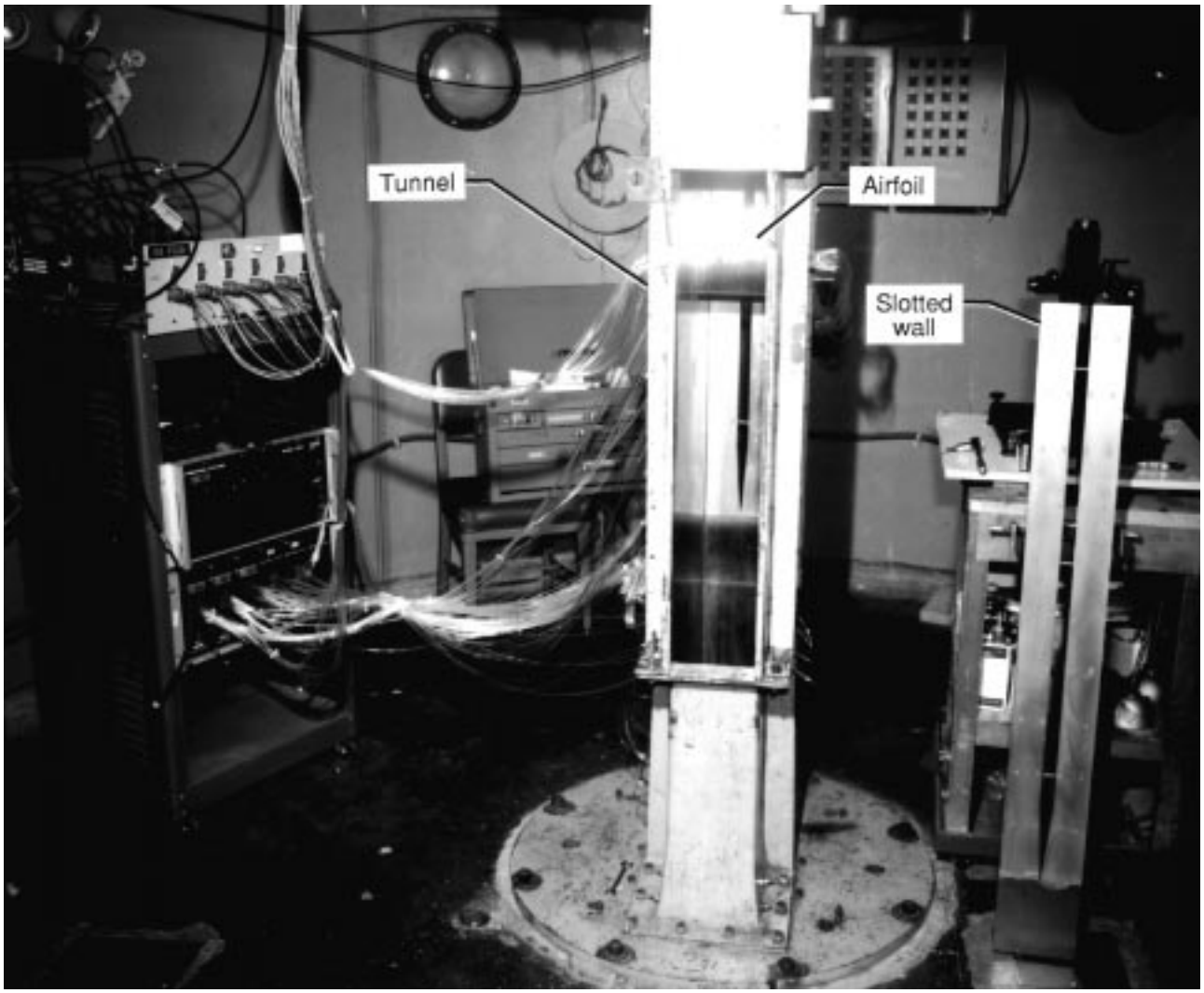

Figure 17. Langley 6- by 19-Inch Transonic Tunnel.

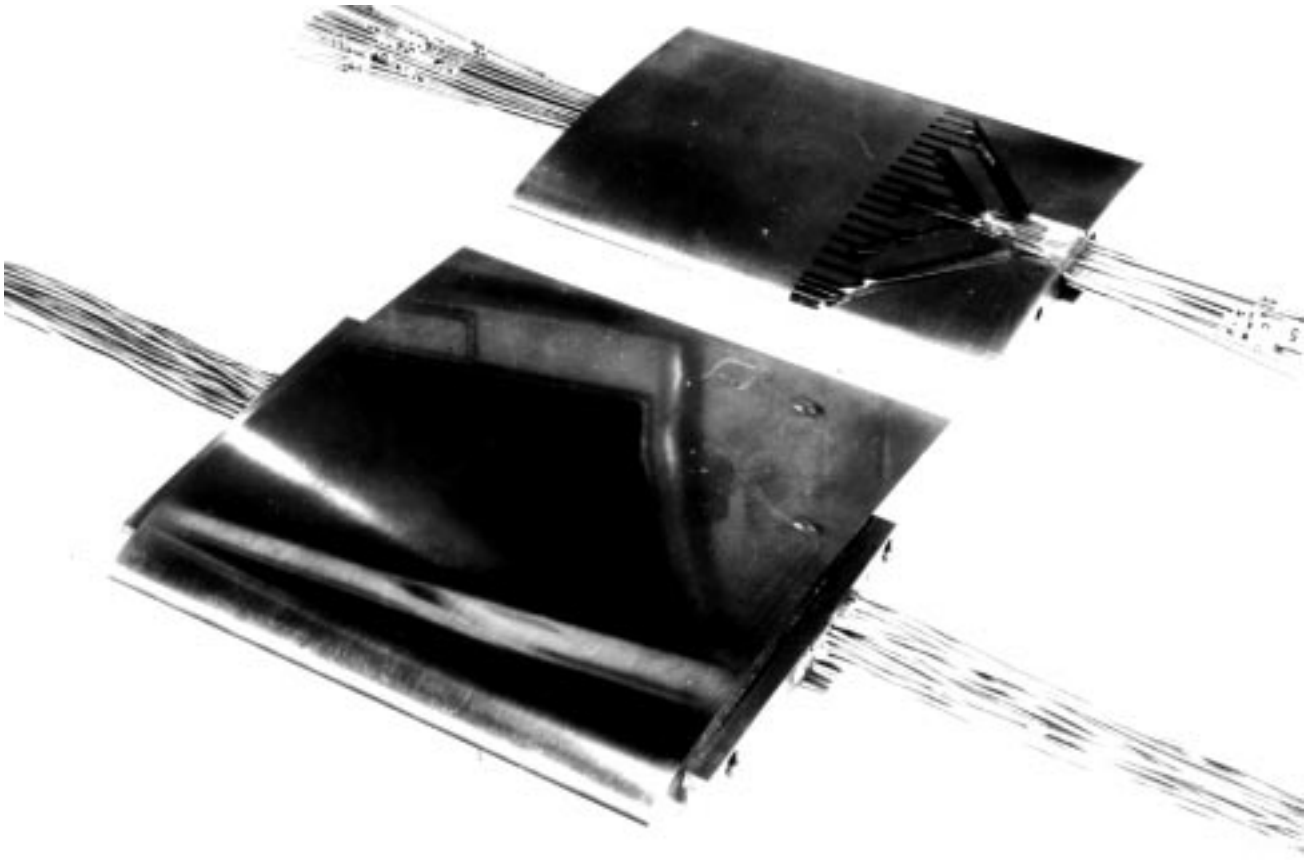

Figure 20. Typical pressure-instrumented airfoil models. In foreground, 6-in. chord; 4-in. chord in background.

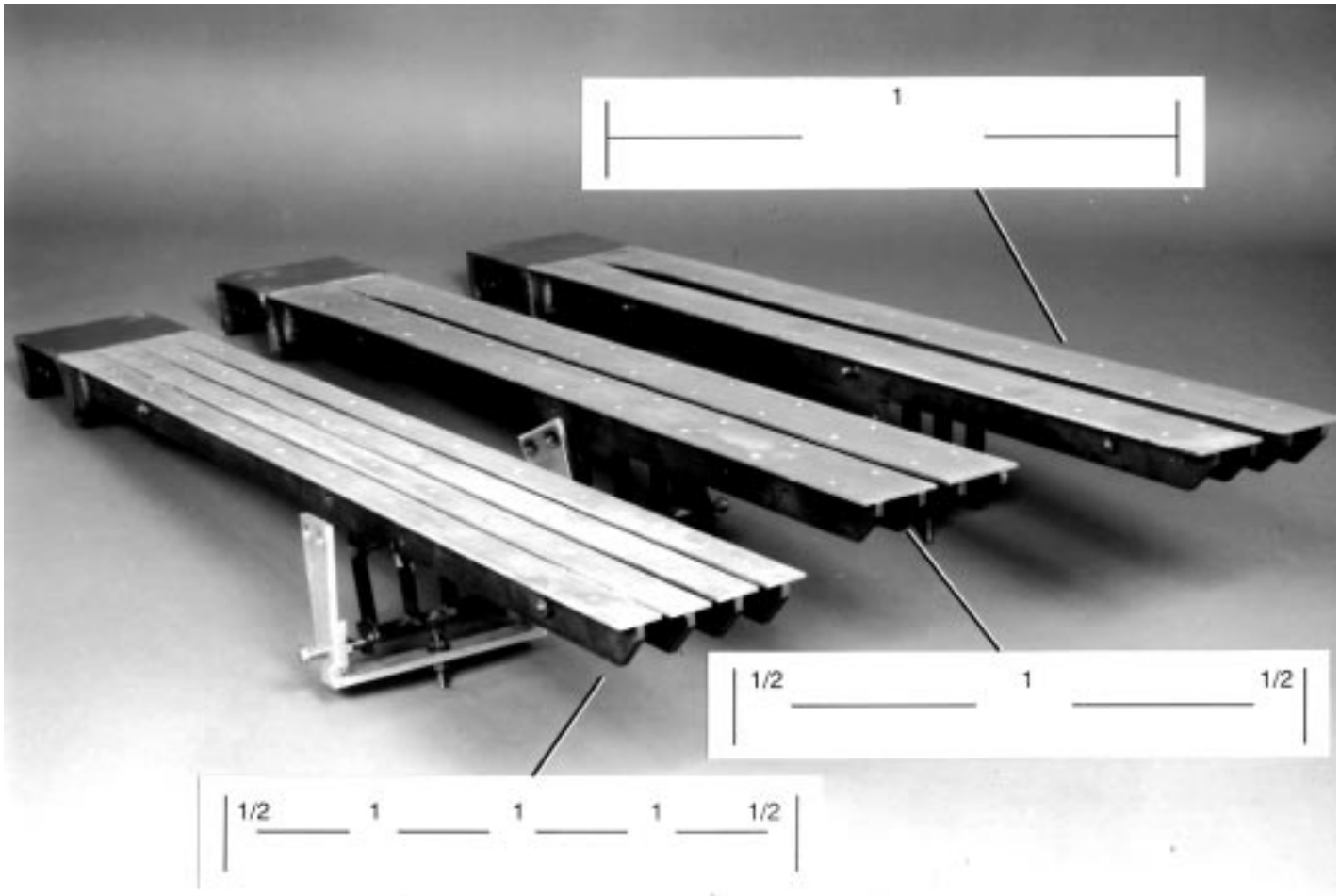
1
1/2
1
1/2
1/2
1
1
1
1/2

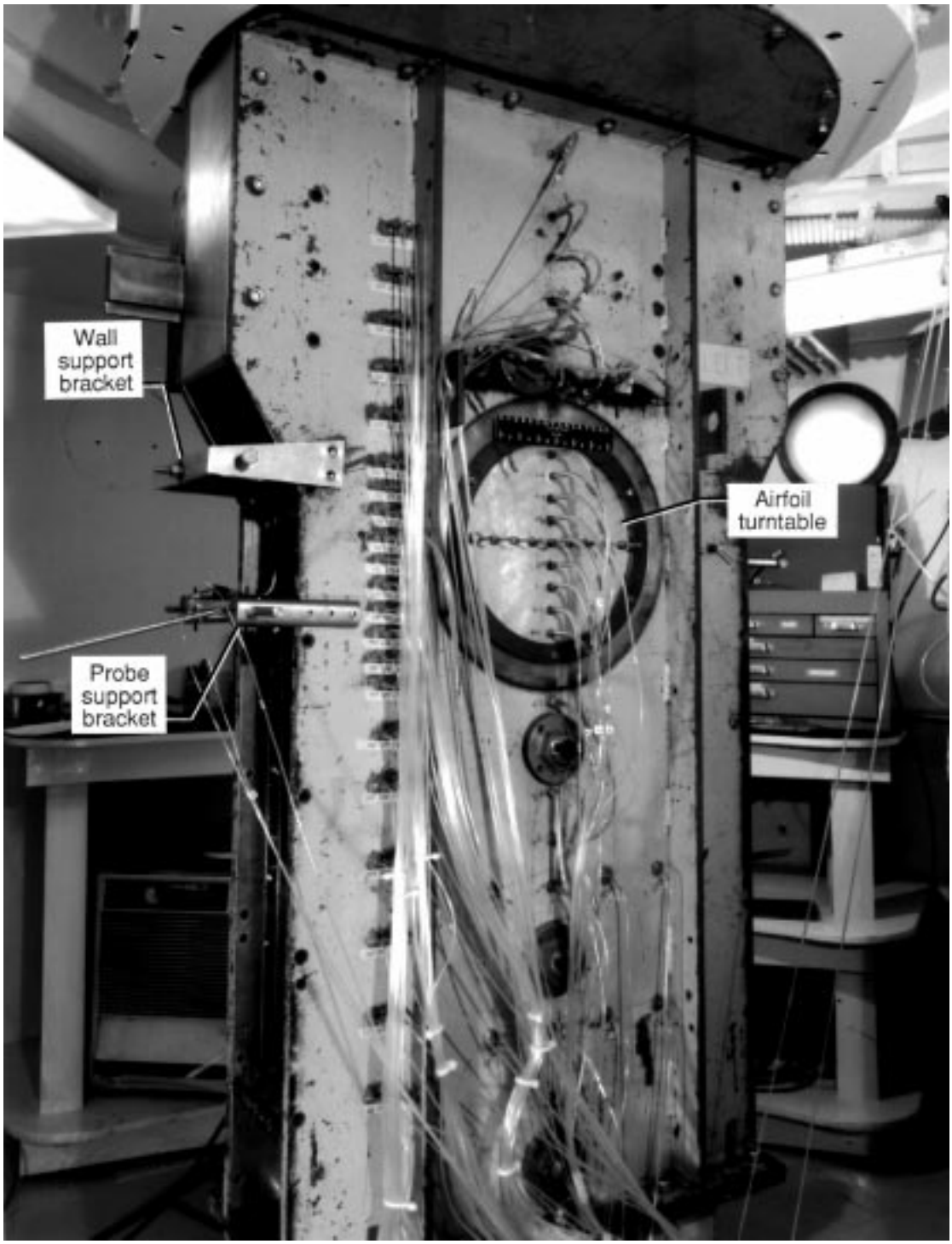

Figure 23. Tunnel sidewall with orifice layout and location of airfoil turntable.

Figure 17. Langley 6- by 19-Inch Transonic Tunnel.

L-84-6641

Figure 20. Typical pressure-instrumented airfoil models. In foreground, 6-in. chord; 4-in chord in background.

Figure 20. Typical pressure-instrumented airfoil models. In foreground, 6-in. chord; 4-in. chord in background.

L-75-234

Figure 22. Fifteen-percent-open wall configurations.

L-85-2176

Figure 23. Tunnel sidewall with orifice layout and location of airfoil turntable.

L-85-2188

REPORT DOCUMENTATION PAGE

Form Approved
OMB No. 0704-0188

1. AGENCY USE ONLY *(Leave blank)*	2. REPORT DATE	3. REPORT TYPE AND DATES COVERED
	April 1994	Technical Paper

4. TITLE AND SUBTITLE
Experimental Studies of Transonic Flow Field Near a Longitudinally Slotted Wind Tunnel Wall

5. FUNDING NUMBERS
WU 506-40-41-01

6. AUTHOR(S)
Joel L. Everhart and Percy J. Bobbitt

7. PERFORMING ORGANIZATION NAME(S) AND ADDRESS(ES)
NASA Langley Research Center
Hampton, VA 23681-0001

8. PERFORMING ORGANIZATION REPORT NUMBER
L-16423

9. SPONSORING/MONITORING AGENCY NAME(S) AND ADDRESS(ES)
National Aeronautics and Space Administration
Washington, DC 20546-0001

10. SPONSORING/MONITORING AGENCY REPORT NUMBER
NASA TP-3392

11. SUPPLEMENTARY NOTES
Part of the information presented in this report was included in a dissertation submitted by Joel L. Everhart in partial fulfillment of the requirements for the Doctor of Science in Fluid Mechanics, The George Washington University, Washington, DC, February 1988.

12a. DISTRIBUTION/AVAILABILITY STATEMENT
Unclassified–Unlimited

Subject Category 02

12b. DISTRIBUTION CODE

13. ABSTRACT *(Maximum 200 words)*
The results of detailed, parametric experiments are presented for the near-wall flow field of a longitudinally slotted transonic wind tunnel. Existing data are reevaluated and new data obtained in the Langley 6- by 19-Inch Transonic Wind Tunnel are presented and analyzed. In the experiments, researchers systematically investigate many pertinent wall-geometry variables such as the wall openness and the number of slots along with the free-stream Mach number and model angle of attack. Flow-field surveys on the plane passing through the centerline of the slot were conducted and are presented. The effects of viscosity on the slot flow are considered in the analysis. The present experiments combined with those of previous investigations, give a more complete physical characterization of the flow near and through the slotted wall of a transonic wind tunnel. .

14. SUBJECT TERMS
Wind tunnels; Transonic; Wall interference; Slotted walls; Boundary conditions; Experiments

15. NUMBER OF PAGES
72

16. PRICE CODE
A04

17. SECURITY CLASSIFICATION OF REPORT	18. SECURITY CLASSIFICATION OF THIS PAGE	19. SECURITY CLASSIFICATION OF ABSTRACT	20. LIMITATION OF ABSTRACT
Unclassified	Unclassified		